Design of Polymeric Membranes for Large-Scale Energy Storage

A Dissertation Presented for the
Doctor of Philosophy
Degree
The University of Tennessee, Knoxville

Michelle Lehmann
May 2022

ACKNOWLEDGEMENTS

I would like to thank my advisor, Dr. Tomonori Saito for his mentorship, patience, and support during my Ph.D. studies. I would also like to thank him for taking a chance in hiring me when I graduated with my BS degree.
I would like to thank my doctoral committee members: Prof. Alexei Sokolov, Prof. Brian Long, Dr. Jagjit Nanda, and Prof. Thomas Zawodzinski for their valuable suggestions, collaborations, and advise during my PhD studies.
I would like to thank Dr. Guang Yang, who taught me many valuable electrochemical techniques, data analysis, and helped extensively with writing my first publications. I am grateful for his assistance in training me to become a worthy scientist.
I also want to thank the OE non-aqueous flow battery team; Dr. Guang Yang, Ethan Self, Frank Delnick, and Landon Tyler for providing guidance, knowledge, and many interesting discussions.
I want to thank the AEMFC and PEMFC collaborators Yu Seung Kim, Daniel Leonard, Thomas Zawodzinski, Pranathi Gangavarapu, and Shane Foister.
I want to thank Dr. Brian long for allowing me to be trained in the norbornene synthesis and Trevor Wilson for taking the time out of his busy schedule give me the run down on the synthesis methods.
I would also like to acknowledge the collaborative efforts and valuable discussions with members in the group: Dr. Alexei Solokov, Dr. Tao Hong, Bingrui Li, Dustin Gilmer, Jackie Zheng, Anis Rahman, Arif Arifuzzaman, and all former group members.
I also want to thank my family for putting up with me during these years of hard work and sometimes long hours. Your patience and wondering ‘what’s for dinner’ has helped keep me grounded and reminded me to make time for you guys.

ABSTRACT

Many countries have enacted renewable energy targets of 32% or more by 2040 to reduce their carbon footprint. However, due to the intermittent nature of renewable energy sources, long-duration energy storage systems are vital for providing a secure electricity supply. To meet this demand, new battery technologies utilizing earth-abundant and low-cost components are necessary. Among them, non-aqueous redox flow batteries represent a transformative energy storage system due to their flexible material selection and wide operating voltage window. A membrane plays a critical role in these next-generation energy storage technologies as it separates the anode and cathode while allowing for facile transport of the charge carrier. In addition to designing and synthesizing novel polymer membranes with improved ion transport, it is imperative to gain a greater understanding of the impact of a non-aqueous electrolyte on membrane properties. The goal of this study is to synthesize new high performance membranes and gain insight into the impact of non-aqueous electrolytes on membrane properties.

In this dissertation, membranes of various composition and architecture are synthesized, and a systematic evaluation of membrane properties in various electrolyte solutions unravels their structure-property relationships. Tailored crosslinking of poly(ethylene oxide) (PEO), a commonly utilized polymer electrolyte, was found to enhance sodium-ion conductivity and mechanical robustness over a wide temperature range compared to the linear polymer. Building upon these findings, a Lewis basic functional group was incorporated to the crosslinked PEO network. The Lewis basic functional group facilitates lithium salt dissolution and enables higher cation transport. Then a trifluoromethanesulfonimide functionalized cation exchange membrane was synthesized and the critical relationships between membrane ion transport and electrolyte salt concentration are unraveled. Tailoring the electrolyte salt concentration enables over an order of magnitude increase in membrane ionic conductivity, while maintaining a transport number >0.75.

Finally, the synthesis of a mechanically robust anion exchange membrane with excellent chemical stability is demonstrated. The membrane is evaluated for use in an aqueous and non-aqueous environment. Insights gained into the effect of organic electrolytes on membrane properties will provide strategies for the development of new polymer electrolyte membranes and performance improvements for a variety of electrochemical technologies.

TABLE OF CONTENTS

LIST OF TABLES

LIST OF FIGURES

INTRODUCTION

Large-scale, long-duration energy storage (LDES) is a key technology to enable the widespread adoption of renewable energy resources (solar, wind, etc.) and to meet the growing demands of an energy intensive economy. The increased renewable energy penetration in the electric grid is essential for decarbonization to address global climate change. Several governments and states have mandated targets to increase electricity generation from renewable sources. For example, the European Union set a 32% target for renewable energy use by 2035,[1] and California plans to achieve net-zero carbon by 2040.[2] The switch to renewable energy sources requires a diverse and flexible energy storage portfolio to meet the power demands of the grid. A recent techno-economic study suggests that for storage between 10-100 hours at rated power, the levelized cost of storage should be $\geq$ \$0.05 kWh^{-1}.[3] Furthermore, The United States Department of Energy long-duration storage shot's recent announcement sets an aggressive goal of reducing grid-scale storage cost by 90% within the next decade for systems delivering 10 plus hours of storage.[4] This target is based on the \$162 kWh^{-1} 2020 capital cost of a 100 MW lithium-ion battery. To meet this demand, new battery technologies utilizing earth-abundant and low-cost components are necessary. Thus, it is imperative to advance alternative battery chemistries for large-scale stationary applications.

Current Li-ion batteries utilize a liquid electrolyte (organic solvent + salt) with a porous separator. Possible next-generation batteries include lithium and sodium-based solid-state batteries, in which a polymer electrolyte replaces the liquid electrolyte (Figure 1a). The use of a polymer electrolyte membrane may enable the use of the ultimate high energy density anode, lithium metal. Traditional research into polymer-based batteries have utilized neutral polymers that can solvate an alkali metal salt or single-ion conducting polymers (Figure 2a and 2b). Salt-in-polymer electrolytes often suffer from low cation transport numbers (< 0.5).[5, 6] The low transport number causes concentration polarization at the electrodes, a reduced electrochemical stability window, and dendrite formation, which limits their practical application for high energy density batteries utilizing an alkali metal anode. Single-ion conducting polymers constrain the mobility of the anion by tethering it to the polymer backbone and exhibit high cation transport numbers (>0.85).[3] However, the use of single-ion conducting polymers in solid-state Li or Na-ion batteries has been limited due to the poor ionic conductivity of these polymers in a dry state (10^{-11} to 10^{-6} S/cm at 30 °C).[7-9] Strategies used to increase the conductivity of single-ion conductors for Li and Na batteries include the use of a cation conducting group with a delocalized negative charge, such as trifluoromethanesulfonimide (TFSI), and the addition of a high dielectric constant carbonate plasticizer.[10-12] For LDES applications, where the weight of a battery is not a limiting factor, solid-state Na-ion batteries are a promising alternative to Li-ion batteries due to the low cost and abundance of sodium compared to lithium.[13]

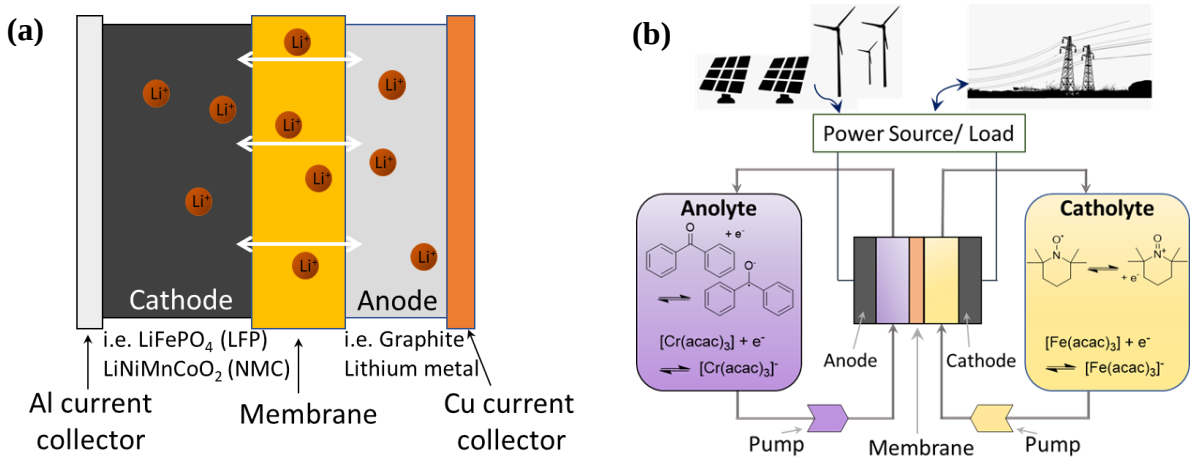

Figure 1. (a) Schematic of a lithium-ion polymer battery. (b) Schematic of a non-aqueous redox flow battery, with examples of organic and metal-based redox couples.

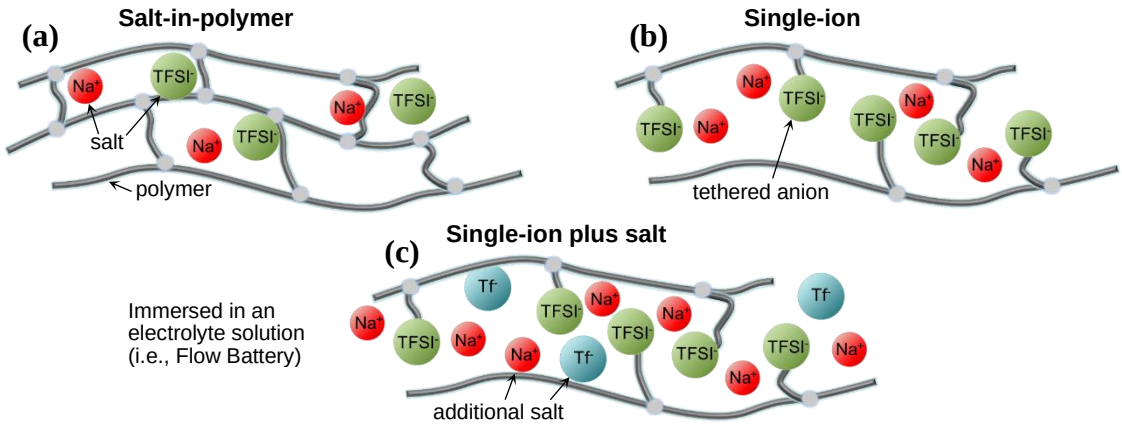

Figure 2. Illustration of a (a) salt-in-polymer electrolyte, (b) single-ion conducting polymer, and (c) single-ion plus salt polymer.

A representative LDES technology is a redox flow battery (RFB). RFBs are well suited for LDES due to their modular design and ability to decouple power and energy performance.[14, 15] RFBs store energy in redox-active species dissolved in a liquid electrolyte as separate catholyte and anolyte solutions (Figure 1b). Non-aqueous RFBs are a potential next-generation LDES option due to their higher operating voltage and higher energy density compared to aqueous flow batteries.[16, 17] A membrane, as a critical component in these non-aqueous electrochemical systems, needs to exhibit high selectivity and conductivity in addition to high chemical, electrochemical, and mechanical stability. Improved membrane performance and the design of new polymeric materials are imperative to aid in the advancement of next-generation batteries. In this dissertation, various strategies are implemented to improve the ionic conductivity, transport number, and mechanical properties of polymer electrolytes. Firstly, several salt-in-polymer electrolytes were developed to improve upon the transport and mechanical properties of linear poly(ethylene oxide) (PEO). Linear PEO has been extensively studied as a polymer electrolyte due to its ability to form complexes with various cations.[18-20] However, linear PEO electrolytes typically exhibit poor room temperature ionic conductivity (10^{-7} – 10^{-6} S/cm) due to its semi-crystalline nature.[21-24] Furthermore, linear PEO loses its mechanical integrity at temperatures above the crystalline melting point of 60 °C.

A crosslinked PEO polymer electrolyte for Na-based batteries was developed utilizing readily available building blocks via a facile single-step synthesis. The crosslinked polymer network provides mechanical robustness over a wide temperature range, even when completely immersed in an electrolyte. Even with a high degree of crosslinking, the membrane remains flexible and completely amorphous, imparting excellent room temperature ionic conductivity. The role of ethylene oxide complexation with sodium triflate (NaTf) and its effect on polymer segmental dynamics and ionic conductivity is elucidated with and without tetraethylene glycol dimethyl ether (TEGDME) as a plasticizer. To explore the impact of adding a Lewis basic group to the polymer network, a novel crosslinked polymer system consisting of branched poly(ethyleneimine) (PEI) and linear PEO was synthesized. Due to the hyperbranched structure, H-bonding, and electrostatic interactions of PEI, the PEI-PEO crosslinked membranes demonstrate unique features of improved salt solvation and lithium-ion transport over linear PEO. The PEI-PEO crosslinked polymer electrolyte system is evaluated for use in a Li metal battery, and the effect of free amine moieties on ion transport and mechanical properties are revealed.

Then a single-ion conducting cation exchange membrane was utilized to gain a fundamental understanding and insight into membrane transport properties in non-aqueous electrolytes (Figure 2c). A commercially available sulfonated pentablock terpolymer was utilized due to its high mechanical strength and capability to form microphase-separated morphology. The sulfonate functional group was converted to a TFSI functional group via a facile two-step

process to provide improved ionic conductivity in a non-aqueous system. Membrane properties such as uptake, conductivity, transport number, and salt absorption were measured to determine the relationships between membrane transport and electrolyte salt concentration. Finally, mechanically robust polynorbornene anion exchange membranes were synthesized and evaluated for use in both aqueous and non-aqueous systems. The impact of the quaternary ammonium tether length and incorporation of hydrophobic groups on aqueous membrane performance was elucidated for this polymer system. The best performing membrane was then selected for evaluation in a non-aqueous environment. Membrane properties of uptake and conductivity were evaluated in several organic electrolyte solutions to determine its efficacy for use in a non-aqueous flow battery.

The insight gained into the effect of organic electrolytes on membrane properties will provide strategies for the development of new membrane materials, performance improvement of existing membrane materials, and stimulate further research into the ion transport mechanisms in non-aqueous electrolytes. The results of this study have the potential to provide an avenue for the significant advancement of Li-ion, Na-ion, and non-aqueous flow batteries. Furthermore, the high-performance membranes synthesized for this work can be applied to other electrochemical technologies.

CHAPTER I
Background: Membrane Properties in Non-Aqueous Electrolytes

A version of this chapter was published by Michelle L. Lehmann, Landon Tyler, Ethan C. Self, Guang Yang, Jagjit Nanda, and Tomonori Saito "Membrane Design for Non-Aqueous Redox Flow Batteries: Current Status and Path Forward" accepted to *Chem*, *10.1016/j.chempr.2022.04.005*

Michelle Lehmann wrote most of the manuscript under the guidance of Tomonori Saito, with input and discussion from Ethan Self and Guang Yang. Landon Tyler wrote a section of the manuscript under the guidance of Jagjit Nanda. Tomonori Saito and Jagjit Nanda provided overall direction and supervision.

Abstract

Redox flow batteries are promising technologies for long-duration, large-scale energy storage applications. Among them, non-aqueous redox flow batteries (NARFB) represent a transformative flow battery system since NARFBs can offer higher energy density and lower cost than aqueous flow batteries. However, many technical challenges remain for NARFBs, including the lack of high performance membranes, low solubility of redox materials, and poor efficiencies of the cells. Membranes serve a vital function in NARFBs, as they allow for selective ion transport while providing separation between the anolyte and catholyte. NARFB membrane development is an emerging research area, and this chapter reviews critical factors that influence membrane properties, including solvent uptake and ion transport. A greater understanding of membrane behavior in non-aqueous solutions provides design principles for developing next-generation membranes for NARFB and lays a strong foundation for the development of electrolytes for solid-state batteries and various other energy storage systems.

Introduction

Large-scale, long-duration energy storage (LDES) is a key technology to enable widespread adoption of renewable energy resources (solar, wind, etc.) and to meet the growing demands of an energy intensive economy. Redox flow batteries (RFBs) are well suited for LDES due to their modular design, ability to decouple power and energy performance.[14, 15] RFBs have been widely studied since first reported by Thaller in 1974.[25] The aqueous RFB was further developed into a vanadium RFB, first reported by Maria Skyllas-Kazakos in 1984,[26] the most common RFB chemistry used today. Non-aqueous RFBs (NARFBs) have emerged as an alternative to aqueous RFBs. The use of an organic solvent offers a much higher operating voltage than aqueous RFBs, which in turn can increase the system's energy density. The potential window of aqueous RFBs is limited to 1.5 V,[17] due to the occurrence of undesirable water-splitting, while organic systems such as acetonitrile based electrolytes have an electrochemical window of up to 5 V.[16] NARFBs show great potential as next-generation RFBs, with some systems having theoretical specific energies over 200 Wh kg^{-1}, almost 10 times greater than aqueous vanadium RFBs.[27] A United

States Department of Energy report predicts the LCOS of utility scale installments for a chromium/iron-based NARFB (200-250 \$ MWh^{-1}) to be half that of an aqueous vanadium RFB (425-475 \$ MWh^{-1}).[28] However, many challenges still need to be addressed before NARFBs can reach commercial viability, including the development of redox-active species with improved stability/solubility and higher performance membranes.

The membrane is a critical component in flow batteries, as it needs to provide high ionic conductivity and separate the anolyte and catholyte compartments. The membrane in a NARFB is constantly exposed to the harsh environment of the organic supporting electrolyte and redox couples. To achieve stable NARFB performance, membranes are required to provide high mechanical strength, high ionic conductivity and selectivity, and excellent chemical and electrochemical stability.[29] Currently, commercially available porous separators and conventional membranes for aqueous RFBs are the most widely used membranes in NAFRBs, due to the unavailability of high-performance membranes designed for NARFBs. In addition, commercially available membranes for aqueous systems often lack the stability in organic solvents to provide suitable performance for NARFBs.

This chapter provides insights into factors that control electrolyte uptake and ion transport in non-aqueous systems. The effect of organic solvents on membrane properties in non-aqueous systems is complex and not well-understood, while these parameters are relatively well studied in aqueous systems. Greater insight into the impact of organic solvents on membrane properties will provide design strategies for improved membranes for NARFBs and other non-aqueous battery technologies.

Membranes for NARFBs

The US DOE's recent announcement sets an aggressive goal of reducing long-duration energy storage costs by 90% within the next decade. To reach such as aggressive target, achieving enhanced performance while reducing component costs are necessary. Furthermore, next-generation RFBs, such as NARFBs, should be able to achieve a minimum of 1250 cycles, or 5 years of operation, to be competitive with Li-ion systems.[30] Realistically, a lifetime of >10 years is expected. The membrane, as a critical component in a NARFB, should exhibit:

1. *High ionic conductivity*

A membrane needs to have low area specific resistance, which requires thin membranes with high ionic conductivity. Darling et al. recommended a target resistance of < 2.3 $\Omega\ cm^2$,[30] where for example, 30 μm membrane would require a conductivity of 1.3 mS cm^{-1}.

2. *Low permeability of redox-active species*
Failure to effectively block the transport of the redox-active species through the membrane can lead to self-discharge and irreversible capacity loss. Maintaining a Columbic efficiency of 99.99% or higher is necessary to achieve stable long-term performance of a flow battery. To achieve such high CE of an operating cell, a membrane needs to have an active species permeability of $\leq 10^{-10}$ cm^2 s^{-1}.

3. *High mechanical stability/ low swelling ratio*
High mechanical and dimensional stability in organic solvents reduces membrane fatigue and enables thinner membranes to be utilized. Excellent mechanical strength also allows the membrane to withstand the pressure induced by flowing liquids in the cell. Excessive dimensional swelling of the membrane reduces its mechanical strength and increases stress when assembled into a device. Furthermore, a membrane with high mechanical strength allows for facile integration into large-scale roll-to-roll manufacturing.

4. *Chemical and electrochemical stability*
Excellent chemical and electrochemical stability mitigates side reactions of the membrane with the electrolyte, which is critical to enable stable device performance. More specifically, the membrane needs to be stable in organic solvents and against highly oxidative and reductive redox couples. Furthermore, to fully utilize the benefits of a non-aqueous system, a wide operating voltage is needed. A simulation study by Chen et al. indicates that many polymers utilized as electrolytes for Li-ion batteries have an electrochemical stability window (ESW) of 4.75 eV.[31] As redox couples are developed that can achieve larger potential windows, the electrochemical stability of the membrane will become a critical factor.

Unfortunately, there is often a trade-off among these performance requirements. High ionic conductivity generally comes at the cost of decreased selectivity,[32] as demonstrated with reported values of conductivity and redox species permeability (Figure 3). In addition, many polymeric systems with high mechanical and chemical stability typically exhibit poor room-temperature ionic conductivity.[33-35] For non-aqueous systems, there are many factors involved that impact a membranes' uptake, conductivity, and active species permeability. For this chapter, membranes are classified into 3 broad categories: anion exchange membrane (AEM), cation exchange membrane (CEM), and porous membranes (Figure 4).

AEMs are the most widely developed membranes for NARFBs. The cation tethered to the polymer backbone aids the transport of an anion while blocking the transport of positively charged species by Donnan exclusion. Many redox couples are positively charged (e.g., ferrocenium cation), with the charge carrier being the anion. Thus, AEMs can serve as the appropriate choice of membrane for these systems. On the other hand, CEMs contain an anion tethered to the polymer backbone, allowing the transport of cations through the membrane while

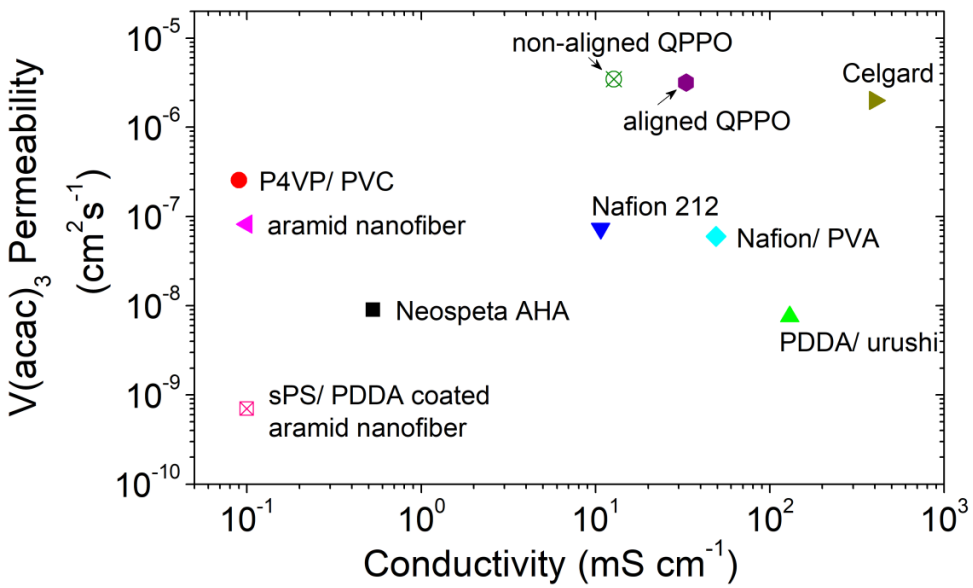

Figure 3. (a) Selectivity of various NARFB membranes. All studies measured the permeability of $V(acac)_3$. References for the data points in the plot are: aligned and non-aligned QPPO, Ref [36]; Celgard, Neosepta AHA and PDDA/ urushi Ref [37]; P4VP/ PVC, Ref [38]; aramid nanofiber and sPS/ PDDA coated aramid nanofiber, Ref [39]; Nafion/ PVA and Nafion 212, Ref [40]. QPPO= quaternary amine form of poly(phenylene oxide), PDDA= poly(diallyl dimethylammonium), P4VP= poly(4-vinyl pyridine), PVC= polyvinyl chloride, sPS= sulfonated polystyrene, and PVA= polyvinyl alcohol.

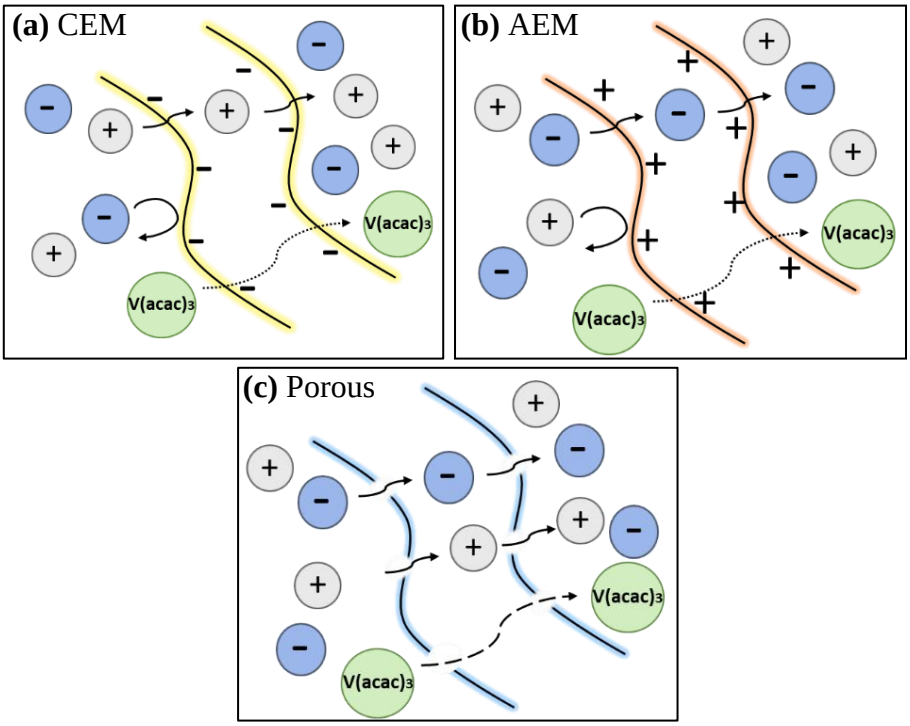

Figure 4. Schematic of the 3 categories of membranes for NARFBs and their ion transport mechanism. (a) Cation exchange membrane, (b) anion exchange membrane, and (c) porous separator. The arrows represent the relative ease of ion transport through the membrane: solid fast transport, dash moderate transport, and dotted slow transport.

blocking the transport of anions. Porous membranes are defined here as separators that do not contain any chemical functionality to inhibit the transport of redox couples or ions. Porous separators block the transport of redox species via size exclusion, though often, the pore size is larger than the solvated redox compound. Porous separators allow for transport of both anion and cation, thus offering no selectivity toward the charge carrier. To date, a handful of ionic groups have been utilized for ion exchange membranes for NARFBs (see Figure 5a). In some cases, membranes containing larger cations (i.e., 1-methylpyridinium) exhibit lower $V(acac)_3$ permeability than those prepared with a smaller cation (i.e., trimethylammonium).[41] Examples of potential ionic groups yet to be explored for NARFB membranes are given in Figures 5b and 5c. While the list of ionic groups in Figures 5b and 5c is by no means comprehensive, the depicted cations demonstrate improved stability in aqueous environments, while the anions show improved conductivity lithium-based battery studies.

Impact of Non-Aqueous Solutions on Membrane Properties

To design membranes for NARFBs, it is imperative to establish an understanding of the structure-property relationships and the dynamics of ion transport in non-aqueous systems.[42, 43] Considering the vast combination of supporting electrolytes and redox-active species possible for NARFBs, developing correlations between the supporting electrolyte composition and membrane properties (i.e., uptake, ion transport, permeability) is imperative for developing high-performance NARFB membranes.

Solvent Uptake.

It is essential to control a membrane's electrolyte uptake and swelling in flow battery applications. A large amount of solvent uptake generally increases ionic conductivity, but excessive uptake results in high permeability and loss of mechanical integrity. On the other hand, when the uptake is limited, the membrane typically exhibits poor ionic conductivity. Uptake is generally correlated with membrane dimensional swelling unless a support layer is utilized (see discussion below). In aqueous solutions, backbone flexibility,[44, 45] polarity,[46, 47] and membrane ion exchange capacity (IEC)[48, 49] have a significant impact on electrolyte uptake. Due to the ionic groups being hydrophilic, water uptake increases with higher IEC in aqueous systems; thus, there is a balance between ionic conductivity and swelling of the membrane. In non-aqueous solutions, the relationship is much more complex. Solvent uptake is affected by the physical properties of the polymer as well as that of the solvent.

The effect of solvent properties on lithiated Nafion (Li-Nafion) uptake has been comprehensively studied by Doyle et al.[43] In general, solvent uptake increased with donor number and dielectric constant. The effect of backbone structure in non-aqueous solvents is not well understood, though it is intuitive that a rigid backbone may experience less swelling than a flexible backbone. While

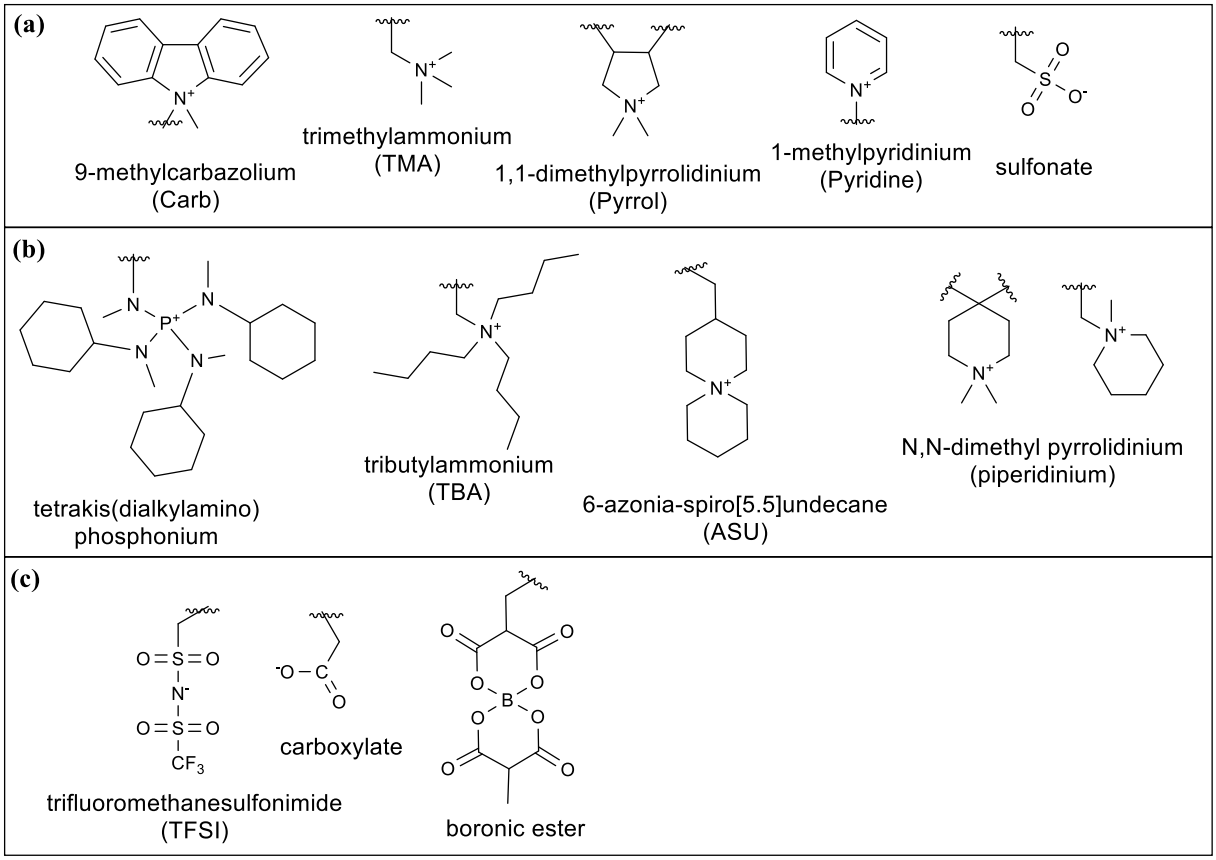

Figure 5. (a) Ionic groups utilized in NARFB membrane studies. (b) Examples of potential cationic groups for anion exchange membranes. (c) Examples of potential anionic groups for cation exchange membranes.

the polarity of the backbone greatly affects water uptake in aqueous solutions, the trend is not well studied and is unclear in non-aqueous solutions. In water, the highly hydrophobic backbone of Nafion exhibits less uptake than a non-fluorinated backbone such as styrene-ethylene/butylene-styrene (SEBS) triblock copolymer.[50, 51] In organic solvents, such as propylene carbonate (PC), acetonitrile (AN), and dimethyloxyethane (DME), Nafion exhibits uptake values of 65%, 19%, and 29%, respectively, while the sulfonated SEBS copolymer had no measurable solvent uptake.[50] The IEC of the membrane also impacts solvent uptake, though the degree to which this occurs depends on the solvent dielectric constant and the electrolyte salt concentration. For Li-Nafion, an increase in DME uptake only occurred at a high IEC (1.27 meq g^{-1}).[50] On the other hand, a gradual increase in PC uptake was observed with increasing IEC, with a sharp increase occurring at IECs >1.0 meq g^{-1} (Figure 6a). The lesser change in uptake for DME may be related to its low dielectric constant. For example, a high dielectric constant solvent exhibited a greater affinity for the ionic regions of sulfonated polystyrene, while a low dielectric solvent had similar affinities toward the backbone and ionic regions.[52] Thus, a change in the IEC would have a greater impact with a high dielectric solvent such as PC than the low dielectric solvent DME. Furthermore, uptake of a poly(phenylene oxide) (PPO) membrane increased significantly when salt was present in an AN-based electrolyte (Figure 6b).[53] This trend is the opposite of many aqueous systems, where the presence of salt generally decreases solvent uptake (Figure 6c).[54] Furthermore, the degree to which uptake increases in the non-aqueous electrolyte solution is more pronounced at higher IEC values (~2× at 0.49 meq g^{-1} and ~3.5× at 1.03 meq g^{-1}).

Ionic Conductivity.

In non-aqueous systems, many factors contribute to the ionic conductivity of a membrane, including the solvent type, functionality of the tethered anion or cation, as well as the counter-ion. Proton transport in aqueous systems generally occurs via the Grotthus mechanism, based on H-bonding between the proton and water molecules. It is difficult to match the proton conductivity of aqueous systems to ion conductivity in non-aqueous systems due to the lack of Grotthus-type of transport. In non-aqueous systems, ion diffusion is a much slower process; thus, developing clear correlations between membrane conductivity, solvent type, and other factors is crucial for improving the entire cell performance in NARFBs.

In general, membrane conductivity in non-aqueous solvents increases with the solvent's donor number and dielectric constant (Figure 7a and 7b). Li-Nafion has a Li^+ conductivity of 5.4×10^{-3} mS cm^{-1} in AN [43, 55, 56] and 2.2×10^{-2} mS cm^{-1} in PC.[43, 55, 56] In contrast, in water, Li^+ conductivity reaches 16 mS cm^{-1}, ~two orders higher than in non-aqueous solvents.[43, 54] The difference between aqueous and non-aqueous conductivity values is partially attributed to the constriction of Nafion's ionically conductive channels. In water, the pore size of Li-Nafion is estimated to be 2.9 nm,[57, 58] which decreases to 0.53 nm in PC.[59] Another reason for the decrease in ionic conductivity is the poor solvation of the Li^+ cation and the perfluoro sulfonate functional group by organic solvents,

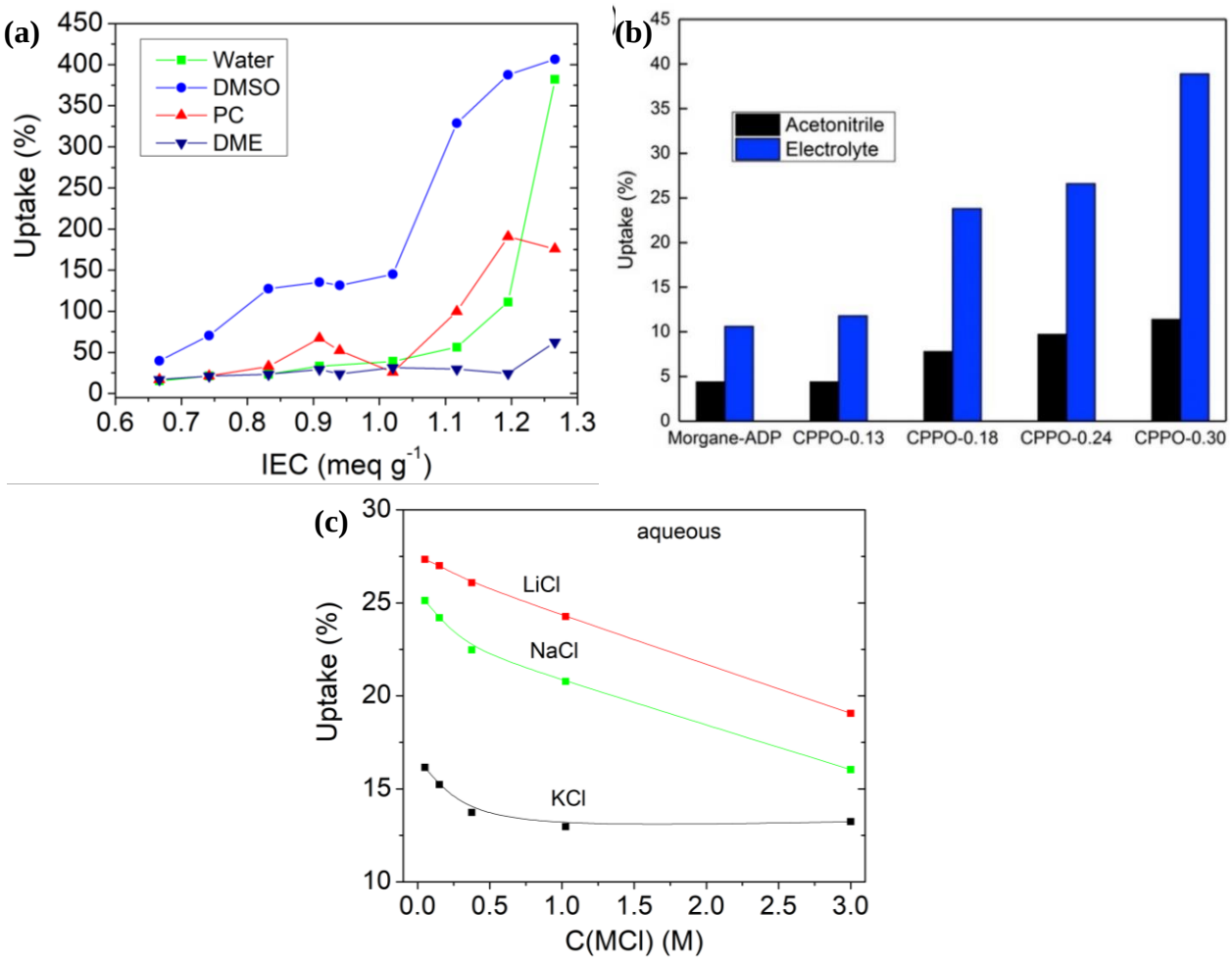

Figure 6. (a) Solvent uptake versus IEC of Li-Nafion in various solvents. Modified and reprinted with permission from Doyle et al.[50] Copyright 2001 American Chemical Society. (b) Uptake of crosslinked poly(phenylene oxide) (PPO) anion exchange membranes of various IECs (0.49, 0.87, 0.89, 1.03) in AN and electrolyte solution. Reprinted with permission from Li et al.[53] Copyright 2018 Elsevier. (c) Uptake of Nafion-117 equilibrated in various concentrations of aqueous salt solutions. Modified and reprinted with permission from Stenina et al.[54] Copyright 2004 Elsevier.

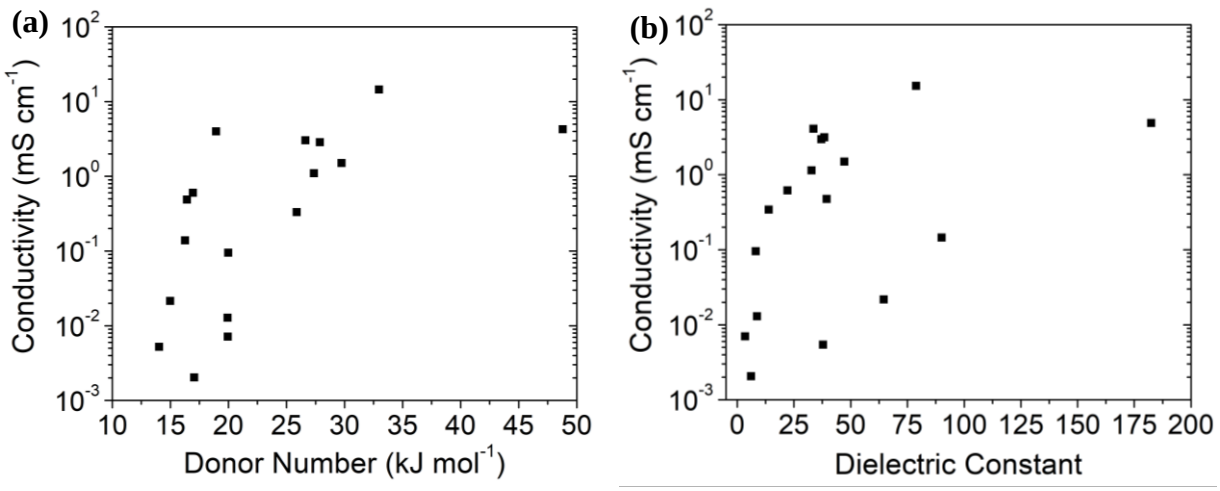

Figure 7. The conductivity of Li-Nafion as a function of solvent (a) donor number and (b) dielectric constant. Modified and reprinted with permission from Doyle et al.[43] Copyright 2001 Elsevier.

causing the Li^+ to be more tightly bound to the anion.[50, 60] A further decrease in Li^+ conductivity was observed in PC for more Lewis basic anions of perfluoro carboxylate and styrene sulfonate. Thus, to promote ion disassociation in organic solvents, a very weak Lewis basic anionic group, such as a sulfonylimide, is a promising route to explore for NARFBs.[50] In Li-ion batteries, the sulfonylimide functional group is proven to provide an order of magnitude increase in Li^+ conductivity due to the highly delocalized charge on the anion.[61] Another method to promote ion disassociation is the use of an organic cation instead of an alkali metal cation.

In non-aqueous solvents, organic cations demonstrate much higher ionic conductivity than Li^+.[43, 60, 62] The conductivity of organic cations increases with increasing size, contrary to the trend observed in aqueous systems (Figure 8a). A perfluorinated 3M membrane (similar chemical structure to Nafion) exhibits a conductivity of 2.4 mS cm^{-1} to 18.3 mS cm^{-1} in AN with an increase in cation size from tetramethylammonium (TMA) to tetrabutylammonium (TBA).[62] In this work, the 3M membrane in lithium form had a conductivity of 1.1 mS cm^{-1}, similar to some reports for Li-Nafion,[60] but also several orders of magnitude higher than values reported elsewhere for Li-Nafion.[43, 55, 56] The conductivity of Nafion can depend on pretreatment conditions and equilibration time, so values here are only compared within the same work. The increase in conductivity for organic cations is attributed to the weaker electrostatic interactions between the larger TBA cation and the sulfonate groups of the polymer. In addition, the membrane in TBA^+ form exhibits a higher AN uptake (127%) than when in TMA^+ (81%) and Li^+ (16.4%) forms, which also contributes to the increase in conductivity (Figure 8b).

The effect of supporting electrolyte concentration on membrane conductivity is well documented for aqueous flow batteries, where an increase in proton conductivity is observed at low acid concentrations, then steadily declines at higher acid concentrations.[63, 64] Reasons behind the decline in proton conductivity include an increase in solution viscosity and dehydration of the membrane. In neutral pH aqueous electrolytes, the conductivity of Nafion 117 depends strongly on the alkali metal cation (Figure 9a).[54] Conductivity increased with increasing salt concentration for both NaCl and LiCl, though the conductivity of NaCl was higher across the concentration range measured (0 M to 3 M). For KCl, the conductivity slightly decreased with increasing salt concentration.

In a non-aqueous solution, a study utilizing Nafion 117 demonstrated that a decrease in Li^+ conductivity is observed with increasing $LiPF_6$ concentration in PC. On the other hand, $LiPF_6$ concentration (0 to 1.5 M) in DMSO electrolytes had little impact on conductivity (Figure 9b).[59] In PC, the decrease in conductivity is attributed to fewer solvent molecules within the membrane as the salt concentration increases. For DMSO, the solvent uptake by Li-Nafion is considerably higher than in PC (136 wt% compared to 65 wt%).[43, 59] Thus, a small decrease in the number of solvent molecules in the ion channels of Nafion soaked in $LiPF_6$ dimethyl sulfoxide solutions has little effect on ionic conductivity. The higher viscosity of concentrated electrolytes may also play

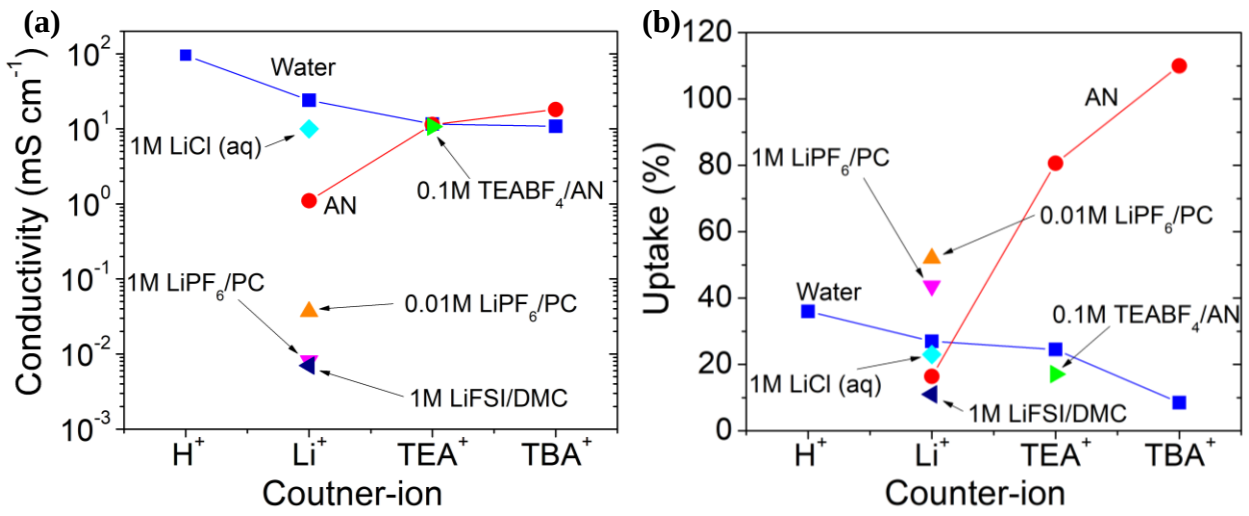

Figure 8. (a) Conductivity of Nafion or 3M perfluourinated membrane in various counter-ion forms in aqueous and non-aqueous solutions. (b) Uptake of Nafion or 3M perfluourinated membrane in various counter-ion forms in aqueous and non-aqueous solutions. AN and water data from Refs[62, 64], 1M LiCl (aq) Ref[54], 0.01M and 1M $LiPF_6$ in PC Ref[59], 1M LiFSI in DMC Ref[65], 0.1M $TEABF_4$ in AN Ref[40].

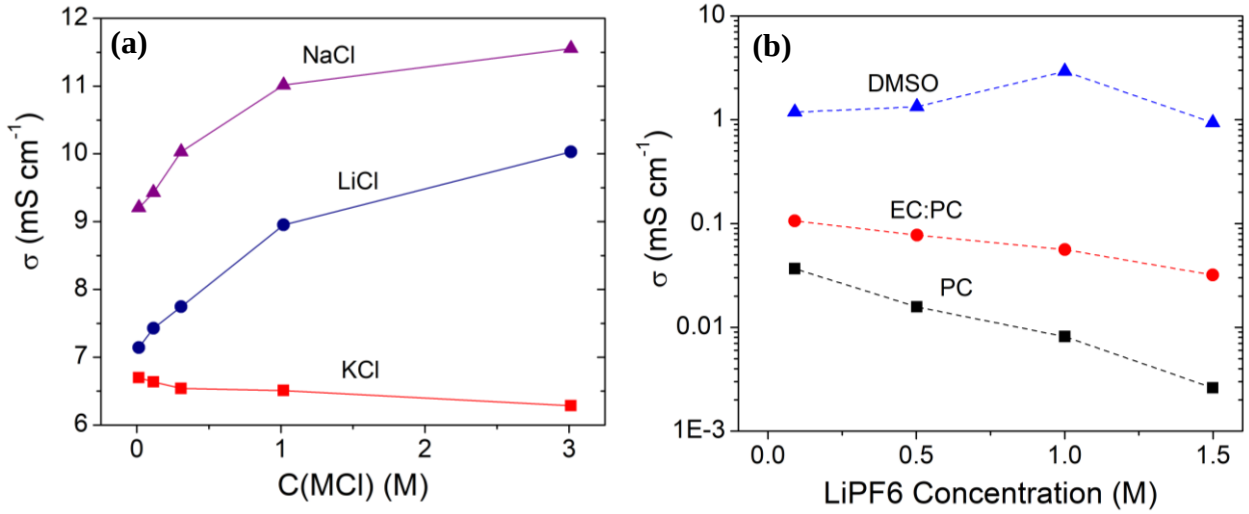

Figure 9. (a) Conductivity of Nafion-117 equilibrated in various alkali metal chloride aqueous solutions as a function of concentration. Modified and reprinted with permission of Ref [54]. Copyright 2014 Elsevier. (b) Conductivity of Nafion-117 equilibrated in various organic electrolyte solutions as a function of $LiPF_6$ concentration. Modified and reprinted with permission of Ref [59]. Copyright 2016 IOP Science.

a significant role. However, there is likely a more complex set of interactions causing the decrease in conductivity that is not yet well understood. Considering that the supporting electrolyte plays such a pivotal role in NARFBs, more research into the effect of the supporting electrolyte composition on membrane conductivity is needed.

Transport Number.

Membrane selectivity for the transportation of the desired charge carrier is an important parameter for NARFB performance. The transport number is the fraction of current which arises from the movement of a given charge carrier. Typically, a high transport number for the desired ion reduces cell polarization.[10] The charge carrier can be the anion or cation depending on the redox couples utilized, but generally, an AEM is utilized for an anion charge carrier and a CEM for a cation charge carrier. From the few studies that have reported the transport number in non-aqueous electrolytes, there appears to be a significant decrease in the transport number from aqueous to non-aqueous environments. These studies utilized the electromotive force (*emf*) method to estimate the transport number. Briefly, the cell potential is measured between compartments containing high and low concentrations of the supporting electrolyte separated by the membrane. The anion transport number ($\bar{t}_-$) through the membrane is then calculated using $V = (1 - 2\bar{t}_-)\frac{RT}{F}\ln(\frac{C_L}{C_H})$ where V is the cell potential, R is the gas constant, T is the temperature in Kelvin, F is the Faraday constant, and C_L and C_H are the low and high electrolyte concentrations, respectively.[66] While relatively dilute solutions are generally utilized to limit the impact of the activity of the electrolyte solution, studies in aqueous systems suggest that the contribution of the non-ideal thermodynamic portion may be significant in certain cases.[67] This is especially true in situations where the ion activity coefficient of the solution increases with increasing electrolyte concentration and needs to be considered for non-aqueous systems. Furthermore, developing methods to accurately determine the ion transport number in more concentrated solutions, such as those utilized in NARFBs, would provide additional insight into improving membrane performance in non-aqueous electrolytes.

Kim et al. measured the BF_4^- anion transport through two AEMs in PC and found that both exhibited a decrease in the anion transport number (0.79 and 0.87) from the Cl^- transport number in water (0.96 for both membranes).[66] Shin et al. observed an even more drastic decrease in the anion transport number of several membranes.[41] A poly(glycidyl methacrylate) (PGMA)/alkyl trimethyl ammonium and a poly(4-vinyl pyridine) (P4VP)/pyridinium crosslinked membranes containing a PVDF/Si support demonstrated Cl^- transport numbers of 0.96 in aqueous solution, consistent with other reports of aqueous transport numbers.[54 68] When immersed in a dilute 0.05 M $TEABF_4$ AN solution, the anion transport number decreased to 0.36 for the PGMA and 0.64 for the P4VP membranes. The commercial AEM, Neospeta AHA, exhibited an anion transport number of 0.98 in an aqueous electrolyte and 0.80 in the non-aqueous electrolyte 0.05 M $TEABF_4$ in AN.[41]

A decrease in transport number could be partially due to the difference in the salts utilized. Stienna et al. demonstrated that the cation transference number is relatively size-dependent in 1M aqueous solutions of NaCl, LiCl, and KCl.[54] The transport numbers of Li^+ and Na^+ were very similar at 0.96 and 0.97, respectively, while the transport number of the larger K^+ ion was 0.89. Furthermore, when the counter-ion was changed to the larger SO_4^{2-} ion, all the transport numbers remained above 0.98. However, even with variations in salt type, the transport numbers in aqueous systems remain significantly higher than that of the transport numbers in non-aqueous systems. Shin et al. attributed the low transport number of the PGMA membrane to charge inversion. The flexible cation in PGMA was proposed to be more accessible to the uptake of the BF_4^- counter-ion to form a Stern layer (a layer of ions counter to those tethered to the membrane) in comparison to the rigid aromatic cation of P4VP (Figure 10). Thus, charge inversion was prevented for the P4VP membrane, and a higher transport number was maintained. Even so, the ability of the membrane to exclude excess ions from entering is reduced in non-aqueous solvents compared to aqueous solutions. The poor exclusion of counter-ions implies that the effect of Donnan exclusion is weaker in organic solvents than in water. The membrane transport number behavior in non-aqueous systems needs to be further investigated to improve ion transport and reduce the redox species' permeability.

Permeability.

Reducing or eliminating the permeation of the redox couples through the membrane remains one of the greatest challenges for NARFBs. A high crossover rate of the redox species leads to low Columbic efficiency and energy efficiency.[41] The most widely studied redox couple to test membrane performance is vanadium acetylacetonate ($V(acac)_3$), which is positively and negatively charged when used as the catholyte and anolyte, respectively. The co-presence of charged and neutral species poses a problem for developing membranes for NARFB's, as many membranes are either cation or anion exchange, as discussed above. A few reports have utilized an aramid nanofiber support coated with layers of cation and anion exchange polymer to create a dual functionality membrane. The membrane exhibits one of the lowest $V(acac)_3$ permeabilities reported (7×10^{-10} cm^2 s^{-1}Table 2).[39] On the other hand, ferrocene (Fc, a smaller molecule than $V(acac)_3$) had several orders of magnitude higher permeability through the dual functionality aramid nanofiber membrane.[39, 69] In addition, the neutral Fc species permeability was found to be higher than Fc^+ (1.1×10^{-7} cm^2 s^{-1} compared to 2.8×10^{-8} cm^2 s^{-1}).[69] The decrease in permeability of Fc^+ is attributed to electrostatic repulsion from the ion exchange layers in the membrane.

Maurya et al. measured $V(acac)_3$ permeability in its cationic, neutral, and anionic forms. The authors found that the permeation of $V(acac)_3$ increased with decreasing ionic size (ionic size: $V(acac)_3^-$ > $V(acac)_3$ > $V(acac)_3^+$) in low crosslink density/high IEC AEMs. However, the permeability of all three species was relatively constant for a high crosslink density/low IEC membrane.[38] If Donnan exclusion were the main factor in determining the permeability of a

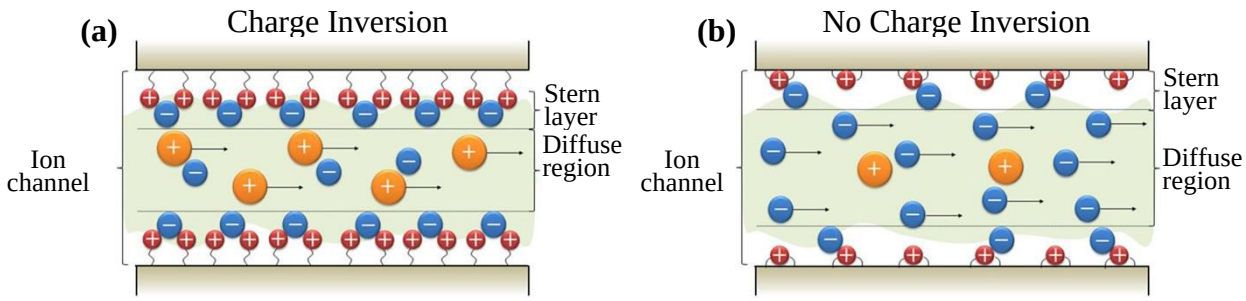

Figure 10. Schematic of ion transport through a membrane (a) with charge inversion (poly(glycidyl methacrylate) (PGMA)) and (b) without charge inversion (poly(4-vinyl pyridine) (P4VP)). Modified and reprinted with permission of Ref [41]. Copyright 2015 Elsevier.

charged species, one would expect the highest IEC membrane should have the lowest permeability for $V(acac)_3^+$, as seen with AEMs in aqueous systems.[68] Furthermore, Mushtaq et al. found that the molar flux of Fc^+ was similar for an AEM (FAP-450) and CEM (Nafion) at ~5 μmol h^{-1}·cm^{-2}.[70] These studies suggest that Donnan exclusion is not the major determining factor in redox species permeability for ion exchange membranes. For neutral species, the polarity of the redox species and the polymer backbone correlate strongly with permeability. In a study utilizing a PPO backbone, neutral species permeability was found to occur through the PPO phase of the membrane rather than the ionic rich regions, thus largely unaffected by the membrane's IEC.[65, 71] Furthermore, the transport of more polar molecules through the membrane was decreased compared to their less polar counterparts. The reduction in permeability of the more polar compounds is due to less favorable interactions with the PPO backbone. This study suggests that the permeability of redox species, especially that of neutral species, may be decoupled from membrane conductivity. Thus, careful design of backbone polarity in addition to ionic groups will be necessary for controlling redox species' permeability. Surprisingly, the permeability of neutral $V(acac)_3$ is an order of magnitude higher in Nafion than Fumasep FAP, even though both polymers have a similar perfluorinated backbone.[66, 72] This discrepancy may be due to differences in membrane microstructure and/or the sidechain ionic groups.

The concentration of the supporting electrolyte also impacts the permeability of redox species. The permeability of Fc^+, Fc, and I^- decreased by 1.5 to 2 orders from a 0.01 M $LiPF_6$/ PC solution to a 1M $LiPF_6$/ PC solution.[59] The reduction in redox species permeability can be attributed to a decrease in electrolyte uptake with the 1M solution. These works demonstrate the complexity of redox species permeability through a membrane in non-aqueous systems. Systematic studies of permeability through polymers of varying polarities with different ionic groups are necessary. In this manner, the permeability of positive, negative, and neutral redox species could be systemically studied to gain greater insight into the factors governing their permeability through a membrane. To control redox species permeability, multiple modes of exclusion may be necessary, such as combining size exclusion with Donnan exclusion (i.e., a nanoporous substrate coated with an AEM).

Design of Membranes for NARFBs

Considering the vast combination of solvents, salts, and redox species candidates for NARFBs, designing a membrane that meets all the performance requirements mentioned above is a highly challenging task. As material selection is narrowed to fewer high-performing candidates, membrane design will also be optimized for these systems. As mentioned in the previous sections, many factors contribute to the overall performance of a membrane in a non-aqueous environment, including backbone polarity, IEC, electrolyte composition, and counter-ion. The polarity and charge of the redox species and composition of the supporting electrolyte all need to be considered when designing a membrane for a NARFB. For relatively non-polar redox species,

a polar backbone may be advantageous to mitigate crossover.[71] The membrane's IEC appears to have less of an impact on the permeability of redox-active species but can significantly alter the ionic conductivity of the membranes.[65] Thus, a membrane with a higher IEC may be more beneficial for non-aqueous systems. In addition, compared to aqueous systems, increasing membrane IEC impacts uptake to a lesser extent in non-aqueous systems, especially for non-polar solvents. But an upper limit often exists on the achievable IEC of a polymer membrane. This upper limit is due to ionic aggregation that causes the polymer to become brittle.[53, 73] The brittleness is especially problematic for non-aqueous systems since the polymers need to be dried thoroughly before use to remove any residual moisture. Methods employed to aid in reducing the brittleness of ion exchange membranes include crosslinking, the formation of a graft or block copolymer, and polymer blending.

As with aqueous systems, controlling membrane uptake and dimensional stability are vital engineering requirements. Methods commonly employed to control membrane uptake and swelling include crosslinking,[74] copolymerization,[75, 76] and the use of a support layer.[72] Crosslinking aids in reducing dimensional swelling and improves solvent resistance. Crosslinking generally reduces solvent uptake and swelling, but can also reduce the membrane's conductivity.[77] Crosslinking alone does not typically control swelling to a sufficient degree when minimal dimensional swelling is required. Another approach includes the use of block copolymers to decouple ionic conductivity and mechanical properties. A block copolymer can have 2 to 5 dissimilar blocks, consisting of ionically conductive block(s) and mechanically robust block(s). Block copolymers have been investigated for use in aqueous systems and have been adopted with varying levels of success.[75-77] For non-aqueous systems, a block copolymer would need to be designed such that the non-aqueous electrolyte has a higher affinity towards the ionic regions rather than the mechanical blocks. This approach has not been investigated for NARFBs thus far and is a pathway worth considering.

Of these methods to control uptake and dimensional stability, the use of a porous support layer, such as Celgard, is the most effective and widely used strategy for NARFB membranes thus far. Utilizing a porous support layer is effective in minimizing dimensional swelling while allowing for a reasonable electrolyte uptake. For example, Bang et al. reported the dimensional swelling of a Celgard/ Nafion composite to be less than 0.5% with an electrolyte uptake (0.1M $TEABF_4$ in AN) of 30%. In comparison, Nafion exhibited a dimensional swelling of 9.3% with a solution uptake of 17%.[40] Methods utilized to prepare composites with a porous substrate include (i) pore filling with a monomer solution,[66, 68, 72] followed by polymerization, (ii) dip coating in a polymer solution (provides surface coating),[78] and (iii) infiltration of a polymer solution into the porous substrate.[79] In addition to controlling dimensional swelling, the use of a composite increases the overall strength of the membrane. The ultimate tensile strength of a composite utilizing a polyolefin separator may be significantly higher (120-150 MPa) than the neat polymer membranes (9 to 30 MPa).[40, 66] Notably, the tensile strength of polypropylene-based separators

depends on the direction of elongation (due to the manufacturing process), with values of 100-150 MPa and 5-15 MPa for elongation along or against the casting direction, respectively.[80]

A composite system commonly utilized in aqueous systems is the use of a polytetrafluoroethylene (PTFE) or expanded PTFE (ePTFE) support matrix. A polymer solution is typically cast with the support matrix to obtain a membrane of excellent mechanical strength. The use of ePTFE is standard for the fabrication of Nafion-based fuel cell membranes, though the use of a composite may increase membrane cost substantially. Another promising pathway for the development of membranes for NAFRB is the use of a ceramic/polymer composite. Most highly conductive ceramic separators are brittle and difficult to fabricate as thin films. A ceramic/polymer composite can offer high single-ion conductivity while maintaining flexibility, providing a mechanically stable membrane that is potentially scalable with roll-to-roll processing. Furthermore, ceramic fillers reduce uptake and swelling of the polymer component and have been shown to aid in the reduction of redox species permeability.[81, 82]

Conclusions

Utility-scale electrical energy storage is expected to play a significant role in enabling the widespread adoption of renewable energy sources and improving the power grid's efficiency. NARFBs are an attractive technology for large scale energy storage due to their potential for high energy density. While much research has focused on the development of redox active species, the development of membranes for NAFRBs is a relatively recent endeavor. Progress has been made toward achieving high performance membranes for NARFBs, with $V(acac)_3$ permeability values in the range of 1×10^{-10} to 7×10^{-10} $cm^2\ s^{-1}$ and reasonable room temperature conductivity (0.1 to 5.4 mS cm^{-1}). However, significant improvements still need to be made before this technology can reach the commercialization stage.

To enable commercially viable NARFBs, improvements in the redox active species, membranes, and cell design are necessary. The Department of Energy (DOE) long duration energy storage shot's recent announcement sets an aggressive goal of reducing grid scale energy cost by 90% within the next decade for systems delivering 10 plus hours of storage.[4] This target is based on the $162/KWh (2020) cost of a 100 MW lithium-ion battery. To fully utilize the benefits of a non-aqueous flow battery, a high concentration of active species (~4 M) and high operating voltage (3-4 V) are necessary.[83, 84] Furthermore, an increase in cell voltage to 4.5 V may relax constraints on membrane/electrolyte area specific resistance (ASR) and redox species concentrations.[84] In addition to active species concentration and cell voltage, performance metrics for a NARFB include a cell resistance (which includes electrodes, electrolyte, and membrane) under 5 $\Omega\ cm^2$ [84] and a Columbic efficiency value higher than 99.99% for an asymmetric and 97% for a symmetric (where the same redox active species is reduced on one side and oxidized on the other) flow battery. [30] While the actual performance requirements are

highly dependent upon the specific system utilized, these metrics provide useful targets. To predict the cost and performance of a flow battery, Crawford et al. reported a chemistry agnostic model based on inputs such as electrolyte and membrane conductivity and kinetic rate constants.[85] Such a model allows for the rapid evaluation of novel chemistries and will expedite the development of future NARFBs.

To further advance NARFB technology, membrane performance needs to be improved. Specifically, to achieve a Columbic efficiency of 99.99%, a membrane needs to be highly selective with good chemical and mechanical stability. Active species permeability of $\leq 10^{-10}$ $cm^2\ s^{-1}$ is required for acceptable long-term performance. The chemical durability of membranes in non-aqueous systems is not well studied. Studying polymers with proven chemical stability in aqueous systems will provide benchmark values for understanding stability in a non-aqueous environment. In particular, polymers containing only hydrocarbons in the backbone have proven to be more stable in strongly basic conditions and against radical species.[44, 86-88] The target ASR of the membrane is $\leq 2.3\ \Omega\ cm^2$.[30, 89] To achieve this goal, a highly conductive thin membrane is required, where for example, a 30 μm membrane needs to have a conductivity of 1.3 mS cm^{-1} to meet the ASR target. Furthermore, solvent uptake by the membrane needs to be minimized to maintain high selectivity and good mechanical properties.

The utilization of a Celgard/polymer composite membrane is the most common and effective method to control swelling thus far. However, Celgard/polymer composites are often limited to operating at lower current densities (0.5 to 2 mAh cm^{-2})[66, 72, 90] and delamination of the composite is a concern during long term operation.[53] Nanoporous membranes (pore size of 0.1-1 nm) have been proposed as a possible candidate for NARFB separators.[30] Additionally, the development of ceramic/polymer composite membranes could be a promising pathway for NARFB membrane improvements. Most highly conductive ceramic separators are brittle and difficult to fabricate as thin films. A ceramic/polymer composite can offer high single-ion conductivity as a flexible and mechanically stable membrane that is potentially scalable into manufacturing platforms such as roll-to-roll. In addition, the ionic group utilized in ion exchange membranes can significantly impact membrane conductivity and redox species permeability. Thus, systematic studies are necessary to determine the optimal tethered ionic groups for NARFBs. A membrane for a NARFB will likely require the combination of a support matrix and a high performance ion exchange membrane to achieve the desired properties.

NARFBs provide a promising energy storage option that utilizes earth abundant and low-cost materials, while they still require much research and optimization before possible commercialization. Continued study on all components of a NARFB is necessary, and the membrane, as a key enabler of the technology, requires significant improvements in durability, selectivity, and conductivity. Furthermore, targeted research on the effect of organic solvents on

membrane transport will provide a deeper understanding of membrane properties in a non-aqueous environment. Establishing the structure-property relationships of the membrane in non-aqueous systems will provide routes for the design of high performance membranes for NARFBs and enable deployment of NARFB technologies.

CHAPTER II
Crosslinked PEO Salt-in-Polymer Electrolyte

A version of this chapter was published by Michelle Lehmann, Guang Yang, Dustin Gilmer, Kee Sung Han, Ethan C Self, Rose E Ruther, Sirui Ge, Bingrui Li, Vijayakumar Murugesan, Alexei P Sokolov, Frank M Delnick, Jagjit Nanda, and Tomonori Saito. "Tailored Crosslinking of Poly(Ethylene Oxide) Enables Mechanical Robustness and Improved Sodium-Ion Conductivity" *Energy Storage Materials*, 2019, 21, 85-96

Jagjit Nanda and Tomonori Saito formulated the concept and managed the entire project. Michelle Lehmann conducted most of the experiments and wrote the manuscript under the guidance of Tomonori Saito. Guang Yang conducted linear PEO experiments, designed experiments for Na striping/plating and transport number measurements, obtained SEM/EDX images and contributed to writing the manuscript. Dustin Gilmer conducted membrane fabrications. Ethan Self and Frank Delink assisted Michelle Lehmann with electrochemical testing. Guang Yang and Rose Ruther conducted FTIR and analyzed the data. Bingrui Li performed DMA and Sirui Gee performed rheology under the guidance of Alexei Sokolov. Kee Sung Han conducted solid state NMR experiments. Kee Sung Han, Vijayakumar Murugesan, and Guang Yang performed NMR data analysis.

Abstract

Sodium-based energy storage systems are promising candidates for electric vehicles and grid-level energy storage applications. The advancement of sodium-based energy storage systems relies on the development of high performance sodium-ion conducting electrolytes and membranes that exhibit high ionic conductivity and mechanical stability. A crosslinked poly(ethylene oxide) based polymer electrolyte was developed that demonstrates high ionic conductivity, as well as excellent mechanical stability over a wide temperature range. The membranes were evaluated in both dry and plasticized states, with the Na^+ transference number decreasing upon plasticization. Ionic conductivities up to 2.0×10^{-4} S/cm at 20 °C and 7.1×10^{-4} S/cm at 70 °C are achieved for the plasticized membrane, almost four orders of magnitude greater than that of the non-plasticized membrane. The membranes are mechanically robust, and the storage modulus of the membrane is maintained at ~1 MPa from -20 to 180 °C even with the addition of plasticizer. This study provides a synthesis approach towards the design of highly ion conducting, mechanically robust gel polymer electrolytes for Na-ion batteries, non-aqueous flow batteries, and many other applications.

Introduction

Sodium-based energy storage systems have gained renewed interest in recent years due to the low cost and abundance of sodium compared to lithium.[13] With the ever-growing need for low-cost renewable energy storage systems, sodium-based batteries are promising candidates for electric vehicles and grid-level energy storage applications.[91, 92] In addition to sodium-based

anodes and cathodes, the developments of high performance sodium-ion conducting electrolytes and membranes are imperative for the success of these emerging technologies.[93, 94] Though much can be learned from the Li-ion field, relatively little work has been done on the development of electrolytes for Na-based energy storage systems. Compared to conventional liquid electrolytes, solid polymer electrolytes (SPEs) offer several advantages, including all solid-state device construction, good mechanical flexibility, low cost fabrication, and high ionic conductivity due to the formation of a stable gel by plasticizing with solvents. In addition to cost reduction, safety is a major concern for any battery technology. Electrolyte instability issues have plagued lithium ion batteries,[95] and SPEs plasticized with ether-based solvents offer a safer alternative to conventional carbonate-based liquid electrolytes.[96]

Poly(ethylene oxide) (PEO) has been extensively studied as a SPE due to its ability to form complexes with various cations.[18-20] However, PEO electrolytes typically exhibit poor room temperature ionic conductivity (10^{-7} – 10^{-6} S/cm) due to the semi-crystalline nature of PEO.[21-24] The addition of plasticizer to the polymer network has been shown to improve the room temperature ionic conductivity of PEO (10^{-6} – 10^{-5} S/cm),[97-99] but the weak mechanical properties of plasticized PEO prevents its use for practical applications. The mechanical strength of linear PEO derives from the well stacked chains in the crystalline phase and chain entanglement, but it loses mechanical integrity at temperatures above the crystalline melting point at around 56 °C. Crosslinking is an effective means to increase the mechanical strength of polymer electrolytes, including PEO-based electrolytes.[100, 101] Several techniques have been developed to fabricate Li-ion conductive crosslinked PEO-based SPEs, including photo-induced [102] and free radical polymerization.[103] On the other hand, thermally induced polymerization can also be effectively used to crosslink the precursors.[104] This method allows for precise control over crosslink density, which is determined by the precursor chain length and is readily tunable.

To date, several crosslinked PEO-based membranes have been studied for lithium systems,[100, 105-108] but few reports exist on gel polymer electrolytes for sodium systems. Gao et.al. reported a radical polymerized crosslinked poly(methyl methacrylate)-TEGDME gel polymer electrolyte for a sodium-sulfur battery that exhibited excellent electrochemical stability,[109] though it required a cellulose layer for mechanical support. Colo et al. reported a photo-crosslinked PEO-based polymer that demonstrated excellent conductivity (1×10^{-3} S/cm) at room temperature; however, this is above the crystalline melting temperature and no room temperature mechanical properties were reported.[110] Bella et al. reported a poly(ethylene glycol methyl ether methacrylate) crosslinked polymer electrolyte plasticized with a 1 M solution of $NaClO_4$ in propylene carbonate.[111] The photo-crosslinked polymer also displayed excellent room temperature conductivity (5.1×10^{-3} S/cm) but showed extensive swelling (200%) when immersed in the electrolyte. Further advancement of mechanically robust and highly Na-ion conductive membranes is necessary to meet the future demand of the technology. This is

especially true for non-aqueous flow battery applications, which require mechanical stability while fully immersed in liquid electrolyte. Thus, this study aimed to create a crosslinked PEO membrane with high ionic conductivity and good mechanical stability after plasticization, along with establishing the structure-property relationships.

Herein, this chapter demonstrates a facile single step synthesis approach that utilizes readily available building blocks to create a mechanically robust crosslinked PEO membrane for Na-based batteries. The PEO-based polymer is designed to be highly crosslinked, providing mechanical robustness over a wide temperature range and when completely immersed in electrolyte. Even with a high degree of crosslinking, the membrane remains flexible and completely amorphous, which imparts excellent ionic conductivity at room temperature. We utilize tetraethylene glycol dimethyl ether (TEGDME) as a plasticizer due to its compatibility with PEO as well as its excellent electrochemical and thermal stability.[96, 112, 113] TEGDME is more stable with respect to reduction than carbonate solvents and is thermally stable to just below 200 °C. The role of ethylene oxide (EO) complexation with sodium triflate (NaTf) and its effect on polymer segmental dynamics and ionic conductivity is elucidated with and without TEGDME as a plasticizer. The mechanical properties of the crosslinked membrane are evaluated using dynamic mechanical analysis (DMA) and rheology.

Experimental

Materials

The crosslinked PEO membrane contained two polymer precursors: (i) Poly(ethylene glycol) diglycidyl ether (PEGDGE, Sigma Aldrich, M_n = 500g/mol) and (ii) Jeffamine® ED 900 (95% purity, Huntsman, M_n = 900g/mol), a diamine with a poly(ethylene glycol) and poly(propylene glycol) backbone. Poly(ethylene oxide) (PEO, Sigma Aldrich, M_v = 600,000 g/mol) was used as the linear PEO reference, and sodium trifluoromethanesulfonate (sodium triflate, NaTf, 98%, Sigma Aldrich) was the salt in all membranes. Diethylene glycol dimethyl ether (diglyme, 99.5%, Sigma Aldrich) was used to cast the crosslinked membranes. All reagents used in the preparation of crosslinked films were used as received, except for TEGDME (≥99%, Sigma Aldrich) which was dried over molecular sieves and stored in an inert atmosphere.

Film Preparation

Crosslinked films were prepared using a solution-casting technique where the NaTf concentration was varied with respect to the polymer from 8 to 40 wt%. The molar ratio of epoxides in PEGDGE to amines in Jeffamine was fixed at 2:1 for all films. The polymers were mixed using a magnetic stir bar for 24 h before adding the desired amount of NaTf (dissolved in 5 ml diglyme). The polymer/solvent/NaTf mixture was mixed for 3-5 h to allow for complexation of the salt with the polymer chains, cast in a Teflon® dish, and cured at 100 °C for

3-3.5 h. All the fabricated membranes were dried under vacuum for 24 h at room temperature to remove any residual solvent. Plasticized samples were prepared in an Ar-filled glove box by soaking the dry membranes in excess TEGDME for 24 h and blotting dry. The initial and final mass of the samples were measured to determine the amount of TEGDME incorporated into the film. All plasticized membranes contained approximately 50 wt% TEGDME. Residual TEGDME from plasticization was evaporated to dryness, and no evidence of NaTf was observed, indicating the TEGDME soaking procedure did not leach NaTf salt from the polymer membrane.

Linear PEO-NaTf membranes were made as follows. The butylated hydroxytoluene (BHT) inhibitor in linear PEO was removed by rinsing 5g PEO with 1L of acetone, followed by drying PEO (M_v = 600,000 g/mol) at 60 °C under vacuum for a minimum of 24 h. NaTf was dried under vacuum at 90 °C for 8 h. PEO and NaTf were dissolved in acetonitrile (Sigma Aldrich, anhydrous, 99.8%) to form 4 wt% and 3 wt% stock solutions, respectively. These two stock solutions were mixed to form a series of PEO-NaTf solutions, with NaTf concentrations ranging from 12 wt% to 40 wt% in the final membrane. One plasticized linear PEO-NaTf sample was prepared by adding 2 moles of TEGDME per 1 mole EO to the solution. The PEO-NaTf solution was then cast into a Teflon® dish and dried under ambient conditions for 8 h, followed by a 16 h drying step under vacuum to evaporate any residual acetonitrile. All membranes were stored in an Ar-filled glove box (H_2O < 0.1 ppm, O_2 < 0.1 ppm) for further use.

Electrochemical Characterizations

Ionic conductivity of the membranes was measured by electrochemical impedance spectroscopy. Samples were punched into circular disks (1.27 cm in diameter) and sealed between two stainless-steel electrodes using heat shrink tubing to prevent moisture exposure during measurements. The impedance for each film was measured at multiple temperatures (20 – 70 °C) over a frequency range of 10^6 - 1 Hz using a 6 mV AC signal. Samples were thermally cycled three times between 20 – 70 °C in 10 °C increments to ensure reproducibility in the impedance measurements. All samples for electrochemical measurements were prepared in a glovebox and were performed using a Biologic VMP3 potentiostat and EC-Lab® software. The electrochemical stability window and Na^+ transference number of dry and TEGDME plasticized 18 wt% NaTf membranes were measured at 40 °C, with an additional transference number measurement at 20 °C with a plasticized membrane. The electrochemical stability window was measured using sodium foil as the counter and reference electrodes with a stainless-steel working electrode by linear sweep voltammetry between open circuit voltage and 6 V (*vs.* Na^+/Na) at a rate of 10 mV per second. For transference number measurements, a sodium foil symmetric cell was used, and a small DC potential of 7.5 mV was applied, and the current decay was monitored over time. Electrochemical impedance spectra at open circuit voltage just before applying the bias potential and after the current reached a steady state value were measured. Sodium stripping

and plating stability test was performed at 40 °C using a sodium foil symmetric cell and a TEGDME plasticized 18 wt% NaTf crosslinked PEO and 18wt% NaTf Linear PEO, cycled at a 73 μA/cm^2 current density.

Thermal Characterizations

Glass transition temperature (T_g) and melting temperature (T_m) of each membrane were measured using differential scanning calorimetry (DSC, TA instruments Q2000). Samples were sealed in aluminum DSC pans in an Ar atmosphere prior to measurement. The samples were cycled at a rate of 5 °C/min from -90 to 90 °C for 2 cycles, and T_g and T_m were recorded from the second cycle. The thermal profile of dry and TEGDME plasticized membranes were performed by thermal gravimetric analysis (TGA, TA Instruments Q50). TGA was conducted under nitrogen from 25 to 800 °C at a heating rate of 20 °C/min.

Mechanical Analysis

Films were prepared into approximately (9 × 4 × 0.1) mm^3 specimens for mechanical analysis. Storage and loss modulus were measured by dynamic mechanical analysis (DMA) at an operating frequency of 1 Hz utilizing a TA Instruments RSA-G2 Solids Analyzer as the samples were heated from 20 °C to 200 °C at 3 °C/min under nitrogen. Tensile measurements were performed according to ASTM D1708 using an Instron 3343 universal tensile meter. Membranes were stretched constant rate of 1 mm/min at room temperature in air until break. Reported tensile properties are an average of 5 samples.

Shear Rheology

Mechanical transitions in linear and crosslinked PEO samples were measured utilizing an AR2000ex rheometer (TA instruments) through temperature sweep tests in an oscillatory shear mode under a nitrogen atmosphere. Two different geometries were applied based on the magnitude of the shear modulus. The temperature range was -60 to 180 °C for the crosslinked PEO sample and -40 to 180 °C for the linear PEO sample. For both samples, the temperature ramp rate was 1 °C/min, and the angular frequency was 1 rad/s. Parallel plates (4 mm in diameter) were employed for measuring the crosslinked PEO sample over the entire temperature range. For the linear PEO sample, parallel plates of 4 mm diameter were used from -40 to 45 °C, and parallel plates of 8 mm diameter were used from 45 to 180 °C. The stress controlled oscillatory mode was set to 25,000 Pa stress for the entire temperature range for the crosslinked PEO sample. For linear PEO, the stress controlled oscillatory mode was set to 25,000 Pa stress for the temperature range of -40 to 45 °C, and the strain controlled mode was set to 0.15% strain for the temperature range of 45 to 180 °C.

Nuclear Magnetic Resonance

For the determination of the ion rotational correlation time, τ_c for Na^+ cation and Tf^- anion, ^{23}Na, and ^{19}F nuclear relaxation times were measured on a 600 MHz solid state NMR spectrometer (Bruker, Germany) equipped with a 2.5 mm magic angle spinning (MAS) probe at 20 °C without spinning the samples. Spin-spin (T_2) and spin-lattice (T_1) relaxation times were determined using a Carr-Purcell-Meiboom-Gill (CPMG) (90°- τ - 180° - τ - acquisition) and the inversion-recovery (180°-τ-90°-acquisition) sequences, respectively. Larmor frequencies (ω_0) for ^{19}F and ^{23}Na relaxation measurements were $2\pi\cdot564.644$ and $2\pi\cdot158.751$ rad·MHz, respectively. The rotational correlation time, τ_c (s) for Tf^- anion and Na^+ cation was estimated from the nuclear relaxation ratio using equation 1.[114]

$$T_2/T_1 = \left[\frac{2}{1+\omega_0^2\tau_c^2} + \frac{8}{1+4\omega_0^2\tau_c^2}\right] / \left[3 + \frac{5}{1+\omega_0^2\tau_c^2} + \frac{2}{1+4\omega_0^2\tau_c^2}\right] \quad (1)$$

From the measured τ_c, the diffusion coefficient of Na^+ cation and Tf^- anion were determined using the Einstein-Smoluchowski equation,[115]

$$D = \frac{a^2}{4.5\tau_c} \quad (2)$$

where a is the ionic radius of Na^+ cation (1.02 Å)[116] and the radius of Tf^- anion (2.95 Å)[117].

Results and Discussion

Fabrication of PEGDGE/Jeffamine Crosslinked Membranes

Crosslinked membranes were prepared via a single step synthesis using amine and epoxide terminated PEO-based precursors (Jeffamine, M_n = 900g/mol, and PEGDGE, M_n = 500g/mol, respectively). The primary amine on Jeffamine reacts with the epoxide on PEGDGE to form a covalent linkage, and the resulting secondary amine further reacts to form a crosslinked network (see Figures 11a and 11b). The molar ratio of epoxides:amines was fixed at 2:1 to form a robust, highly crosslinked network. Constraining the PEO segments in a crosslinked network is anticipated to reduce the crystallinity associated with linear PEO. All membranes are flexible and translucent (see Figure 11c). The membranes are mechanically stable, even with the addition of plasticizer and became slightly stiffer with increasing NaTf concentration. To evaluate the effect of NaTf concentration on their T_g and ionic conductivity, the membranes were prepared with NaTf concentrations ranging from 8 to 40 wt% with respect to polymer mass (EO/Na = 32 to 4).

Impact of NaTf and TEGDME on T_g

Figure 12a shows the DSC curves for non-plasticized crosslinked membranes with linear PEO shown for comparison. All crosslinked membranes exhibit a single T_g and no melting peak,

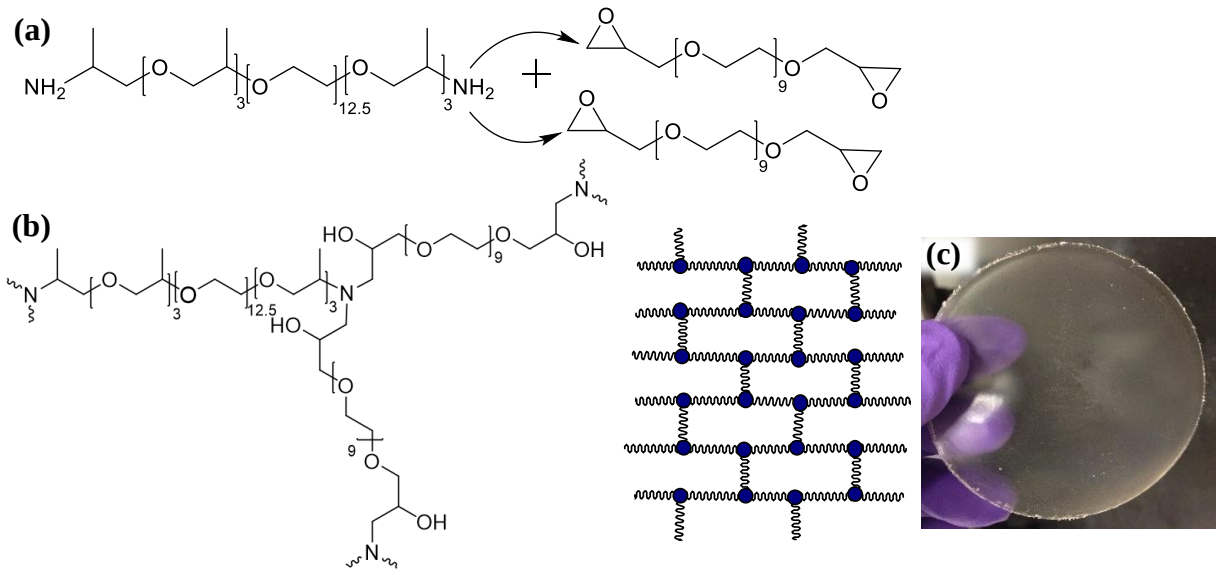

Figure 11. (a) Reaction scheme of PEGDGE and Jeffamine to produce a crosslinked PEO-based network, (b) Schematic of a crosslinked PEO network where dots represent nitrogen and lines represent PEGDGE and Jeffamine, and (c) photograph of a free standing crosslinked membrane containing 24 wt% NaTf.

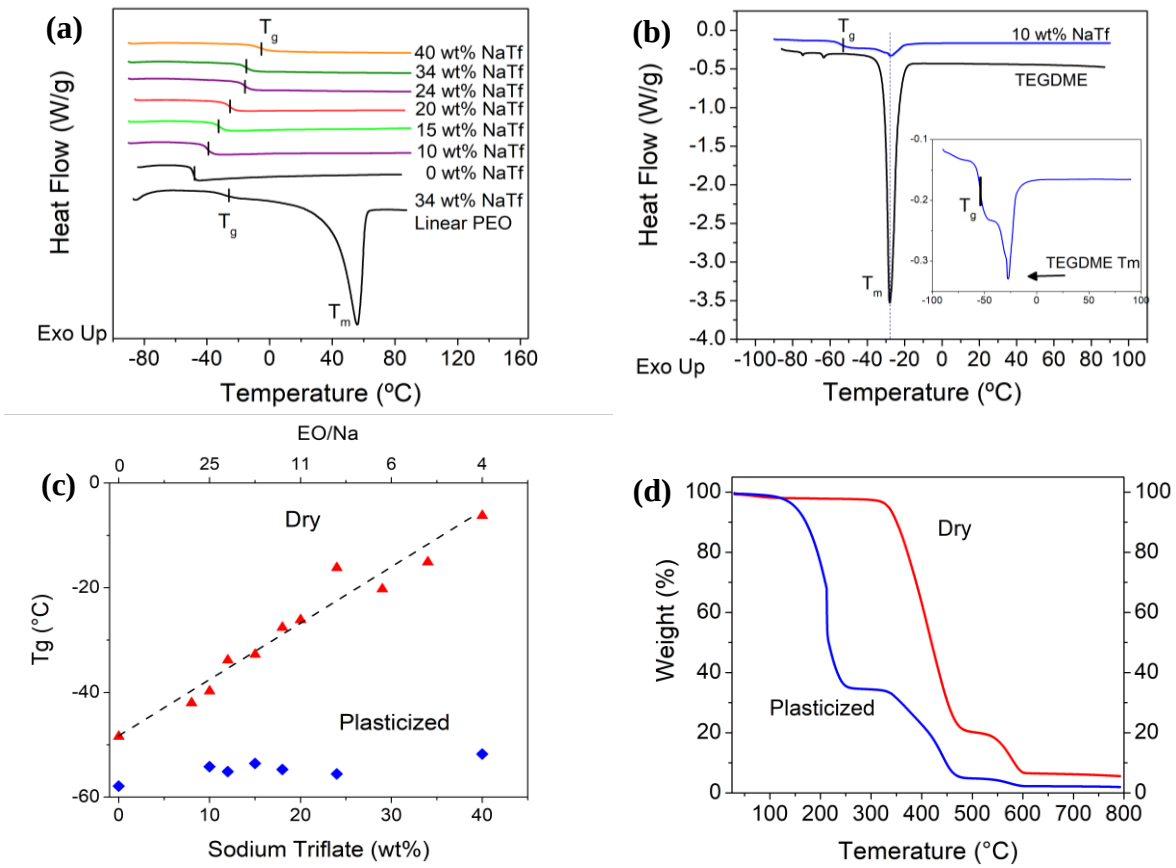

Figure 12. (a) DSC plots for non-plasticized crosslinked and linear PEO. (b) DSC plot for 10 wt% NaTf crosslinked PEO plasticized with TEGDME with pure TEGDME shown as reference, insert: enlarged view of T_g and T_m of plasticized 10 wt% NaTf crosslinked PEO. (c) Effect of NaTf concentration in the membrane on T_g for non-plasticized and plasticized crosslinked membranes. (c) TGA analysis of non-plasticized and plasticized crosslinked PEO.

which indicates suppression of PEO crystallization. In comparison, linear PEO with 34 wt% NaTf shows a T_g at -30 °C and a crystalline melting temperature (T_m) of 56 °C. T_g of the dry crosslinked membranes linearly increases with NaTf concentration from -48 °C at 0 wt% to -6 °C at 40 wt% (Figure 12c). These results are consistent with the report by He et al. for a non-plasticized crosslinked PEO-Lithium bis(trifluoromethanesulfonyl)imide (LiTFSI) electrolyte.[118] The increase in T_g and broadening of the glass transition for dry samples is attributed to ion-dipole interactions between the Na^+ and the ether oxygens on PEG segments.[97, 119] These ion-dipole interactions act as physical crosslinks within the matrix which increases T_g. This conclusion is further supported by the depression of T_g for plasticized samples, which remains fairly constant at ca. -54 °C (Figure 12c), as TEGDME solvates the ions, reducing the ether oxygen-Na^+ interactions. T_g of the plasticized sample containing no salt is slightly lower at -58 °C, indicating that there are some weak interactions between EO and Na^+ in the plasticized membranes that also prevents leaching of the salt during plasticization. As shown in Figure 12b, the melting temperature of TEGDME is -28 °C for both pure TEGDME and TEGDME incorporated into the polymer network. The percent crystallinity of TEGDME is significantly reduced when incorporated into the polymer network. Pure TEGDME is 60% crystalline, and the crystallinity of TEGDME in 1M NaTf-TEGDME is 38%. TEGDME crystallinity is reduced to roughly 8% in the membrane, indicating that Na^+ forms physical crosslinks between TEGDME EO and polymer EO units, preventing TEGMDE from forming a crystalline phase. This conclusion is further supported by the slight increase in T_g for the plasticized sample with the highest salt concentration.

TGA analysis of dry crosslinked PEO shows that the polymer has only a 2% weight loss up to 350 °C, while the plasticized membrane shows TEGDME evaporation occurring at 200 °C, consistent with a report by Carbone et. al who studied the electrochemical and thermal properties of various ether-based/LiTf electrolytes (Figure 12d).[96]

Ionic Conductivity

The ionic conductivity of crosslinked and linear PEO membranes containing up to 40 wt% NaTf were measured over 20 – 70 °C using AC impedance spectroscopy. As shown in Figure 13a, the ionic conductivity of the non-plasticized crosslinked PEO membranes decreases with increasing salt concentration. The slope of log(conductivity) vs. reciprocal temperature shows no significant change, indicating that there is no phase change of the polymer, which is consistent with the DSC measurements. In principle, the ion conduction mechanism in a polymer electrolyte is based on the coupling between ion transport and the segmental relaxation of the polymer chains. Increasing NaTf concentration reduces the polymer segmental motion in the dry samples (indicated by higher T_g shown in Figure 12c), which causes a decline in ionic conductivity. The highest conductivity for the non-plasticized membranes is 6.4×10^{-5} S/cm at 70 °C for the 10 wt% NaTf sample (Figure 13a), which is in agreement with other PEO-based crosslinked

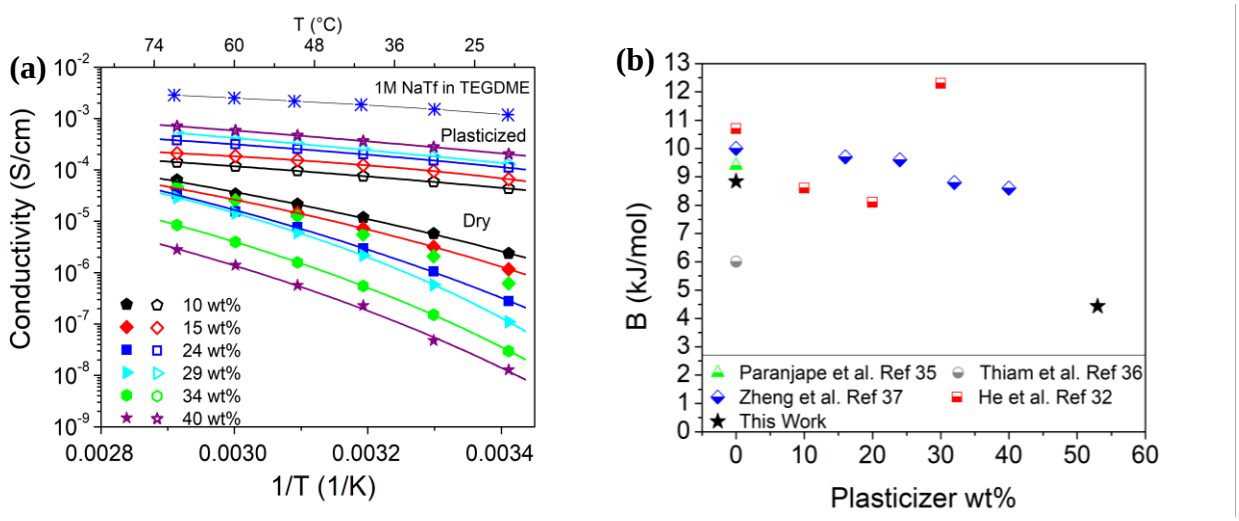

Figure 13. (a) Conductivity as a function of temperature for selected wt% NaTf crosslinked PEO membranes. Lines indicate fit to the VFT model. 1 M NaTf in TEGDME (liquid electrolyte) is included for reference, (b) VFT parameter B of this work compared with previous reports as a function of plasticizer wt%, at a salt concentration of ~12 wt% (EO:M^+ = 20:1, where M = Li or Na).

systems using LiTFSI.[118] Unlike the dry samples, the conductivity of the plasticized films increases with increasing NaTf concentration (Figure 13a), while T_g remains fairly constant (Figure 12c). An increase in conductivity with ion concentration is expected at constant T_g. Overall, plasticization results in a nearly four orders of magnitude increase in ionic conductivity at room temperature for the crosslinked membrane containing 40 wt% NaTf, consistent with conductivity values reported by Kim et al for a PVDF-HFP/TEGDME/NaTf composite system.[120]

As shown in Figure 13a, the ionic conductivity over 20 – 70 °C for these crosslinked PEO-based polymers can be fit well to the Vogel-Fulcher-Tammann (VFT) equation [121]:

$$\sigma = \sigma_0 \exp\left(\frac{-B}{R(T-T_0)}\right) \quad (3)$$

where σ is the conductivity, σ_0 is the pre-exponential factor, and B and T_0 are the VFT parameters. The VFT parameter B for dry membranes (8.8 to 12 kJ/mol) is similar to those for other PEO-based crosslinked systems (6.0 to 10.0 kJ/mol) [109, 122-124]. Parameter B for plasticized membranes is highly dependent upon the wt% of plasticizer within the membrane. A comparison of VFT parameter B versus plasticizer wt% for a fixed salt concentration of ~12 wt% (EO:M = 20:1) can be found in Figure 13b. The VFT parameter B for the plasticized membranes in this work (~ 4 kJ/mol) is lower than other reported values (Figure 13b) and is closer to that of 1M NaTf in TEGDME (1.8 kJ/mol) than that of the dry membranes (~ 9 kJ/mol), an indication that ion conduction is preferentially through TEGDME, and governed by salt-TEGDME interactions in preference to salt-polymer interactions [99].

To determine the impact of crosslinking on conductivity, crosslinked and linear PEO membranes containing various NaTf concentrations were compared. The conductivity of crosslinked and linear PEO with 12 wt% NaTf is shown in Figure 14a as a function of temperature. Linear PEO exhibits a sharp decrease in conductivity at T < 60 °C due to crystallization, whereas the conductivity of the crosslinked membrane shows no significant change in slope over the same temperature range. At 20 °C, the ionic conductivity of the crosslinked membrane is almost an order of magnitude greater than that of linear PEO (1.6×10^{-6} vs. 4.1×10^{-7} S/cm, respectively). As seen in Figure 14b, the conductivity for non-plasticized crosslinked membranes strongly decreases above 10 wt% NaTf concentration, while linear PEO exhibited a maximum conductivity around 20 wt% NaTf. The optimal salt concentration for the highest ionic conductivity shifted from 20 wt% NaTf for linear PEO to 10 wt% NaTf for crosslinked PEO. It should be noted that the conductivity obtained for a given polymer electrolyte depends on many factors such as the polymer segmental dynamics, crystallinity, ion concentration and their dissociation (see discussion of the FTIR data below), as well as the coordination/mobility of charge carriers.[125-127] The conductivity of plasticized crosslinked PEO shows a higher value than

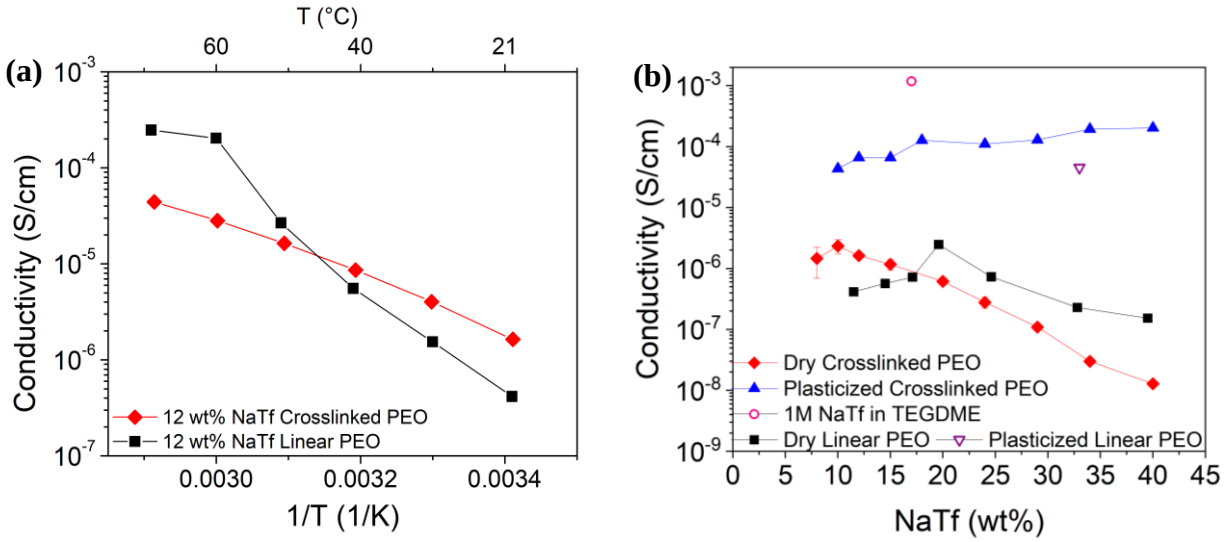

Figure 14. (a) Conductivity of dry 12 wt% NaTf linear PEO and crosslinked PEO from 70 °C to 20 °C, (b) Comparison of conductivity as a function of wt% NaTf at 20 °C for non-plasticized and plasticized crosslinked and linear PEO, and 1 M NaTf in TEGDME.

that of plasticized linear PEO (Figure 14b). To put these membrane conductivity values in perspective, the conductivity of a liquid electrolyte containing 1M NaTf in TEGDME (Figure 13a and Figure 14b) was also measured, which sets the upper limit of the ionic conductivity of the current polymer membrane system. Compared to 1M NaTf in TEGDME, the plasticized crosslinked PEO exhibits only an order of magnitude lower conductivity. Since most polymeric systems typically result in several orders of magnitude lower conductivity than their liquid counterparts, this plasticized crosslinked PEO presents significant promise toward maintaining high ionic conductivity.

Transport Number

The transport number of Na^+ (t_c) was evaluated using both the diffusion coefficients determined by NMR and the Bruce-Vincent method [128, 129] for non-plasticized and plasticized crosslinked PEO membranes given by the following formulas:

Na^+ ion transference number, $t_{c(NMR)}$ from the diffusion coefficient determined by NMR:

$$t_{c(NMR)} = \frac{D^+_{NMR}}{D^+_{NMR} + D^-_{NMR}} \quad (4)$$

where D^+_{NMR} and D^-_{NMR} are the Na^+ cation and Tf^- anion diffusivities, respectively.

Bruce-Vincent:

$$t_{c(BV)} = \frac{I_{ss}(\Delta V - I_0 R_0)}{I_0(\Delta V - I_s R_{ss})} \quad (5)$$

where I_0 and I_{ss} are the initial and steady-state currents (Figure 15a); ΔV is the bias voltage, set as 7.5 mV; R_0 and R_{ss} are the initial and steady-state interfacial resistances, which were obtained by electrochemical impedance spectra at open circuit voltage before and after applying the bias potential (Figures 15b and 15c).

The relaxation times (T_1 and T_2), rotational correlation time (τ_c) and estimated diffusion coefficients (D_{NMR}) for Na^+ cation and Tf^- anion for the crosslinked PEO membranes obtained from NMR are summarized in Table 1. As can be seen from Table 1, the relaxation time is too short to apply pulse field gradient (PFG) NMR to these samples, except for the Tf^- anion in the plasticized sample. Thus, for the plasticized sample, the Tf^- anion diffusion coefficient was determined both from rotational correlation time, τ_c using Equations 1 and 2, and ^{19}F PFG-NMR. PFG-NMR gives a Tf^- anion diffusion coefficient of $D_{PFG} = 9.0 \times 10^{-12}$ m^2/s, which is in reasonable agreement with $D^-_{NMR} = 2.13 \times 10^{-11}$ m^2/s, estimated from τ_c. Thus, it is believed that the diffusion coefficients estimated from τ_c are useful to calculate the Na^+ ion transference numbers ($t_{c(NMR)}$). As seen in Figure 15d, the value obtained by the Bruce-Vincent method at 20

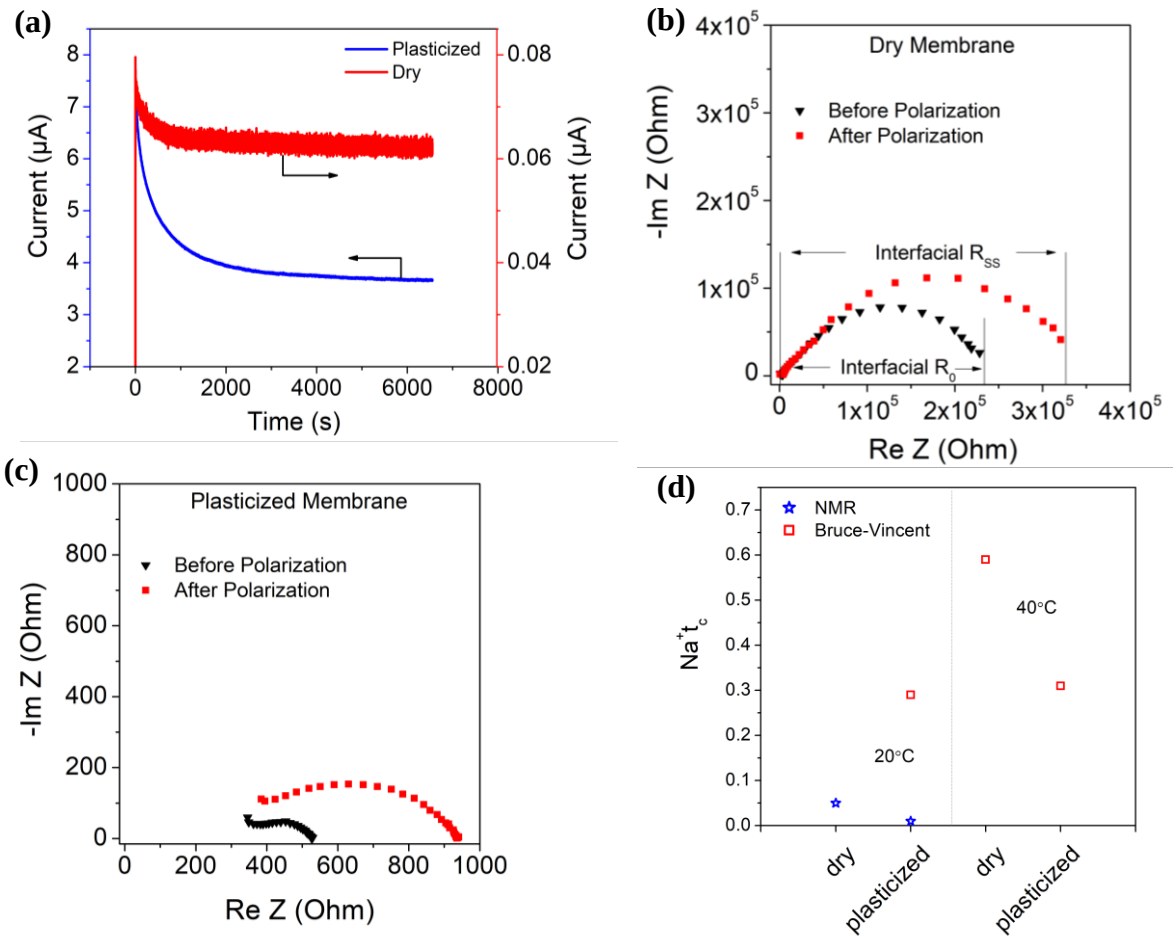

Figure 15. (a) Current decay over time after applying a bias potential of 7.5mV, (b) Electrochemical impedance of non-plasticized crosslinked PEO before and after bias potential is applied, (c) Electrochemical impedance spectroscopy of TEGDME plasticized crosslinked PEO before and after bias potential is applied, (d) Transference number for dry and plasticized crosslinked PEO measured by NMR and Bruce-Vincent methods.

Table 1. Relaxation times (T_1 and T_2), rotational correlation times (τ_c), and diffusion coefficient calculated from τ_c (D_{NMR}) and directly measured by PFG-NMR (D_{PFG}).

	Samples	T_1 (s)	T_2 (s)	τ_c (s)	D_{NMR} (m^2/s)	D_{PFG} (m^2/s)
^{19}F (Tf$^-$)	**Dry**	6.26×10^{-1}	1.46×10^{-3}	9.67×10^{-9}	1.99×10^{-12}	N/A
	Plasticized	6.36×10^{-1}	6.64×10^{-2}	9.05×10^{-9}	2.13×10^{-11}	9.0×10^{-12}
^{23}Na	**Dry**	1.67×10^{-3}	4.78×10^{-6}	2.15×10^{-8}	1.07×10^{-13}	N/A
	Plasticized	4.72×10^{-4}	6.60×10^{-6}	9.67×10^{-9}	2.39×10^{-13}	N/A

°C for the plasticized membrane is higher than that obtained from NMR relaxation time measurements. We attempted to obtain a value for the dry membrane using the Bruce-Vincent method at 20 °C, but due to the high resistance of the membrane, the steady state current was too noisy to obtain a reliable value.

To determine the expected agreement of t_c between the Bruce-Vincent method and NMR relaxation time measurements, an ideality parameter (β) can be applied, given by the formula [130]:

$$\beta = \frac{\sigma RT}{F^2 c\,(D^+_{NMR}+D^-_{NMR})} \qquad (6)$$

where σ is the ionic conductivity, R the gas constant, T is temperature, F is Faraday's constant, c is the bulk molar salt concentration and D^+_{NMR} and D^-_{NMR} are the cation and anion self-diffusivities obtained by NMR. A β value close to 1 indicates that a good agreement is expected for transference numbers obtained from NMR and galvanostatic polarization methods, while a $\beta < 1$ indicates the values are expected to be different. The ideality parameter provides a measure of how much the diffusivities, D^+ and D^-, obtained by NMR relaxation time measurements are due to disassociated ions (β close to 1) or a combination of associated and disassociated ions ($\beta < 1$), which results in a lower self-diffusion value by NMR than that of the charged species diffusivity measured by galvanostatic methods. The calculated β value for the dry membranes is 0.006 and 0.174 for the plasticized membrane (Table 2). This indicates that we should not expect reasonable agreement between the two methods. The t_c value (0.3) of the plasticized membranes measured at 20 °C and 40 °C by the Bruce-Vincent method are in reasonable agreement with those typically reported for linear PEO (t_c, 0.2-0.5).[5, 128, 131] An interesting finding is that t_c decreases upon plasticization (Figure 15d) by both NMR and Bruce-Vincent methods. The higher t_c value for the dry membrane may be due to the crosslinked 3D network restricting triflate anion migration. The decrease in transference number with plasticization indicates that the addition of TEGDME to the polymer matrix changes the mechanism of ion transport. Adding TEGDME provides improved solvation and diffusivity of both ions (confirmed by IR, Figure 16) and decreased T_g of the matrix (Figure 12c)), resulting in an increase in ionic conductivity (Figure 13a), but migration of the larger triflate ion is increased to a greater extent than the cation (Table 1).

FTIR Spectral Analysis of Dry and Plasticized Membranes

Vibrational spectroscopy provides an additional means to understand the effect of NaTf coordination chemistry on T_g and ionic conductivity of the membranes. FTIR spectra were acquired for non-plasticized and plasticized crosslinked membranes at various NaTf concentrations. The vibrational modes of the triflate anion are sensitive to changes in coordination, and the FTIR spectra in Figures 16a and 16b show that the degree of ion association increases with NaTf concentration, as expected. The CF_3 in-plane bending mode, δ_s

Table 2. Values used to calculate Ideality parameter β.

Sample	20°C Ionic Conductivity (S/m)	Molar NaTf Concentration (mol/m^3)	Diffusivity Na^+ (m^2/s)	Diffusivity Tf^- (m^2/s)	Ideality Parameter (β)
Dry	8.13×10^{-5}	1778	1.07×10^{-13}	1.99×10^{-12}	0.006
Plasticized	1.27×10^{-2}	889	2.39×10^{-13}	2.13×10^{-11}	0.174

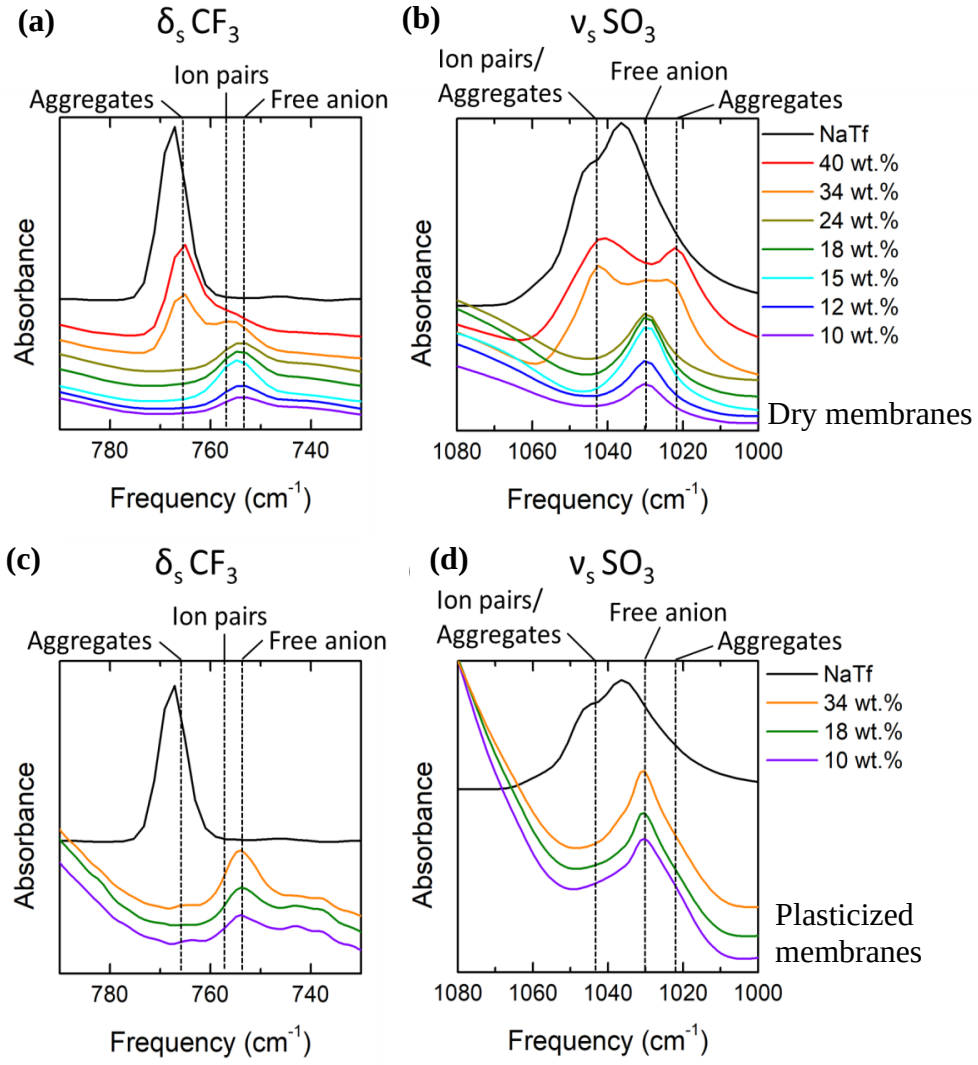

Figure 16. (a-d) FTIR spectra of crosslinked PEO membranes with different wt% NaTf with pure NaTf shown for comparison, (a-b) Non-plasticized and (c-d) TEGDME plasticized, (a,c) Region for CF_3 in-plane bend ($\delta_s CF_3$), (b,d) Region for SO_3 symmetric stretch.

CF_3, occurs near 753 cm^{-1} for the free anion, 757 cm^{-1} for the ion pair, and 761 cm^{-1} for the triple ion $[Na_2Tf]^+$. δ_s CF_3 shifts to higher frequencies ≥ 764 cm^{-1} for more highly associated aggregate species [132, 133]. Up to 24 wt% NaTf, the triflate anion appears to exist primarily as the free anion or as ion pairs with weak interactions in the non-plasticized membranes [134]. At higher triflate concentrations, the appearance of a strong band at 767 cm^{-1} is clear evidence for the formation of aggregates. These trends are further confirmed by analysis of the SO_3 asymmetric stretch, ν_s SO_3. The band at 1030 cm^{-1} is assigned to free triflate anions. The band around 1042 cm^{-1} is attributed to triflate anions with higher degrees of cation association and may consist of overlapping contributions from ion pairs, triple ions, and aggregates [134-136]. The band at 1022 cm^{-1} is attributed to aggregate triflate species [135]. Differences in the free ion concentration within the polymer matrix are one contributing factor to the ionic conductivity of the membranes [137]. The addition of TEGDME to the crosslinked membrane results in a shift of δ_s CF_3 and ν_s SO_3 to 753 cm^{-1} and 1030 cm^{-1}, respectively for the 34 wt% NaTf sample. The shift in δ_s CF_3 and ν_s SO_3 to a lower frequency indicates the presence of free anions (Figures 16c and 16d). The disappearance of ν_s SO_3 bands at 1042 cm^{-1} and 1022 cm^{-1} for the 34 wt% NaTf sample is a clear indication that NaTf preferentially interacts with TEGDME over the polymer chains. The preferential solvation of NaTf by TEGDME is reflected in the almost constant T_g and provides an additional explanation for the significant increase in ionic conductivity of the plasticized membranes.

Mechanical Comparison of Membranes

Plasticization significantly improves the conductivity of crosslinked and linear PEO, but the plasticized membrane must also exhibit high mechanical stability to be useful in practical devices. Mechanical properties of the non-plasticized and plasticized membranes were evaluated using DMA and rheology, respectively (Figures 17a and b). Due to the very weak mechanical properties of linear PEO at $T > T_m$ (56 °C), a rheometer was used to accurately measure the modulus of plasticized membranes. Linear PEO exhibited a fairly high modulus at $T < T_m$, but showed a significant decrease in the storage modulus once above 56 °C for both non-plasticized and plasticized samples. The low modulus of linear PEO above 56 °C does not provide a stable membrane, preventing its use at operating temperatures above T_m. The presence of a crystalline phase in linear PEO provides a fairly high modulus at low temperatures, but it also inhibits ionic conductivity. The crosslinked membranes show excellent mechanical properties with no significant change in the modulus over the temperature range measured. The modulus for the plasticized crosslinked membrane is maintained at ~1 MPa in the temperature range of -20 – 180 °C, which is a reasonable modulus for a gel polymer electrolyte and sufficiently high to be easily handled. Furthermore, the modulus ~1 MPa is a tenfold increase from previous reports of plasticized crosslinked membranes.[100, 124, 138] The stress-strain curve for dry and plasticized membranes is shown in Figure 17c. The tensile strength of the membranes is 0.924 ± 0.03 MPa and 0.521 ± 0.07 MPa for dry and plasticized membranes, respectively (Table 3), consistent

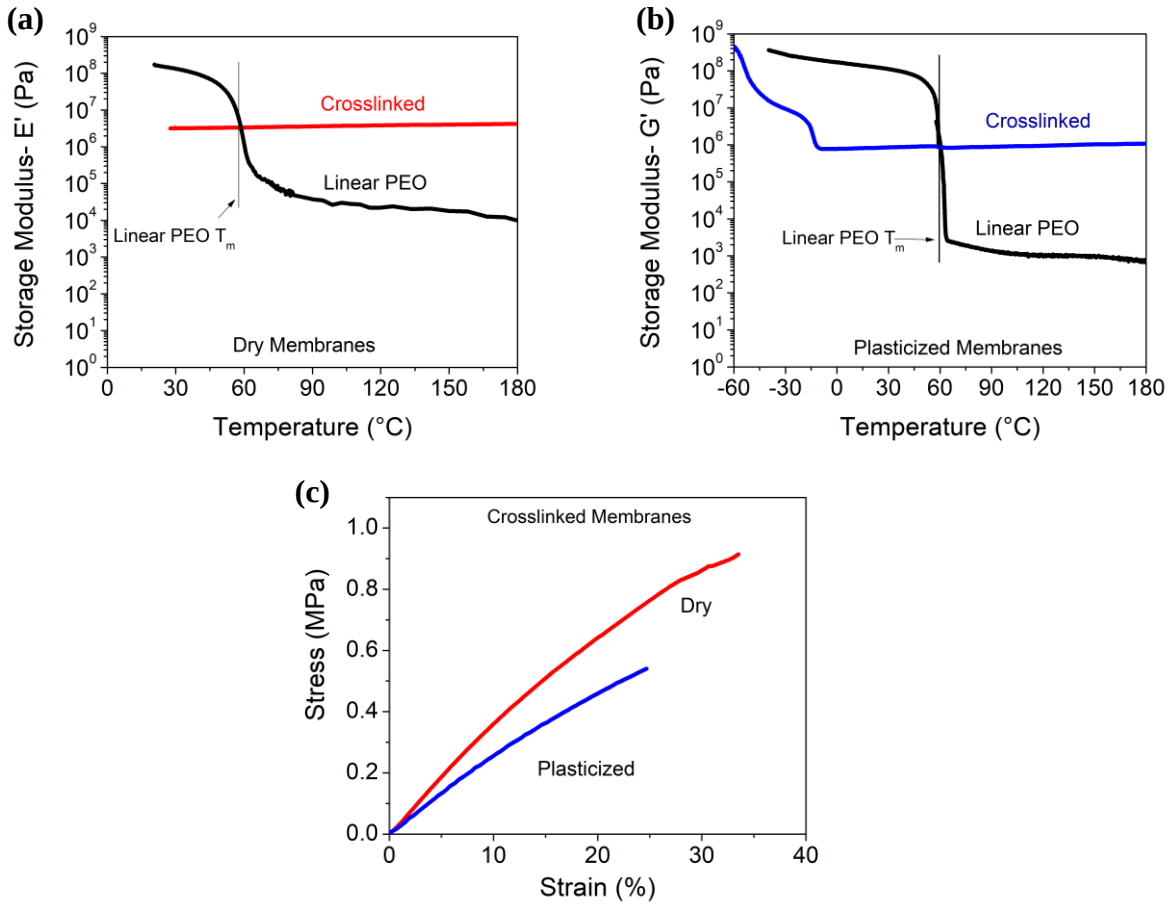

Figure 17. Mechanical analysis of crosslinked PEO and linear PEO, (a) DMA of non-plasticized membrane, (b) Rheology of TEGDME plasticized membrane and (c) Stress-strain curve of non-plasticized and plasticized crosslinked PEO membranes at 21 °C.

Table 3. Mechanical Properties of Dry and Plasticized 18 wt% NaTf crosslinked PEO membrane at 21 °C

Sample	Youngs Modulus (MPa)	Tensile Strength (MPa)	Elongation at Break (%)
Dry	3.41 ± 0.25	0.924 ± 0.03	33.0 ± 2.5
Plasticized	2.32 ± 0.16	0.521 ± 0.07	24.3 ± 4.3

with other crosslinked polymer electrolytes.[118, 139] The high degree of crosslinking enables good tensile strength while maintaining reasonable ductility, resulting in a Youngs Modulus of 3.41 ± 0.25MPa and 2.32 ± 0.16 MPa for non-plasticized membranes and plasticized membranes respectively (Table 3). Many prior works on PEO-based crosslinked gel polymer electrolytes did not report the mechanical properties of their membranes,[109, 111, 118, 122, 140, 141] possibly due to the inherently weak nature of gel polymer electrolytes. The mechanical stability and excellent conductivity over a wide temperature range combined with the thermal and electrochemical stability of TEGDME provides a path for a highly conductive membrane that is useful for a variety of battery applications.

Conclusions

A robust crosslinked PEO-based membrane has been developed that demonstrates high ionic conductivity and mechanical stability. The crosslinked films were prepared via a single step synthesis of an amine and epoxide-terminated PEO-based precursors with varied NaTf concentrations. T_g of the dry membranes increased with NaTf concentration due to ionic crosslinking between the salt and polymer chains, and this was reflected in a strong decrease in conductivity with increasing salt concentration. Plasticization of the membranes with TEGDME significantly reduced ionic crosslinking within the polymer matrix due to ion solvation, and this correlated with a much lower T_g that is essentially independent of salt concentration. The addition of TEGDME increased the ionic conductivity of the membranes by 4 orders of magnitude to 2×10^{-4} S/cm at 20 °C, just slightly lower than that of a TEGDME-based liquid electrolyte (1×10^{-3} S/cm). The membranes are sufficiently robust to resist short-circuit by sodium dendrites over the course of 180 hours when cycled in a Na metal symmetric cell, and have a Na^+ transference number of 0.58 in the dry membranes and 0.31 in plasticized membranes at 40°C. In addition, the mechanical properties of the crosslinked membrane were maintained with the addition of plasticizer. The membranes were stable over a wide temperature range with a constant storage modulus of ~1 MPa from -20 °C to 180 °C. The excellent mechanical stability of the crosslinked PEO-based membrane combined with the electrochemical and thermal stability of TEGDME provides a highly conductive gel polymer electrolyte suitable for a variety of Na-based electrochemical energy storage applications.

CHAPTER III
Improving Cation Transport in Salt-in-Polymer Electrolytes

A version of this chapter was published by Michelle L. Lehmann, Guang Yang, Jagjit Nanda, and Tomonori Saito. “Well-designed Crosslinked Polymer Electrolyte Enables High Ionic Conductivity and Enhanced Salt Solvation” *Journal of the Electrochemical Society*. 2020, 167, 070539.

Michelle Lehmann fabricated the membranes, performed experiments, and wrote the manuscript under the guidance of Tomonori Saito. Guang Yang assisted in experimental design, performed FTIR and battery measurements under the guidance of Jagjit Nanda.

Abstract

A new facile single-step method to fabricate crosslinked polymer electrolyte membranes consisting of branched poly(ethyleneimine), (PEI) and poly(ethylene oxide), (PEO) is demonstrated. The membranes exhibit excellent ionic conductivity (1.2×10^{-3} S/cm at 80 °C) with minimal addition of plasticizer (20 wt%). The amine functional group in the PEI-PEO crosslinked matrix provides Lewis basic and hydrogen bonding characteristics that facilitate the dissolution of lithium salt and enables a higher cation transport number than a PEO crosslinked matrix. The glass transition temperature, degree of crystallinity, and room temperature storage modulus increases with decreasing crosslink density and increasing ratio of free amines. The resultant ionic conductivity and mechanical strength can be flexibly tailored by varying the molar ratio of free amine moieties in the crosslinked PEI-PEO matrix. This study provides an improved synthesis method, in-depth characterization, and fundamental insights on the effect of free amine moieties on the transport properties of a highly conductive gel polymer electrolyte.

Introduction

Polymer electrolytes have applications in solid-state Li-ion[100, 101, 138, 140, 142] and Na-ion[23, 109, 126] secondary batteries, as well as medium to large scale energy storage such as flow batteries. Poly(ethylene oxide) (PEO) is one of the most widely studied polymers for use as a polymer electrolyte,[18-20, 24] but generally exhibits low room temperature ionic conductivities of 10^{-7} – 10^{-6} S/cm[21-24] due to the formation of a crystalline phase at ~60 °C. In contrast, relatively few reports exist on the study of poly(ethyleneimine) (PEI) as a polymer electrolyte. Linear PEI is a highly crystalline material and exhibits a lower room temperature ionic conductivity (10^{-8} S/cm) than PEO.[143, 144] On the other hand, branched PEI is an amorphous, viscous liquid at room temperature due to the highly disordered hyperbranched structure and exhibits conductivity values similar to that of PEO.[145] In addition, hyperbranched structures have been shown to improve the cation transport of PEO-based polymer electrolytes when incorporated into the polymer matrix.[146, 147]

The vast majority of studies with PEI have focused on a blend of PEI with various polymers, including blends of PEI with poly(vinyl acetate),[148, 149] sulfonated polyetheretherketone,[150] PEO,[151, 152] and polyvinyl pyrrolidone.[153] In particular, the blend of linear PEI with PEO improved the room temperature ionic conductivity of PEO due to the reduction of PEO crystallization.[151, 152] A blend of PEI with poly(vinyl pyrrolidone) also demonstrated enhanced performance of a Li-sulfur battery when used as a binder for the anode.[153] The fabrication of crosslinked membranes containing both PEI and PEO has been reported previously by Zhou et al.[154] The crosslinked membrane demonstrated excellent ionic conductivity (400% plasticizer uptake) and inhibition of lithium polysulfide shuttling, though the fabrication method yielded yellowed membranes indicative of oxidation of the amine functional groups.[155, 156]

While solid-state polymer electrolytes offer a safer alternative to liquid electrolytes for lithium-ion batteries,[95] the low ionic conductivity of dry polymer electrolytes typically limits their practical application. The addition of a small molecule plasticizer significantly increases ionic conductivity, but adversely weakens the mechanical properties of polymers. Crosslinking is a promising strategy for improving the mechanical strength of a gel polymer electrolyte, in addition to reducing PEO crystallization and providing high-temperature dimensional stability.[100, 105-108, 157, 158]

In this chapter, an improved synthesis method and in-depth characterization of a novel crosslinked polymer system consisting of branched PEI and linear PEO is presented. Due to the hyperbranched structure, H-bonding and electrostatic interactions of PEI, the PEI-PEO crosslinked membranes demonstrate unique features such as improved salt solvation and lithium ion transport over the linear PEO system of our previous work.[74] The PEI-PEO crosslinked polymer electrolyte system is evaluated for use in a Li metal battery, and the effect of free amine moieties on ion transport and mechanical properties are unraveled. Furthermore, the design and elucidated structure-property relationships indicate many potential applications for composite systems.

Experimental

Materials

The crosslinked PEI-based membranes consist of the following polymer precursors: (i) Poly(ethylene glycol) diglycidyl ether (PEGDGE, Sigma Aldrich, M_n = 500 and 2000 g/mol) and (ii) Branched poly(ethyleneimine) (PEI, Sigma Aldrich, M_n = 600 g/mol). Bis(trifluoromethane)sulfonimide lithium salt (LiTFSI, 99.95%, Sigma Aldrich) was the salt in all membranes and isopropanol (IPA, 99.9%, Sigma Aldrich) was used to cast the membranes. LiTFSI was dried at 90 °C for 16 h and tetraethyleneglycol dimethyl ether (TEGDME, ≥99%, Sigma Aldrich) was dried over molecular sieves and stored under an inert atmosphere.

Membrane Synthesis

The membranes were prepared by varying the molar ratio of amines in PEI (M_n = 600 g/mol) to epoxides in PEGDGE. Two molecular weights of PEGDGE were used, M_n = 500 g/mol and M_n = 2000 g/mol, as an additional method to control the resulting crosslink density. The molar ratio of amine:epoxide () was 1:1, 2:1 and 4:1 for the 2000 g/mol PEGDGE (i.e. described as 1:1 2000) and 1:1 for 500 g/mol PEGDGE (1:1 500). The ratio of LiTFSI was fixed to the number of ethylene oxide (EO) units in PEGDGE to be EO:Li = 12:1. The desired molar ratio of PEI and PEGDGE were dissolved in 0.5 ml deionized water before LiTFSI and IPA were added. The resulting solution was mixed with a magnetic stir bar for 30 min, cast into a Teflon® dish and cured at 85 °C for 2 h. One reference sample was prepared from Jeffamine-ED® 900 (Huntsman, M_n= 900 g/mol) and PEGDGE 2000 using the same EO:Li ratio and procedure as above. All membranes were dried under vacuum for 48 h at 50 °C, then transferred to an argon-filled glove box. Plasticized membranes were prepared in a glove box by adding the desired mass ratio of 1M LiTFSI in TEGDME to the membrane, and equilibrated for 24 h.

Electrochemical Characterizations

Samples for electrochemical characterizations were prepared in an argon-filled glovebox and measurements taken using a Biologic (VMP3) potentiostat. For electrochemical impedance spectroscopy (EIS) measurements, samples were sandwiched between Li foil and stainless-steel blocking electrodes then sealed with heat shrink tubing. Samples were cycled between 20 – 80 °C three times, and the impedance measured over the frequency range of 1 MHz - 1 Hz using a 6 mV AC signal. The Li^+ transport number was measured at 40 °C with an applied DC potential of 7.5 mV, and the current monitored over time. EIS measurements were taken at open-circuit voltage just before applying the bias potential and after the current reached steady-state. The electrochemical stability window was determined by linear sweep voltammetry (LSV) between open-circuit voltage and 6 V (vs. Li^+/Li) using lithium foil as the counter and reference electrodes and a stainless-steel working electrode at a scan rate of 10 mV/s.

For full cell characterization, cathode slurries were prepared by mixing lithium iron phosphate (LFP) powder ($LiFePO_4$, Hydro-Québec), Super P carbon black, and poly(vinylidene fluoride) (PVDF) (65/20/15 weight ratio) in N-methyl-2-pyrrolidone (NMP). The slurry was cast with a doctor blade onto a carbon-coated Al foil current collector and dried overnight under vacuum before preparing the electrochemical cells. The final active material ($LiFePO_4$) loading is estimated to be 1.4 mg/cm^2. For the full cell test, a coin cell configuration (CR2032) composed of an LFP cathode, a PEI-PEO crosslinked membrane (plasticized with 20wt% TEGDME), and a lithium foil anode was used. All full cell tests were performed at 75 °C.

Thermal Characterizations

The glass transition temperature (T_g) and melting temperature (T_m) of the membranes were determined using differential scanning calorimetry (DSC, TA instruments Q2000). The samples were cycled from -90 to 90 °C at a rate of 10 °C/min for 2 cycles, with T_g and T_m recorded from the second heating cycle. The thermal stability of the membranes was determined by thermal gravimetric analysis (TGA, TA Instruments Q50). The samples were heated from 25 °C to 600 °C under nitrogen at a rate of 10 °C/min, with the thermal decomposition temperature (T_d) measured at 5% mass loss.

Mechanical Analysis

The storage modulus of the membranes was determined by dynamic mechanical analysis (DMA) at an operating frequency of 1 Hz using a TA Instruments Q800 DMA. The samples were heated from -60 °C to 200 °C at a rate of 10 °C/min under nitrogen. One plasticized sample was measured over the temperature range of 10 °C to 90 °C with a heating rate of 10 °C/min. For tensile measurements, the membranes were elongated at a rate of 1 mm/min under ambient conditions until break using an Instron 3343 universal tensile meter. Reported tensile properties are an average of at least 3 samples.

Fourier Transform Infrared Spectroscopy (FTIR)

FTIR measurements were performed using a Fourier Transform Infrared Spectrometer (Bruker, ALPHA) with a diamond attenuated total reflection (ATR) accessory. The FTIR measurements were performed in an argon-filled glove box.

Results and Discussion

Membrane Synthesis

The crosslinked membranes were synthesized via a single-step procedure using branched PEI and epoxy terminated PEO (Figure18a and b). The crosslink density was varied by adjusting the PEO crosslinker molecular weight and the molar ratio of PEO epoxy groups to amine NH groups. The ratio of amine:epoxide ( : ) was 1:1, 2:1 and 4:1 for the 2000 g/mol PEO (i.e. described as 1:1 2000) and 1:1 for 500 g/mol PEO (1:1 500) with a fixed ethylene oxide to lithium ratio of 12. A small amount of water was used for the dissolution of the PEO 2000 and IPA was used to cast the membranes into a Teflon® evaporation dish. The resulting membranes are flexible and elastic, ranging from clear to opaque as the number of free amines increases (Figure 18c). Free amines are defined here as any remaining -NH and -NH_2 groups in the crosslinked network. The primary amines are anticipated to react first, followed by the secondary amines. The presence of a single broad peak at 3370 cm^{-1} in the FTIR spectra of the 4:1 2000 membrane confirms that the majority of the NH_2 functional groups have reacted (Figure 19).

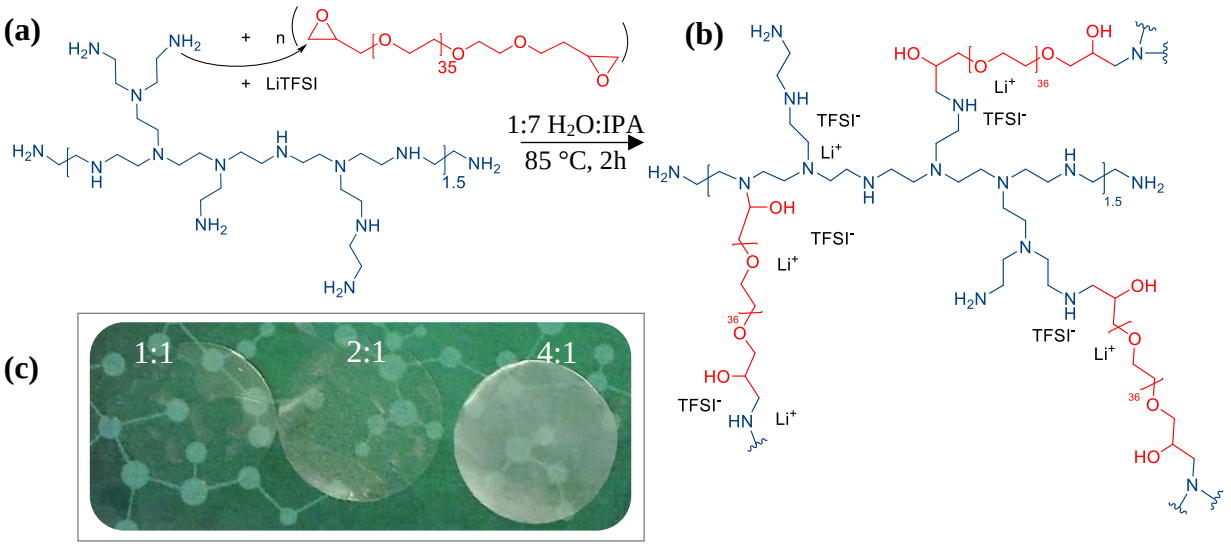

Figure 18. (a) Reaction scheme for PEI and PEGDGE 2000, where n represents various ratios of PEGDGE used. (b) Schematic of the crosslinked network for 4:1 2000 membrane. (c) Membrane images for each PEI-PEO 2000 ratio.

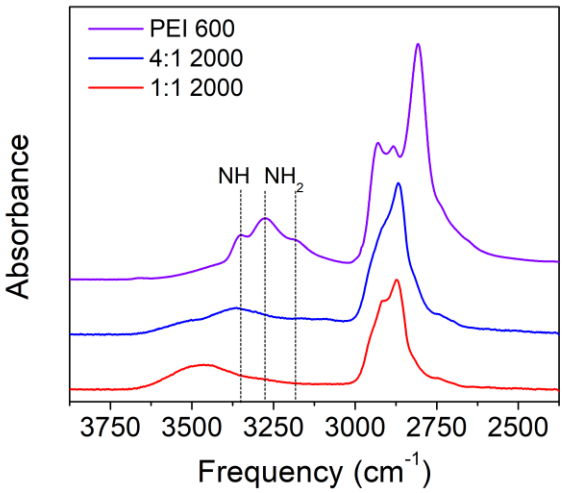

Figure 19. FTIR spectra in the region of the O-H and N-H stretching vibrations.

Membranes with excess NH groups (the 2:1 and 4:1 2000 samples) are expected to have a significant amount of H-bonding and electrostatic interactions. The presence of H-bonding can be beneficial for increasing the interfacial contact between the polymer and other components to create a strong interface at the molecular level,[159, 160] as well as improving mechanical properties.[161, 162] The band centered at 3470 cm^{-1} for the 1:1 2000 membrane is indicative of O-H stretching vibrations formed during the ring opening of the epoxide on PEGDGE and shows little indication of N-H stretching observed in the 4:1 sample and pure PEI. The broad peak centered at 3370 cm^{-1} with an upfield shoulder for the 4:1 membrane is likely due to the over lapping of the OH and NH stretching vibrations[154, 163, 164]. The 4:1 sample shows little indication of the doublet at 3260 cm^{-1} and 3180 cm^{-1} that is attributed to the presence of NH_2 functional groups[145].

Conductivity and Transport Number

The structure and composition of the PEI-PEO membranes significantly influences their ionic conductivity performance (Figure 20a). The conductivity of the dry 1:1 2000 sample is almost 2 orders of magnitude higher than that of the 1:1 500 sample (8.9×10^{-6} S/cm and 2.4×10^{-7} S/cm, respectively at 30 °C). The theoretical crosslink density of the 1:1 500 membrane is ~4 times higher than the 1:1 2000 sample due to the polymer length between crosslinks being ~4 times smaller. The higher crosslink density of 1:1 500 membrane results in a 30 °C higher glass transition temperature (T_g), (Table 4). For polymer electrolytes, ionic conductivity is typically coupled to polymer segmental motion. Thus, a polymer electrolyte with a low T_g is desirable for achieving higher conductivity. Due to the improved conductivity of the 2000 g/mol PEO samples, this series was selected for further characterizations. For the 1:1 and 2:1 2000 membranes, the ionic conductivity increases with decreasing crosslink density (8.9×10^{-6} S/cm and 2.7×10^{-5} S/cm, respectively at 30 °C) as expected for crosslinked membranes. The ionic conductivity for the 4:1 2000 membrane decreases slightly from the 2:1 2000 membrane (1.8×10^{-5} S/cm from 2.7×10^{-5} S/cm, respectively at 30 °C), likely due to a combination of a higher T_g, the presence of a crystalline phase and abundant H-bonding. Interestingly, a sharp increase in conductivity is not observed for the 4:1 2000 sample above T_m, as observed for other PEO-based polymer electrolytes.[97, 102, 129] With the addition of 20 wt% plasticizer (1M LiTFSI in TEGDME), ionic conductivity increases over an order of magnitude from 8.9×10^{-6} S/cm to 1.7×10^{-4} S/cm at 30 °C for the 1:1 2000 sample (Figure 20a). The slightly higher conductivity of the plasticized 1:1 2000 sample over the 2:1 and 4:1 2000 samples (1.7×10^{-4} S/cm, 1.4×10^{-4} S/cm, and 9.8×10^{-5} S/cm respectively at 30 °C) is likely due to the sample having a higher salt content due to the greater number of EO repeat units in the sample (Table 5).

The ionic conductivity data was fit to the Vogel-Fulcher-Tammann (VFT) equation,[121] which describes the viscous behavior of polymers and can be related to ionic conductivity through equation 3. The dry membranes exhibit a VFT activation energy (parameter *B*) (4.3-5.4 kJ/mol)

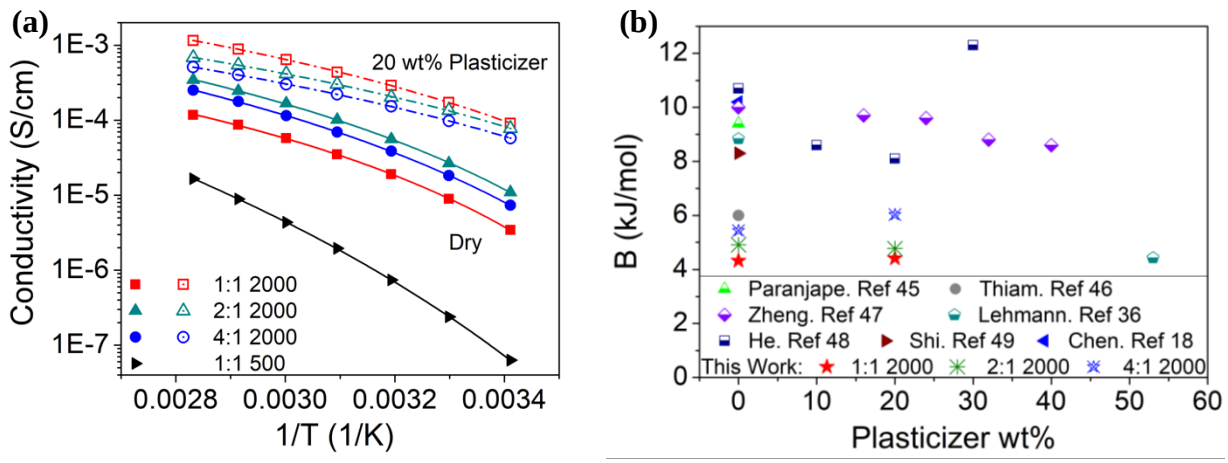

Figure 20. (a) Ionic conductivity as a function of PEI-PEO ratio, with PEO molecular weights of 2000 g/mol and 500 g/mol. Ionic conductivities are presented as dry and with 20 wt% 1M LiTFSI in TEGDME. (b) VFT parameter B for PEO-based polymer electrolytes as a function of plasticizer loading.

Table 4. Electrochemical and thermal properties of dry membranes and thermal properties of plasticized membranes.

Sample	Dry		Dry				Plasticized		
	t_+	σ (40 °C) (S/cm)	T_g (°C)	T_m (°C)	% Crystallinity	T_d^* (°C)	T_g (°C)	T_m (°C)	% Crystallinity
PEI 600	0.76	1.5×10^{-6}	-65	--	--	222	Not measured		
PEO 2000	N/A	N/A	-61	52	84	350	Not measured		
1:1 500	0.54	7.6×10^{-7}	-12	--	--	317	-31	--	--
1:1 2000	0.55	1.9×10^{-5}	-42	--	--	338	-55	--	--
2:1 2000	0.55	5.6×10^{-5}	-43	19	5	314	-58	11	6
4:1 2000	0.76	3.9×10^{-5}	-33	32	20	320	-59	19	13

Table 5. Mass fractions of PEI and LiTFSI salt in the dry PEI-PEO membranes.

Sample	Mass Fraction PEI	Mass Fraction LiTFSI
1:1 500 dry	0.15	0.27
1:1 2000 dry	0.04	0.33
1:2 2000 dry	0.08	0.32
1:4 2000 dry	0.15	0.30

that is lower than values reported for other PEO-based crosslinked membranes (6.0 to 10.0 kJ/mol)[118, 122-124, 165], including a hyperbranched PEO-based network polymer[146] (Figure 20b). The VFT activation energy of the dry membranes is similar to that of a TEGDME plasticized crosslinked PEO system from our previous work.[74] For the PEI-PEO membranes, there is no significant change in VFT parameter B (4.4-6.0 kJ/mol) upon plasticization, suggesting that there is little change in the coordination chemistry of the salt within the polymer matrix (see FTIR discussion below).

The effect of the PEI moiety on the cation transport number was investigated using the Bruce-Vincent polarization method (Equation 5).[128] R_0 and R_{ss}, the initial and steady-state interfacial resistances, obtained from EIS measurements at open-circuit voltage before and after polarization, are shown Figures 21a and b. I_0 and I_{ss}, the initial and steady-state current are shown in Figure 21c. The cation transport number was found to be higher than typical PEO-based polymer electrolytes (0.2-0.5),[5, 6] with values of 0.55 for the 1:1 and 2:1 2000 samples, and 0.76 for the 4:1 2000 sample (Table 4). To the best of our knowledge, this is the first time that the transport number has been reported for a PEI based polymer electrolyte. The increase in Li^+ transport number for the 4:1 2000 membrane is likely due to several factors, including H-bonding between the anion and amine, and the lone pair on the nitrogen heteroatom facilitating lithium ion transport. Several spectroscopy studies with PEI have reported interactions between the lithium ion, triflate anion and amine ($Li^+ \cdots :N\text{-}H \cdots {}^-SO_3CF_3$) that could decrease the anion transport number.[145, 163, 164] Molecular dynamics simulations suggest that the lone pair on the nitrogen atom can interfere with anion transport and facilitate lithium ion transport in a similar PEI-PEO crosslinked system.[154]

Thermal and Mechanical Properties

T_g of the 1:1 and 2:1 2000 membranes are relatively constant at ~-43 °C, while the 4:1 2000 membrane exhibits a 10 °C increase in T_g (Figure 22a). T_g is generally expected to decrease with decreasing crosslink density, as observed for other crosslinked systems.[166] An increase in T_g for the 4:1 2000 sample is due to abundant intermolecular electrostatic interactions and H-bonding between the amine groups in PEI and the oxygen atom in PEO.[118] The increased crosslinking density in the 1:1 500 sample exhibits a T_g 30 °C higher than that of the 1:1 2000 sample (Table 4). A PEO crystalline melting point (T_m) is observed for the 2:1 and 4:1 2000 samples at 11 °C and 32 °C, respectively, though the PEO T_m and percent crystallinity is significantly reduced from that of pure PEO 2000 (52 °C and 84%), (Figure 22a and Table 4). The decrease in PEO crystallinity is attributed to the restriction of PEO chain mobility through crosslinking,[74, 118] and H-bonding between the amine and ether oxygen.[151, 152] Once plasticized, T_g decreases and remains relatively constant for all the 2000 series membranes, consistent with previous studies of crosslinked PEO-based membranes.[74] A decrease in T_g with plasticization is partially attributed to the solvation of the ions by TEGDME, decreasing the ion-dipole interactions between Li^+ and

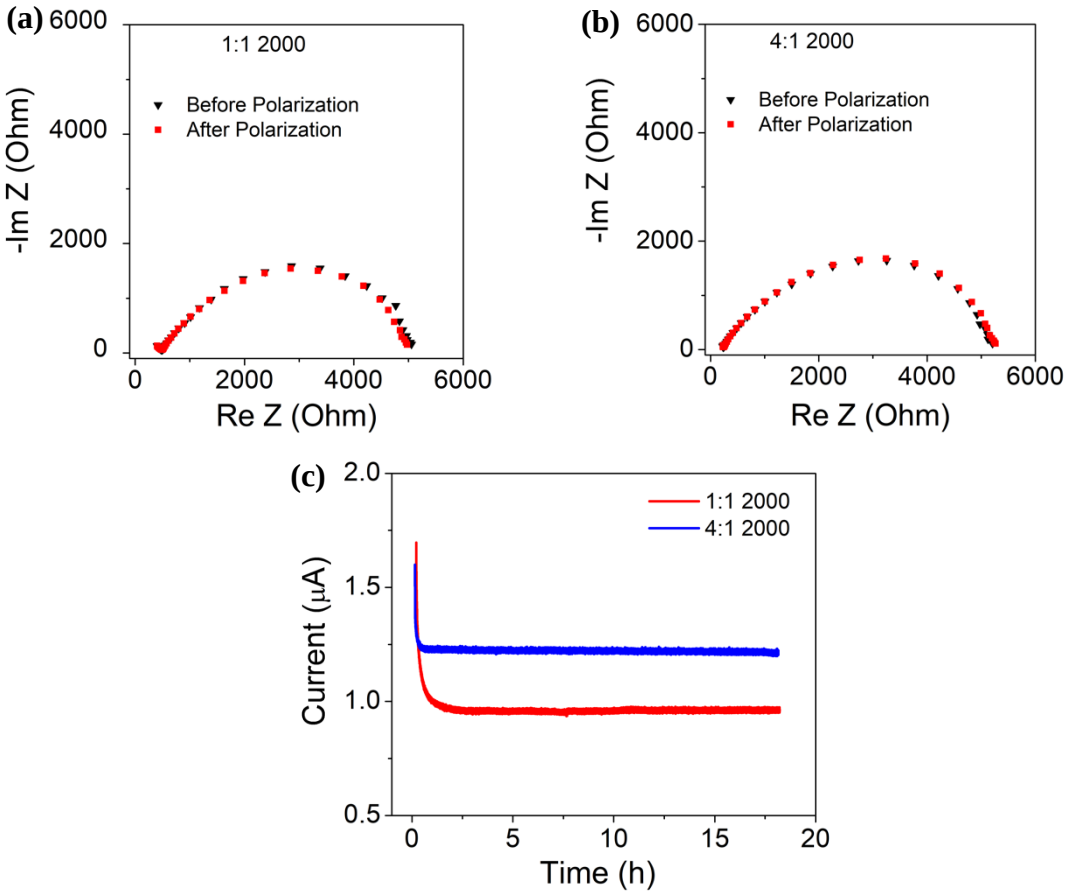

Figure 21. (a) EIS of the 1:1 2000 membrane. (b) EIS of the 4:1 2000 membrane. (c) Current profile after the bias potential (7.5mV) was applied for the 1:1 2000 and 4:1 2000 membranes.

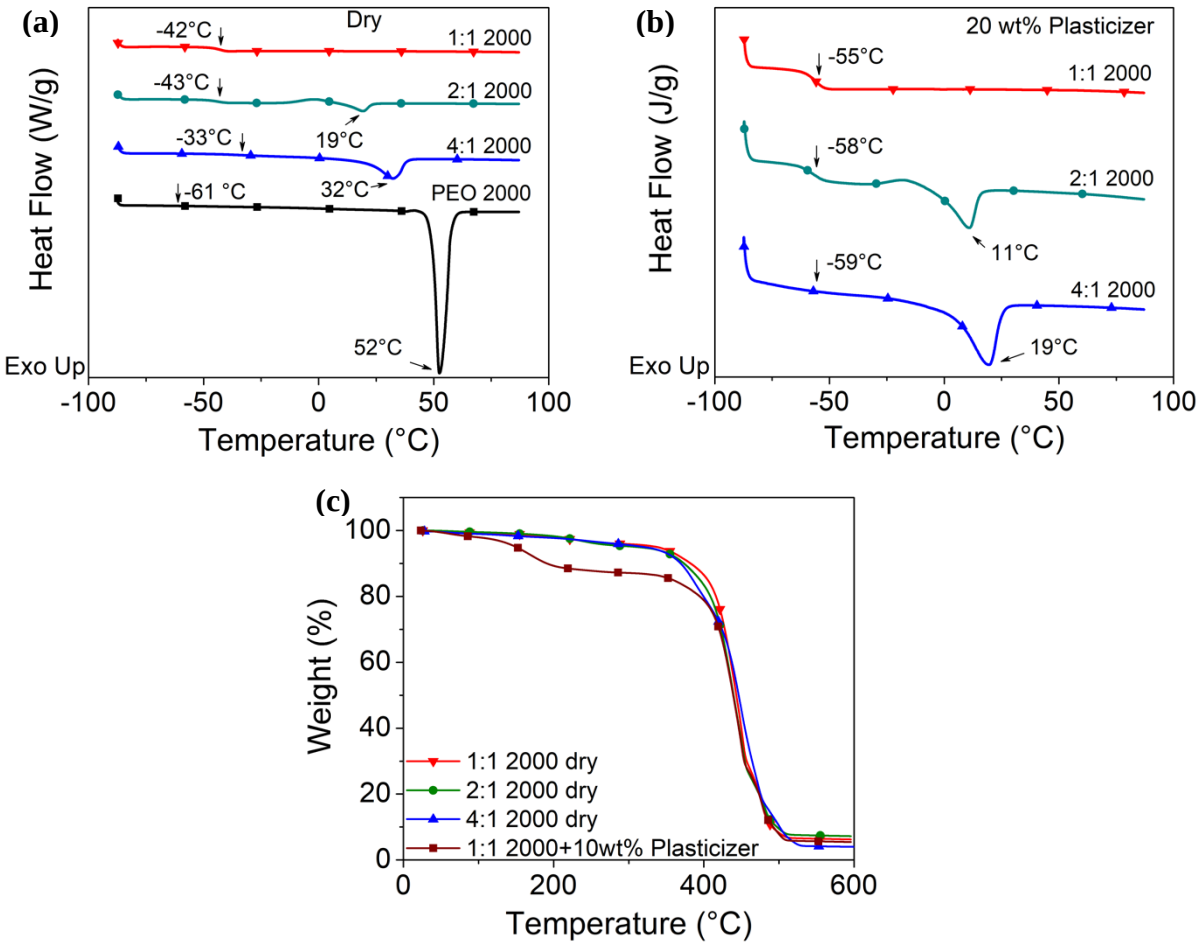

Figure 22. DSC traces for a) dry PEI-PEO 2000 membranes and PEO 2000. b) Plasticized (1M LiTFSI in TEGDME) PEI-PEO 2000 membranes. c) TGA of 2000 series membranes.

the polymer matrix, allowing for greater polymer segmental motion. The degree of crystallinity remains constant or decreases upon plasticization (Table 4), while T_m of the plasticized membranes lowers to below room temperature (Figure 22b). TGA analysis shows that the decomposition temperature (T_d) of the membranes roughly decreases with increasing mass fraction of PEI (Table 5). The 1:1 2000 membrane contains the lowest mass fraction of PEI with a T_d occurring at 338 °C, while the 1:1 500 and 4:1 2000 membranes have the highest mass fraction of PEI with T_d occurring at 317 °C and 320 °C, respectively (Table 4). TEGDME evaporation is observed for the plasticized membrane at approximately 150 °C, well below its boiling point of 275 °C, consistent with a report by Carbone et al.[96]

The effect of the composition and chemistry of the membranes on their mechanical properties was evaluated by tensile measurements and DMA, as shown in Figure 23 and Table 6. The membranes maintain their mechanical properties over a wide temperature range with a rubbery plateau modulus of 0.6, 0.7, and 0.5 MPa for the 1:1, 2:1, and 4:1 2000 membranes, respectively (Figure 23a), typical values for rubbery polymers.[167] The higher room temperature storage modulus of the 4:1 2000 membrane is due to the presence of a crystalline phase and significant H-bonding that provides increased mechanical strength until 65 °C. The tensile properties of the dry 1:1 2000 membrane exhibit an excellent combination of ultimate tensile strength and elongation, at 1.34 MPa and 90%, respectively (Figure 23b). With decreasing crosslink density, the tensile strength also decreases for the 2:1 and 4:1 2000 membranes. The 4:1 2000 membrane exhibits a tensile curve similar to that of an entangled linear polymer, with elongation continuing well after the yield point.[168, 169] While tailored crosslinking provides enhanced mechanical stability in a plasticized state, as seen with other rubbery crosslinked membranes,[74] the tensile strength and elongation decreases upon plasticization due to the polymer chains being partially extended when swollen with plasticizer (Figure 23c).

FTIR Spectroscopy

To better understand the coordination chemistry of crosslinked PEI with the alkali salt, LiTFSI, the 1:1 2000 PEI-PEO sample and the reference sample Jeff900-PEO2000 were investigated by FTIR spectroscopy. Between the 780 cm^{-1} and 900 cm^{-1} frequency regions, an additional band occurs at 867 cm^{-1} for the PEI-PEO membrane, whereas the Jeffamine-PEO membrane shows a less distinguished shoulder (Figure 24a). This mode is assigned to the O_n-M (ether oxygen-alkali metal ion) breathing mode, due to the local crown ether-like interactions with the Li^+ cation.[170] Our previous studies indicate that such an O_n-M breathing mode is more apparent in a short-chain PEO-alkali salt solution, resembling the IR spectrum of sodium triflate in TEGDME.[171] At the same salt concentration, such an O_n-M breathing mode at 867 cm^{-1} does not appear in either a linear PEO nor a crosslinked PEO system.[74] Therefore, it is reasonable to conclude that the interaction of PEI with the alkali metal salt and the ether moiety in PEO contributes to better

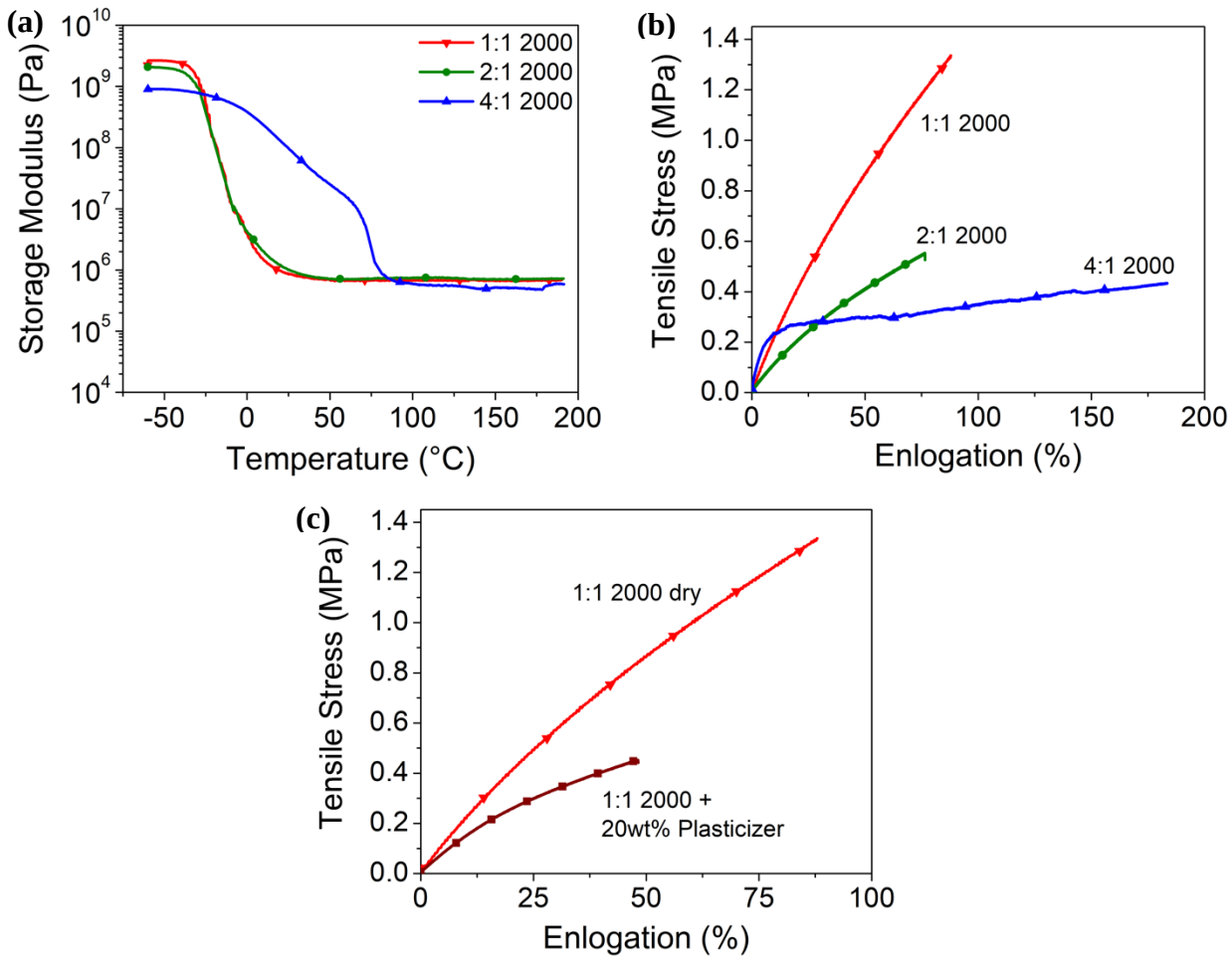

Figure 23. (a) Storage modulus of dry membranes over the temperature range of -60 to 200 °C. (b) Tensile measurement of dry membranes. (c) Tensile measurement of dry and plasticized 1:1 2000 membrane.

Table 6. Mechanical Properties of the 2000 series PEI-PEO membranes at 25 °C

Sample	Youngs Modulus (MPa)	Tensile Strength (MPa)	Elongation at Break (%)	Storage Modulus (MPa)
1:1 2000 dry	2.11 ± 0.10	1.34 ± 0.09	89.2 ± 4.04	0.86
2:1 2000 dry	0.952 ± 0.09	0.468 ± 0.08	71.4 ± 5.12	1.02
4:1 2000 dry	2.68 ± 0.19	0.470 ± 0.01	193 ± 71.9	98.5
1:1 2000 + 20wt% Plasticizer	1.13 ± 0.31	0.418 ± 0.06	51.0 ± 6.00	0.52

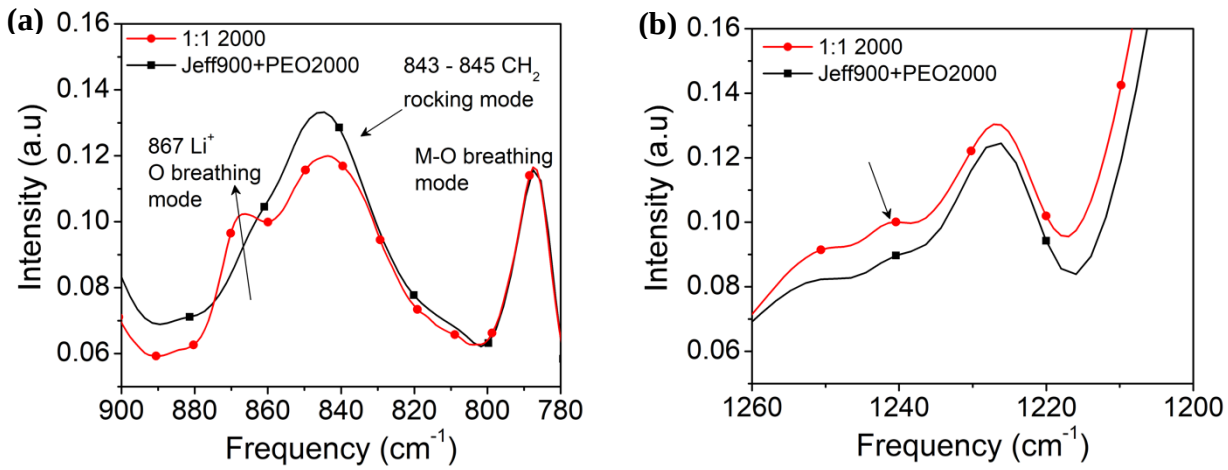

Figure 24. (a) Infrared spectra of 1:1 2000 PEI-PEO and Jeffamine 900-PEO2000 crosslinked membranes between 780 cm^{-1} and 900 cm^{-1}. (b) Infrared spectra of 1:1 2000 PEI-PEO and Jeffamine900-PEO2000 crosslinked membranes in S-O stretching region.

dissociation of the salt, similar to a plasticized system. This conclusion is supported by the low VFT activation energy (parameter *B*) of the dry membranes, which is similar to that of a TEGDME plasticized crosslinked PEO membrane. The frequency region between 1240 and 1255 cm^{-1} comprises S-C and C-F stretching vibrational modes, with the band centered around 1241 cm^{-1} ascribed to dissociated $TFSI^-$ ions (Figure 24b).[172] The PEI-PEO membrane exhibits a higher intensity at the 1241 cm^{-1} band, indicative of a high concentration of solvated Li^+ and $TFSI^-$ ions. The conclusion of well-solvated ions is in good agreement with the strong local interaction of the PEO ether oxygen with the Li^+ cation, as shown in Figure 24a.

Conclusions

An improved synthesis method for fabricating a novel PEI-PEO crosslinked membrane has been demonstrated that provides high ionic conductivity and improved salt solvation. The membranes were synthesized via a single-step procedure utilizing branched PEI and epoxide terminated PEO with varying amine NH to epoxide ratios. The resulting PEI-PEO crosslinked matrix consists of membranes with no free amine NH groups (1:1 2000) to abundant free amine NH groups (4:1 2000). The membranes exhibit an increasing amount of hydrogen bonding with an increasing number of free amines, resulting in an increased cation transport number and storage modulus for the 4:1 2000 membrane. T_g and the degree of crystallinity of the dry membranes increases with decreasing crosslink density, though due to crosslinking and H-bonding, the degree of crystallinity is significantly reduced compared to neat PEO. Light plasticization of the membranes with 1M LiTFSI in TEGDME reduces T_g, T_m, and % crystallinity, resulting in almost two orders of magnitude increase in ionic conductivity. With plasticization, the ionic conductivity of the 1:1 2000 membrane reached 1.7×10^{-4} S/cm at 30 °C and 1.2×10^{-3} S/cm at 80 °C. The highly conductive membranes demonstrate reasonable cycling in a lithium metal full cell under harsh conditions (75 °C) and have many potential applications in electrochemical storage devices.

CHAPTER IV
Unraveling Ion Transport of a Cation Exchange Membrane in Non-Aqueous Electrolytes

A version of this chapter is submitted for publication by Michelle L. Lehmann, Guang Yang, Jagjit Nanda, and Tomonori Saito. “Unraveling Ion Transport in Trifluoromethanesulfonimide Pentablock Copolymer Membranes in Non-Aqueous Electrolytes” *submitted Macromolecules*.

Michelle Lehmann conceived and performed experiments and wrote the manuscript under the guidance of Tomonori Saito. Guang Yang provided guidance and assistance on performing electrochemical tests. Jagjit Nanda and Tomonori Saito provided overall direction and supervision.

Abstract

Single-ion conducting ion exchange membranes provide a key function in various non-aqueous energy storage technologies such as lithium-ion, sodium-ion, and redox flow batteries. The membranes in flow batteries are constantly exposed to a liquid electrolyte, while plasticization of the membrane with an electrolyte solution is often used to increase performance of solid-state Li-ion batteries. As such, understanding the role of a non-aqueous liquid electrolyte on ion transport through a membrane is imperative for optimizing the performance of various energy storage systems, but their structure-property relationship is often unclear. This study unravels the relationships between membrane ion transport and electrolyte salt concentration. We utilize a trifluoromethanesulfonimide (TFSI)-based pentablock copolymer membrane with a polar (propylene carbonate, PC)) and non-polar (tetraethylene glycol dimethyl ether, TEGDME) organic electrolyte solutions. Furthermore, the delocalized negative charge on the TFSI anion, combined with its placement in the center of the pentablock copolymer facilitates ion transport, while the outer blocks provide mechanical robustness. Membrane properties such as electrolyte uptake, ionic conductivity, transport number, and salt absorption were evaluated as a function of electrolyte salt concentration. Over an order of magnitude increase in membrane conductivity is achieved by tailoring the electrolyte salt concentration. Moreover, the tethered anions in the membrane restrict the mobility of free anions, maintaining a high cation transport number (>0.75) across the concentration range for PC and at moderate electrolyte concentrations for TEGDME. This study reveals critically important design parameters for key energy storage systems utilizing non-aqueous electrolytes, such as Li and Na-ion batteries and non-aqueous flow battery technologies.

Introduction

Cation exchange membranes (CEMs) are essential for various aqueous and non-aqueous technologies such as fuel cells, desalination, redox flow batteries, and solid-state batteries. Ion transport in these systems is a crucial factor, as the selectivity and conductivity of the ion through the membranes need to be tailored for the specific application. In addition, the type and concentration of the supporting electrolyte (or brine solution for desalination applications) play a

pivotal role in membrane performance. The use of CEMs in aqueous systems is relatively mature, and membrane properties such as uptake, ion transport, and selectivity are well studied as a function of electrolyte salt concentration. For example, the impact of NaCl aqueous solutions (0.1 to 1M) were studied in CEMs with pendant sulfonate groups. The studies revealed that an increase in NaCl concentration increased ionic conductivity and decreased water uptake, while the cation transport number remained relatively constant (~0.97).[54, 173] For aqueous vanadium redox flow batteries, proton conductivity was found to increase at low acid concentrations before declining as the acid concentration increases.[63, 64] In contrast to aqueous systems, the correlation among CEM properties and salt concentration in non-aqueous electrolytes is not established.

In non-aqueous redox flow batteries, the CEM is bathed in an electrolyte solution of various salt concentrations depending on the solubility of both the salt and redox couple. Often, the effect of the chosen electrolyte concentration on membrane performance is not considered. In a study by Li et al., membrane uptake was found to increase when a crosslinked poly(phenylene oxide) polymer was immersed in an acetonitrile-based electrolyte solution compared to acetonitrile without salt.[53] This is in contrast to aqueous systems where membrane uptake generally decreases in an electrolyte solution compared to pure water. In addition, the charge carrier transport number is typically lower in non-aqueous electrolytes compared with aqueous electrolytes (0.64 to 0.79 compared to 0.96).[41, 66] Maurya et al. proposed that the Donnon exclusion effect, where oppositely charged ions are excluded from entering the ion exchange membrane, is less effective in organic solutions than in water. Thus, a greater understanding of membrane properties in non-aqueous electrolytes is imperative for improving the performance and selectivity of polymeric membranes in non-aqueous flow batteries.

CEMs (or single-ion conductors) are also a vital component for use in Li and Na-ion solid-state batteries. The use of CEMs in solid-state Li or Na-ion batteries has been limited due to the poor ionic conductivity of these polymers in a dry state (10^{-11} to 10^{-6} S/cm at 30 °C)[8, 9, 174]. While salt-in-polymer electrolytes can reach higher conductivity values than that of CEMs, much of the conductivity of salt-in-polymer electrolytes is contributed by the anion, resulting in cation transport numbers (t_+) below 0.5.[5, 6, 11] A high cation transport number is desirable for reducing polarization effects at the electrodes, which can be detrimental to the life of the battery. The benefit of a CEM in a solid-state battery is providing a high cation transport number (>0.85), improving battery cycle life.[10, 11, 174, 175] Strategies used to increase the conductivity of CEMs for Li-ion batteries include the use of a cation conducting group with a more delocalized negative charge, such as trifluoromethanesulfonimide (TFSI), and the addition of a high dielectric constant carbonate plasticizer.[10-12] The addition of a small molecule plasticizer to a CEM improves the ionic conductivity, but an upper limit exits due to a trade-off in the amount of plasticizer and the number of charges in the system, i.e., number of tethered anions that can be

added to the polymer backbone. Plasticizing a CEM with a salt-containing electrolyte solution provides a means to breakthrough this upper limit by providing additional charges within the membrane, thus increasing the ionic conductivity.

It is critical for the development of next-generation energy storage systems to gain a greater understanding of CEM ion transport in the presence of non-aqueous media. This study thus aims to unravel relationships between membrane transport properties and salt concentration of equilibrating electrolyte solutions. A commercially available midblock sulfonated pentablock terpolymer was selected as a base polymer due to its high mechanical strength and capability to form microphase-separated morphology. The superior mechanical strength enables stable thin membranes to be fabricated. The midblock of the copolymer was converted from a sulfonate functional group to a TFSI functional group via a facile two-step process. Furthermore, the tethered anion is expected to aid in restricting the mobility of free anions, allowing a high cation transport number to be maintained. The selected electrolyte solvents are propylene carbonate (PC) and tetraethylene glycol dimethyl ether (TEGDME). These solvents are of similar viscosity (~3.3 mPa s), and widely differing dielectric constant (ε) (ε_{PC}=65, ε_{TEGDME}=7.8).[176, 177] Sodium triflate (NaTf) was selected as the salt due to its solubility in glyme solvents and demonstrated compatibility with highly reactive redox species.[27] Membrane properties such as uptake, conductivity, transport number, and salt absorption were measured as a function of electrolyte concentration to determine the relationships between membrane transport and electrolyte salt concentration. The results of this study provide important design parameters for the advancement of high performance non-aqueous energy-storage technologies.

Experimental

Materials

Trifluoromethanesulfonamide (TFSA, TCI America, 98%), sodium hydroxide (Fisher Scientific, 97%), anhydrous dimethylformamide (DMF, Sigma, 99.8%), triethylamine (TEA, Sigma, 99.5%), anhydrous tetrahydrofuran (THF, Sigma, 99.9%) and thionyl chloride (Sigma, 99%) were used as received. Tetraethylene glycol dimethyl ether (TEGDME, Sigma, 99%) and propylene carbonate (PC, Sigma, 99%) were dried over molecular sieves; sodium trifluoromethane sulfonate (NaTf, Sigma, 98%) was dried at 80 °C for 72 h and stored in a glove box before use. Nexar™ pentablock terpolymer, poly(*t*-butylstyrene-*b*-ethylene-*r*-propylene-*b*-sulfonatedstyrene-*b*-ethylene-*r*-propylene-*b*-*t*-butylstyrene), (MD-9200) was kindly provided by Kraton Corporation. The center block is selectively sulfonated to obtain an ion exchange capacity of 2.0 mmeq/g.

Synthesis and Fabrication of TFSI Na Membranes

The Nexar polymer was dried from the as-received cyclohexane solution and washed with deionized water to remove any residual impurities from polymerization. For conversion to sulfonyl chloride form, 3g (6.0 mmol SO_3) of polymer was dissolved in THF (100 ml). A catalytic amount of DMF was added (0.60 ml, 7.7 mmol), and the solution cooled to 0 °C. Thionyl chloride (1.8 ml, 24 mmol) was added dropwise, and the polymer solution was kept at 0 °C for 1 h, then reacted at room temperature for 6 h under an argon atmosphere. The polymer solution was stored in the freezer overnight before precipitating into ice water. The polymer was collected via vacuum filtration and washed several times with cold water, then dried under vacuum at 50 °C for 48 h. The obtained product is a white fluffy polymer. The TFSI functionalized polymer was prepared by dissolving the sulfonyl chloride intermediate in THF (100 ml) and purging with argon. The solution was cooled to 0 °C before TFSA (1.8 g, 12 mmol) and TEA (2.8 ml, 20 mmol) in 5 ml of THF was added dropwise. The reaction proceeded at 0 °C for 1 h, then room temperature for 3 h. The solution was chilled in the freezer before precipitating into ice water. The resulting light brown polymer was collected via vacuum filtration and dried at 65 °C for 24 h. Conversion to TFSI (H) from was confirmed by elemental analysis (C= 54.7 mmol/g, N=1.77 mmol/g, H=84.2 mmol/g).

The sulfonate membranes were fabricated by casting a 3 wt% polymer in 3:1 THF/DMF solution into a Teflon® evaporating dish. The solvent was slowly evaporated, followed by drying under vacuum at 65 °C overnight. The membranes were exchanged to sodium form by soaking in a 1 M NaOH aqueous solution for 24 h. The solution was replaced with fresh NaOH three times. The membranes were rinsed well with deionized water and dried under vacuum at 65 °C for 24 hours. To prepare the TFSI membranes, the polymer was converted to Na^+ or H^+ form first, then cast using the same procedure as above. The membranes were approximately 50 µm thick.

Membrane Characterizations

Small-angle x-ray scattering (SAXS) was performed using a Xenocs Xeuss 3.0 system with dual-source Cu and Mo x-ray beam (50 kV, 0.60 mA, λ=0.154 nm). The sample to detector distance was 900 mm. The samples were probed for 15 min, with scattering information collected with a triple-axis Pilatus3 R 300K detector. The q range scanned was 0.004 to 3.2 nm^{-1}. The glass transition temperature (T_g) of the membranes was determined by dynamic mechanical analysis (DMA) using a TA Instruments Q800 DMA. Samples of a 15×5 mm size were measured at an operating frequency of 1 Hz and heated at a rate of 10 °C/min from -80 to 250 °C. T_g of the membranes was recorded from the loss modulus peaks. Differential scanning calorimetry (DSC, TA instruments Q2000) was used as an additional method to determine the T_g of the ethylene/propylene block. Samples were prepared in an argon-filled glovebox and heated at a rate of 10 °C/min from -90 to 120 °C for 1 cycle, then from -90 to 200 °C for 1 cycle. T_g was recorded from the second heating cycle. The decomposition temperatures of the dry membranes

were determined by thermal gravimetric analysis (TGA, TA Instruments Q50). TGA was conducted under nitrogen at a heating rate of 20 °C/min, with the thermal decomposition temperature (T_d) measured at 5% mass loss. The tensile strength of the membranes was measured using an Instron 3343 universal tensile meter according to ASTM D1708. Membranes were stretched constant rate of 1 mm/min under ambient conditions until break.

The electrolyte uptake of the membranes soaked in the various electrolyte solutions was determined using:

$$Uptake\ (\%) = \frac{m_w - m_d}{m_d} \times 100 \qquad (7)$$

where m_w is the mass of the polymer after soaking in the electrolyte solution and m_d is the mass of the dry polymer. The amount of salt absorbed into the membranes was determined using inductively coupled plasma optical emission spectroscopy (ICP-OES, Agilent Technologies 5110). Electrolyte equilibrated membranes were dried to remove the residual organic solvent, then heated overnight in a known volume of 1 M nitric acid to transfer the salt into the aqueous phase. The moles of Tf^- in the aqueous solutions was determined by measuring the concentration of sulfur against analytical standards.

Electrochemical Characterizations

Samples for electrochemical measurements were prepared in a glovebox and equilibrated in the various solutions for at least 3 d. Tests were performed using a Biologic VMP3 potentiostat and EC-Lab® software. Electrochemical impedance measurements were performed by a direct contact method.[178] Samples were sealed between two stainless-steel blocking electrodes, and the impedance measured while heating from 25 to 60 °C and cooling from 60 to 20 °C. The frequency range of 1 MHz - 1 Hz was used, with a 6 mV AC signal. The Na^+ transport number was determined by the Bruce-Vincent polarization method.[128] The equilibrated membranes were sandwiched between sodium foil and sealed. A 10 mV DC potential was applied, with the current monitored over 10 h at 50 °C. Electrochemical impedance was measured just before the potential was applied and at 10 h. The cation transport number (t_+) is determined using equation 5.

Results and Discussion

Membrane Synthesis

Nexar was selected for this study due to its ability to form microphase-separated ionic domains, mechanically robust backbone, and availability in sulfonated form. The pentablock terpolymer, poly(*t*-butylstyrene-*b*-ethylene-*r*-propylene-*b*-sulfonatedstyrene-*b*-ethylene-*r*-propylene-*b*-*t*-butylstyrene), (Nexar™, MD-9200), has an ion exchange capacity (IEC) of 2.0 meq/g in acid

form (H^+) (structure shown in Figure 25a). The polymer combines a rigid poly(*t*-butyl styrene) outer block for mechanical support, a flexible low T_g poly(ethylene-*r*-propylene) inner block, and a sulfonated polystyrene ionic center block (Figure 25a). In addition to providing mechanical rigidity, the *t*-butyl styrene structure also prevents sulfonation of the outer block, enabling selective sulfonation of the center block.[179] The original sulfonic acid group was converted to a TFSI functional group via a two-step process. The polymer was reacted with thionyl chloride to form the sulfonyl chloride intermediate. The sulfonyl chloride intermediate was then reacted with trifluoromethanesulfonamide to form the styrene TFSI functional group (Figure 25a). Images of the dried polymer at each step is shown in Figure 25b. The polymer was then exchanged to sodium form to provide a sodium-ion conducting membrane. The IEC of the sodium sulfonate pentablock polymer is 1.9 meq/g, and the sodium TFSI polymer is 1.6 meq/g. Membranes were cast from a 3:1 THF/DMF solvent mixture, thoroughly dried, and transferred to a glove box for plasticization. Plasticization was carried out by equilibrating pieces of membrane in an excess of electrolyte solution consisting of 0 to 1 M NaTf in either TEGDME or PC. The TFSI functional group was selected for this study as it is shown to provide improved conductivity in polymer electrolytes for Li-ion batteries over the sulfonate functional group.[180] In addition to the anion type, phase separation of a polymer into ionic domains facilitates ion transport, depending on the morphology of the membrane.[181, 182]

Morphology of the Pentablock Copolymer Membranes

The neat pentablock copolymer, Nexar, in sulfonic acid form, exhibits microphase separation into various morphologies depending on the casting solvent. For example, Huang et al. reported that Nexar cast from cyclohexane exhibited a disordered structure, while utilization of THF as the casting solvent produced membranes with a laminar/hexagonal morphology.[182] The proton transport of the membranes increased from 4.5 to 47.8 mS/cm (25 °C in water) with the change in casting solvent from cyclohexane to THF. Troung et al. studied the effect of incrementally increasing the casting solvent polarity using toluene/n-propanol mixtures.[183] With 29 wt% n-propanol, the membranes exhibited a highly ordered lamellar morphology with multiple peaks at higher q in small-angle x-ray scattering (SAXS). When the solvent mixture reached 40 wt% n-propanol, membrane morphology switched to a disordered lamellar structure that was more favorable for proton transport under moderate humidity conditions. Proton conductivity increased from 0.004 to 0.015 mS/cm (25 °C, 52% relative humidity) with an increase in n-propanol in the casting solution from 29 wt% to 40 wt%. Here we compare the morphology of the SO_3Na and TFSI Na pentablock copolymer membranes cast from the same solvent mixture (Figure 26). The primary q for the sulfonated membrane occurs at a lower value (0.136 nm^{-1}) than that of the TFSI membrane (0.214 nm^{-1}), indicating a larger feature size. The SAXS profile of the SO_3Na membrane is similar to that of Nexar SO_3H cast from THF,[182] indicating that the polar solvent DMF in the casting solution had minimal effect on membrane morphology, unlike alcoholic co-solvents as mentioned above. Both membranes show a distinct primary peak with

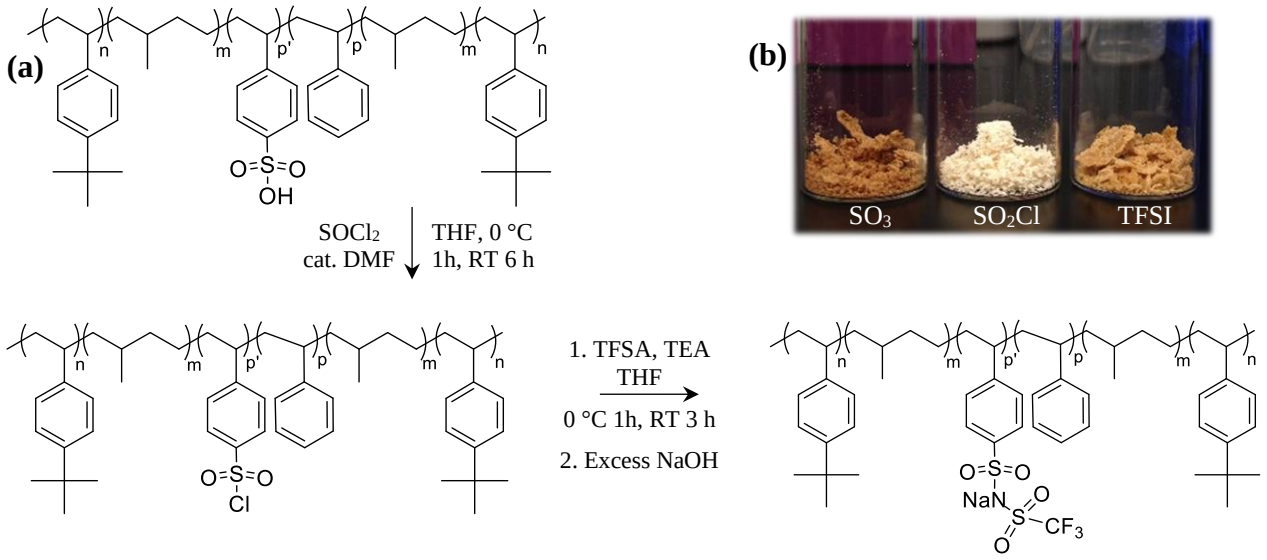

Figure 25. (a) Synthesis of TFSI functionalized pentablock copolymer from the sulfonic acid functionalized base polymer, Nexar. (b) Image of precipitated polymer in sulfonate, sulfonyl chloride and TFSI forms.

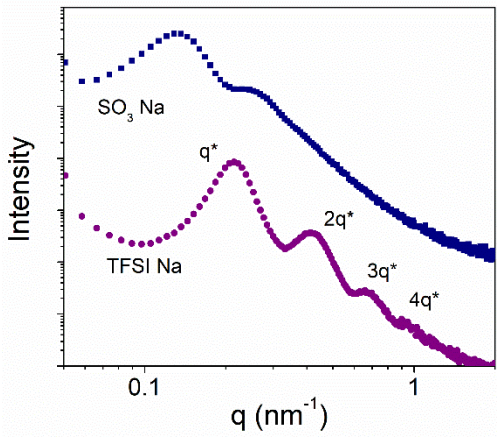

Figure 26. SAXS profiles for sodium sulfonate and TFSI pentablock copolymer membranes.

additional peaks at higher q values. The scattering patterns of both membranes indicate the presence of lamellar morphology. The appearance of the additional peaks of 3q* and 4q* observed for the TFSI membrane indicate longer-range order.[181, 183] The corresponding domain spacing, $d_1 = 2\pi/q^*$, of the SO_3Na membrane and the TFSI Na membrane is 48.9 nm and 29.3 nm, respectively. The obtained domain spacing for the sodium sulfonate membrane is slightly larger than that reported for the sulfonate membrane in proton form (43- 44 nm).[182, 183] The smaller domain size of the TFSI membrane suggests that the TFSI anion allows the ionic regions to be more densely packed, possibly increasing the available percolating pathways for ion transport.[184]

Thermal and Mechanical Properties

The thermal properties of the sulfonate and TFSI membranes are compared in both proton and sodium forms. The first glass transition temperature, $T_{g,1}$, corresponds to the ethylene/propylene block. As expected, there is no change in T_g of this block between the sulfonate and TFSI membranes or between proton and sodium forms (Table 7, Figure 27a). There is a slight decrease in $T_{g,1}$ (2 to 4 °C decrease) when the membrane is plasticized with TEGDME and PC. This slight decrease in T_g is due to plasticization of the ethylene/propylene backbone by the solvent. The impact of plasticization is minimal compared to a more polar polymer, such as poly(ethylene oxide), where its T_g decreases 10 to 20 °C upon plasticization with TEGDME.[4, 74, 99] A minor change in T_g of the uncharged block also indicates that the majority of solvent molecules are adsorbed into the ionic regions of the polymer. T_g of the remaining blocks is not easily measured by DSC for these polymers, thus DMA was employed. DMA of the solvent equilibrated samples was not performed due to excessive moisture adsorption by the polymer when exposed to air. As can be seen from the E" curves in Figure 27b, a broad $T_{g,2}$ transition occurs from ~90 to 140 °C, close to reported values of T_g for poly(*t*-butyl styrene) at ~130 °C[179, 185]. Thus, this $T_{g,2}$ region is attributed to the poly(*t*-butyl styrene) block and occurs at a similar temperature (~115 °C) for all the membranes except the TFSI H sample. The increase in $T_{g,2}$ for the TFSI H sample is due to a combined transition corresponding to poly(*t*-butyl styrene) and polystyrene TFSI. Reported T_g of polystyrene TFSI is 110 °C,[186] a much lower temperature than polystyrene SO_3H. The T_g of highly sulfonated polystyrene typically occurs at temperatures >170 °C.[187] The E' curve for the TFSI H sample shows a rapid decrease in modulus once above $T_{g,2}$, whereas the SO_3H sample exhibits a broad decline in modulus in this region. This broadening is due to increased ionic interactions in the SO_3H sample that slow chain relaxations.[188] The terminal region E' and E" curves of the TFSI H and SO_3H samples correspond well to the expected T_g of polystyrene TFSI and polystyrene sulfonic acid. Furthermore, when converted to sodium form, both membranes exhibit a relatively insignificant decline in E' above $T_{g,2}$, an indication of much stronger ionic interactions between the sodium ion and both the SO_3^- and $TFSI^-$ anions. The strong interaction between the anion and sodium cation is also demonstrated in the thermal decomposition of the

Table 7. Thermal and mechanical properties of pentablock copolymer membranes.

Sample	$T_{g,1\ DSC}$ (°C)	$T_{g,2\ DMA}$[a] (°C)	T_d (°C)	E'[b] (GPa)	Stress[b,c] (MPa)	Strain[b] (%)	Toughness (MJ/m^3)
SO_3H	-52	115	246	1.3	10 ± 1	45 ± 13	4.3 ± 1.2
SO_3Na	-52	116	318	1.7	11 ± 2	25 ± 6	1.7 ± 0.4
TFSI H	-52	127	302	2.3	17 ± 1	57 ± 5	4.9 ± 1.6
TFSI Na	-52	112	395	1.8	19 ± 1	26 ± 5	3.6 ± 1.2

[a] T_g taken from the loss modulus peak. [b]Values taken at 20 °C. [c]Maximum tensile stress.

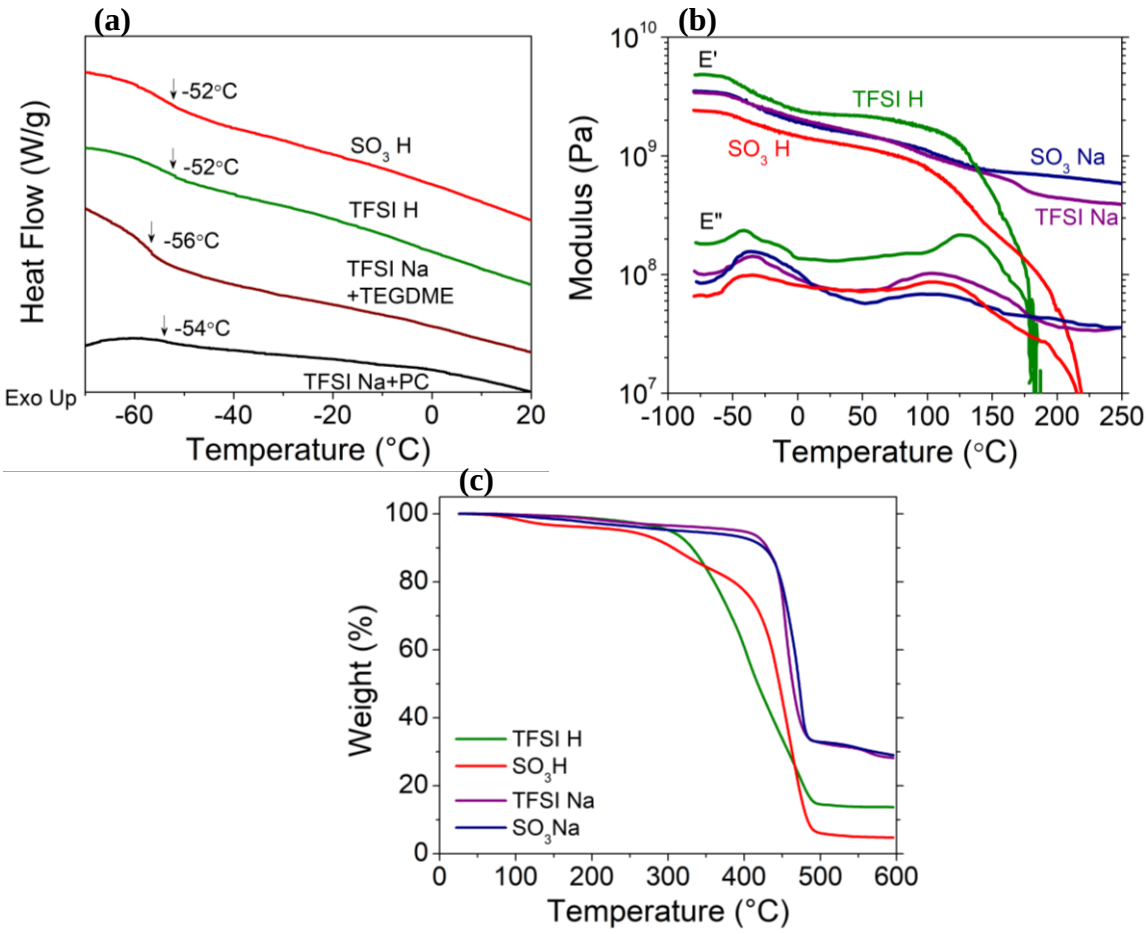

Figure 27. (a) DSC traces of dry membranes in sulfonic acid and TFSI H forms and plasticized TFSI Na membranes. (b) Modulus of the pentablock copolymer membranes in sulfonate and TFSI forms, E' is storage modulus and E" is loss modulus. (c) TGA traces for the pentablock copolymer membranes.

membranes (Figure 27c). T_d of the membranes in sodium form is 60 to 90 °C higher than in proton form (Table 7).

The increased ionic interactions of the membranes in sodium form are also evident from tensile measurements of the membranes (Figure 28a). The sodium form of the membrane exhibits a higher maximum tensile stress than the proton form and decreased elongation (Table 7). The strong ionic interactions between the TFSI anion and the sodium cation increase strength and cause the polymer to become stiffer and less elastic. Even so, these membranes have excellent toughness (both strong and flexible), with values of 4.9 and 3.6 MJ/m^3 for the proton and sodium TFSI membranes, respectively (Table 7). The tensile strength and elongation at break of the TFSI H membrane (16 MPa and 57%) is greater than that of the SO_3H membrane (9 MPa and 46%),[189, 190] indicating that the conversion reaction from sulfonate to TFSI did not damage the backbone structure and even enhanced mechanical strength. The TFSI Na membrane exhibits a significantly higher tensile strength (19 MPa) than that of the SO_3Na membrane (11 MPa), likely due to the change in morphology,[191, 192] as shown in Figure 26. Furthermore, the GPa range storage modulus of the membranes (from DMA, Figure 27b) is another indication of the exceptional mechanical strength of these pentablock copolymers. The high mechanical strength combined with reasonable elasticity allows the fabrication of thin membranes (20 – 30 μm) that enable low area specific resistance of the cell and easy assembly into an electrochemical device.

Single-ion Conductivity

Thermal and mechanical analysis of the membranes suggests that there is a strong association between both the SO_3 and TFSI anions with the sodium ion, while the delocalized charge on the TFSI anion is expected to improve sodium ion dissociation. As a dry polymer, the switch from sulfonate to TFSI forms is shown to improve Li-ion conductivity at least 1 order of magnitude.[61] Plasticization of a membrane with an organic solvent aids in the dissociation of the anion and sodium cation and the extent is evidenced by membrane ionic conductivity. The sodium-ion conductivity of the plasticized membranes increases over 2 orders when in TFSI form compared to sulfonate form (Figure 29). This increased conductivity supports that the larger delocalized anion significantly improves sodium-ion conductivity in non-aqueous solvents. Membranes plasticized with the high dielectric solvent PC exhibit a single-ion conductivity of 1.5×10^{-5} S/cm compared to 1.8×10^{-7} S/cm at 30 °C for the sodium TFSI and sulfonate membranes, respectively. These results are comparable values reported for lithiated Nafion, which exhibits a Li^+ conductivity of 2.2×10^{-6} - 1×10^{-5} S/cm in PC.[43, 56] Furthermore, the extent of solvent uptake can influence the conductivity of the membranes. Solvent uptake for the TFSI form of the membrane is 33% higher in TEGDME and 13% lower in PC compared to the sulfonated form of the membrane (TEGDME uptake is 77% and 99%, PC uptake is 116% and 103% for the sulfonate and TFSI membranes, respectively). This difference in uptake influences the relative increase in conductivity between the sulfonate and TFSI membranes in TEGDME and PC. The

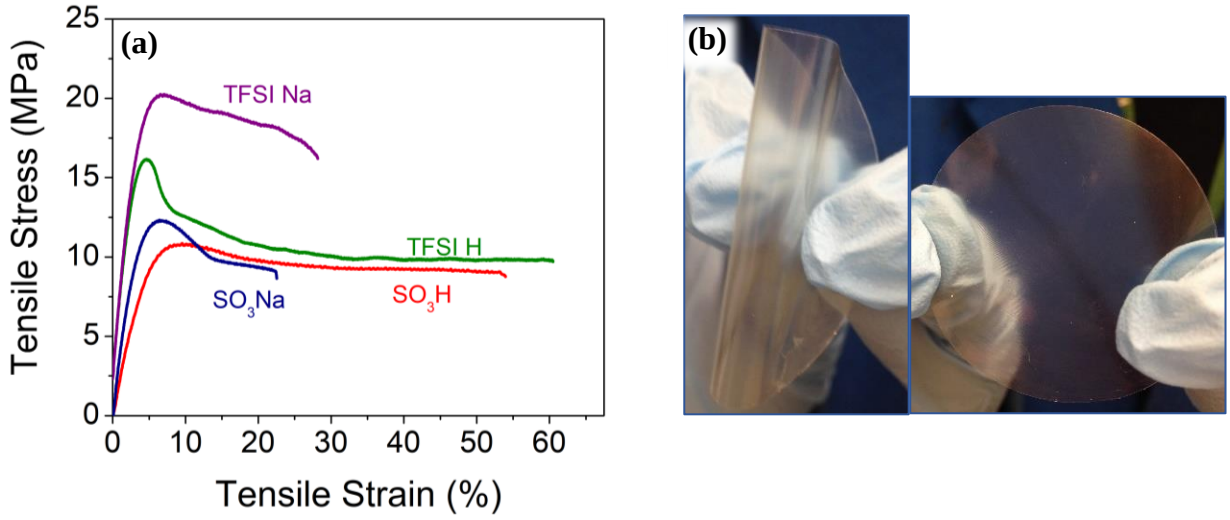

Figure 28. (a) Representative stress-strain curves for the pentablock copolymer membranes. (b) Image of TFSI functionalized membrane.

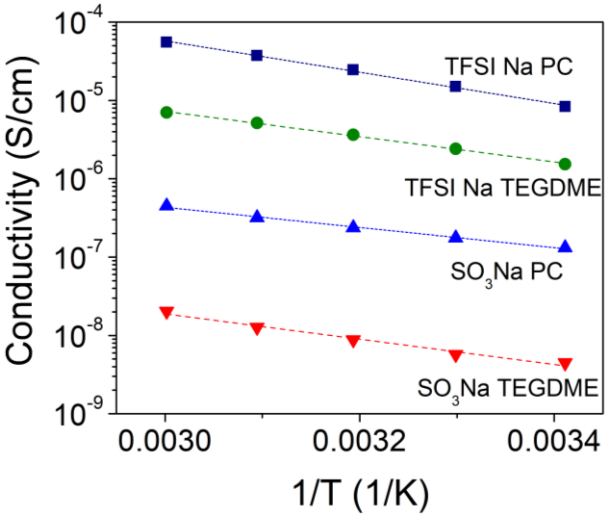

Figure 29. Conductivity of the pentablock copolymer membranes in sodium sulfonate and sodium TFSI forms, equilibrated in TEGDME and PC.

conductivity of the TFSI membrane equilibrated in TEGDME increases almost 3 orders, while the conductivity of the membrane equilibrated in PC increases 2 orders. The demonstrated improvement in conductivity is important for non-aqueous systems, which inherently have a lower conductivity than aqueous systems. Furthermore, glymes are a commonly used class of solvent in non-aqueous systems due to their superior electrochemical stability compared to carbonate solvents.[82, 193] Thus, improving the conductivity of a membrane plasticized with a glyme-type solvent (i.e., TEGDME) is important in the applications such as Li-metal battery and non-aqueous flow battery technologies. In an electrolyte solution, factors such as salt absorption into the membrane and electrolyte uptake also play a role in membrane conductivity, in addition to solvent type.

Impact of Electrolyte Salt Concentration on Membrane Properties

Often there is a trade-off between electrolyte uptake, mechanical strength, conductivity, and selectivity of the membrane. An increase in electrolyte uptake increases conductivity but decreases mechanical integrity, limiting the application of the membrane for non-aqueous flow or solid-state batteries. In addition, the effect of non-aqueous electrolyte uptake and electrolyte salt concentration on cation selectivity of CEMs has not been studied previously. To identify optimal performance of the membrane, a greater understanding is needed for the effect of an electrolyte on membrane transport, selectivity, and electrolyte uptake. Studying membrane properties in an electrolyte solution is also important for non-aqueous flow battery applications, where the membrane is constantly bathed in an electrolyte solution. In most cases, the effect of the chosen electrolyte concentration on membrane performance is not considered when performing flow battery tests. Furthermore, plasticizing a membrane with a salt-containing electrolyte solution is a method to increase the number of charges within the membrane to improve ionic conductivity for solid-state batteries. To systematically study the effect of a non-aqueous electrolyte on membrane performance, membranes were equilibrated in solutions consisting of 0 to 1 M NaTf in either PC or TEGDME. Membrane parameters including uptake, conductivity, and transport number were then studied. In addition, the amount of salt absorbed into the membrane at the varying salt concentrations was quantified.

The electrolyte uptake of the membrane steadily increases with increasing salt concentration for TEGDME, while the opposite trend is observed for PC (Figure 30a). For PC, a similar trend was observed by Su et al., where electrolyte uptake decreased with increasing $LiPF_6$ concentration.[59] The decrease in uptake with an increase in salt concentration is also commonly seen in aqueous systems.[54, 194] Counter to this trend, the electrolyte uptake increases with increased salt concentration for TEGDME. The change in uptake behavior may be correlated with the lower dielectric constant of TEGDME. A similar observation occurred when an anion exchange membrane was equilibrated in an acetonitrile-based electrolyte compared to neat acetonitrile.[53] Uptake of the membrane increased from 12% in neat acetonitrile to 38% in the electrolyte.

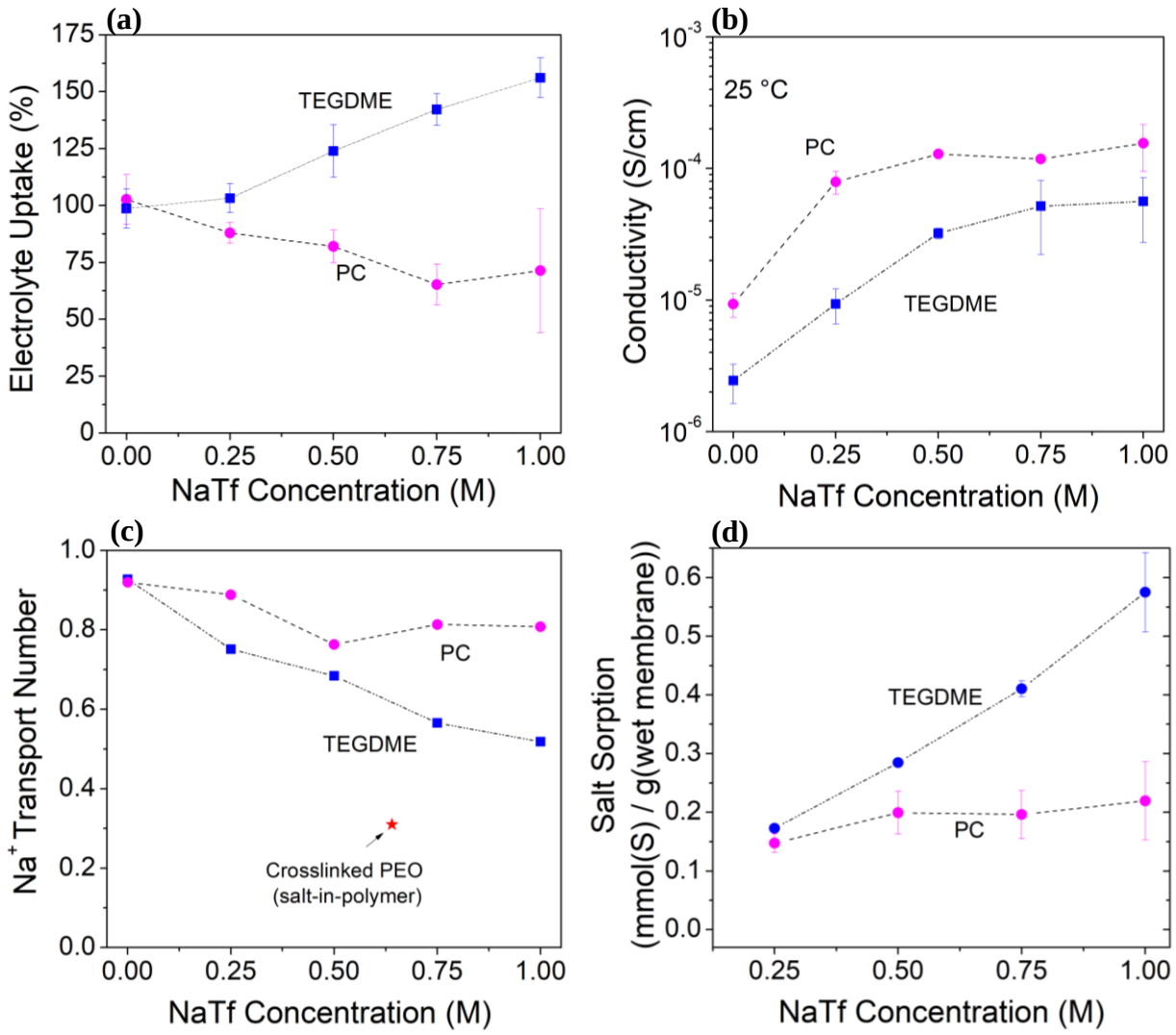

Figure 30. (a) Electrolyte uptake of the TFSI Na pentablock copolymer membranes. (b) Room temperature conductivity of TFSI Na membranes. (c) Cation transport number, with a TEGDME plasticized salt-in-polymer crosslinked poly(ethylene oxide), (PEO), membrane as reference. (d) Sulfur uptake (from Tf^-) into TFSI Na membrane, at various salt concentrations in PC and TEGDME. Error bars represent the standard deviation of 3 samples. No error bars are present for transport number experiments.

Furthermore, a change in uptake with increasing salt concentration can be attributed to a change in the ionic activity coefficient of the solution,[54, 173, 194] a value not commonly measured for non-aqueous electrolytes. Xin et al. measured the mean activity coefficients of $LiPF_6$ in several organic solvents.[195] The results showed an almost 2 order decrease in the activity coefficient for the low dielectric solvent dimethyl carbonate (0.006) compared to the moderate dielectric constant solvent acetonitrile (0.115) at a concentration of 0.5 kg/mol. These values are significantly lower than that measured for LiCl in water (0.74).[196, 197] The low mean activity coefficient for dimethyl carbonate is attributed to ion-pairing, a factor that would impact the ionic conductivity of a membrane in addition to electrolyte uptake.

The membranes demonstrate a 3x increase in conductivity when equilibrated in a 0.25M NaTf electrolyte solution, compared with the neat plasticizer without salt (Figure 30b). The conductivity continues to increase with higher electrolyte salt concentration, reaching a room temperature conductivity of 1.3×10^{-4} S/cm at 0.5 M NaTf for PC and 5.2×10^{-5} S/cm at 0.75 M NaTf for TEGDME. While a direct comparison between this system and others is difficult due to different salt/polymer/counter-ions used, the values obtained here are similar to a poly(phenylene oxide) CEM utilized in a non-aqueous flow battery study. The poly(phenylene oxide) CEM with a tri-sulfonate side chain exhibited a conductivity of 6.0×10^{-5} S/cm in a 1 M LiFSI/dimethyl carbonate electrolyte.[65] In another study, Nafion exhibited a conductivity of 1.6×10^{-5} S/cm and 8.1×10^{-6} S/cm in a 0.5 M and 1 M $LiPF_6$/PC electrolyte, respectively.[59] Conductivity of the membranes equilibrated in the TEGDME and PC electrolytes follow a similar trend as salt absorption (Figure 30d), indicating the conductivity increase is directly related to the number of 'free' ions within the membrane. These results demonstrate that the addition of even a low concentration of free ions into a CEM via the plasticizing solution significantly improves ionic conductivity.

While the bulk conductivity of a membrane is important, measuring the transport number provides information on the contribution of the cation to conductivity. Maintaining a high transport number is critical for reducing cell polarization and improving battery performance.[10] The transport number of ion exchange membranes in aqueous electrolyte solutions is generally higher than in organic electrolyte solutions.[41, 66] This phenomenon may be due to a difference in the Donnan exclusion potential (the ability of an anionic polymer to exclude anions) and a significantly lower mean activity coefficient between organic solvents and water. The decrease in transport number for organic solutions is likely due to a weaker interaction between the ionic groups in the polymer and the solvent, allowing for a higher number of free ions to enter the membrane, thus decreasing the transport number. This phenomenon is evidenced by the lower transport number of membranes equilibrated in solutions with the low dielectric constant solvent TEGDME compared to the high dielectric solvent PC (Figure 30c). The cation transport number is maintained at a higher value for the PC electrolyte, while the transport number in the

TEGDME-based electrolyte continues to decline with increasing salt concentration. In addition to the difference in the Donnan exclusion potential between PC and TEGDME, the ethylene oxide units of TEGDME preferentially coordinate with the cation, reducing its mobility.[99, 198, 199] Thus, the transport number of the TEGDME system is lower than the PC system. Few studies have reported membrane transport number in an organic electrolyte solution, and none were found that have reported the transport number as a function of electrolyte concentration. The anion transport number was measured by Kim et al. in a 0.05 M $TEABF_4$/PC electrolyte. The BF_4^- transport number was found to be 0.87 through a synthesized styrene-divinyl benzene anion exchange membrane,[66] consistent with that reported here at the lowest concentration of the PC electrolyte (0.89). Notably, the cation transport number is maintained above 0.75 for PC and 0.5 for TEGDME. The high transport number demonstrates that the tethered anion within the polymer aids in restricting the mobility of the free anions introduced into the membrane from the equilibrating solution. The degree to which this depends on a specific tethered anion is unknown. The TFSI anion's improved sodium ion dissociation may contribute to promoting cation transport and excluding free anions to a greater extent than the sulfonate anion and warrants further investigation. The high transport number demonstrated here is a significant improvement over salt-in-polymer systems, where the transport number is typically below 0.5.[5, 128, 131] For example, a TEGDME plasticized crosslinked poly(ethylene oxide) membrane utilizing the same salt (NaTf) as this study exhibits a Na^+ transport number of 0.31 (Figure 30c).[74]

Measuring the amount of salt adsorbed into the membrane provides a quantitative measure of the role of Donnan exclusion in non-aqueous systems. Salt sorption by the membrane equilibrated in the various concentrations of electrolyte solutions was measured by the moles of free sulfur (from Tf^- anion) within the membrane. The equilibrated membranes were dried to remove the organic solvents, then heated in a known volume nitric acid to extract the salt from the membrane. Utilizing ICP-OES, the moles of sulfur in the aqueous acid solution were measured. The moles of sulfur absorbed into the membrane, normalized to the mass of the electrolyte equilibrated membranes, shows an almost linear increase with salt concentration for TEGDME, while for the PC electrolyte, the adsorption of the anion into the membrane increases slightly above 0.5M NaTf (Figure 30d). The amount of salt absorbed into the membrane increases with increasing electrolyte concentration for TEGDME, and to a lesser extent for PC. Thus, the effect of Donnan exclusion is weaker in TEGDME than PC, especially at high electrolyte concentrations. This also explains the trends observed for transport number and conductivity. The continued increase in anion sorption for TEGDME increases conductivity but results in a continued decrease in transport number. The difference in Donnan exclusion between these two solvents is due to their vastly different dielectric constants, in addition to their salt solvating properties.[200] PC exhibits better Donnan exclusion due to its ability to dissociate the anion and cation within the membrane into free ions, creating a higher electrostatic repulsion. In contrast, TEGDME associates with the cation, creating solvent separated ion pairs and a lower electrostatic potential within the membrane, enabling more salt to enter the membrane.

In non-aqueous redox flow batteries with a cationic charge carrier, electrolyte concentrations are typically in the range of 0.6 to 1 M in PC, TEGDME, diglyme, or dimethyl carbonate.[27, 65, 201, 202] This study suggests that the best membrane performance is obtained at moderate electrolyte concentrations (0.5 to 0.75M), especially for low dielectric constant solvents. In addition, plasticization of a CEM with an electrolyte solution of low to moderate salt concentration is demonstrated to improve ionic conductivity while maintaining a transport number above 0.75, a desirable combination of factors for solid-state Li-ion, Na-ion, and Li-metal batteries. Furthermore, this study demonstrates the importance of studying membrane performance in various non-aqueous electrolytes at differing concentrations to obtain optimal membrane performance for each specific application.

Conclusions

Performance improvements of CEMs for non-aqueous energy storage systems have primarily been limited to modifications of the polymer structure and plasticization with small molecule solvents. Here, we presented a method for improving the conductivity of membranes for non-aqueous energy storage through plasticization with a tailored electrolyte solution. Furthermore, the facile modification of a commercially available sulfonated penta-block copolymer, Nexar, to TFSI form significantly improves membrane conductivity over two orders of magnitude. Membrane conductivity further increases to 7.2×10^{-5} S/cm and 1.4×10^{-4} S/cm at 25 °C when equilibrated in a 0.5 M NaTf TEGDME or PC-based electrolyte, respectively. Importantly, a high cation transport number (>0.75) was maintained across the concertation range for PC and at low salt concentrations for TEGDME. This study provides insights into the factors that govern membrane performance in non-aqueous systems, where optimum membrane performance, a balance between uptake, conductivity, and cation selectivity; can be achieved at a moderate electrolyte salt concentration. Moreover, we demonstrate that plasticization of a CEM with an electrolyte solution is an effective method to improve membrane performance, providing a new design system for Li and Na-ion batteries. Insights gained from this study provide a strong foundation for the development of polymer electrolytes for flow batteries, solid-state batteries, and other non-aqueous energy storage systems.

CHAPTER V
Synthesis of Anion Exchange Membranes for Aqueous and Non-Aqueous Applications

Abstract

Anion exchange membranes are an important component for a variety of applications such as electrolyzers, fuel cells, and both aqueous and non-aqueous flow batteries. Vinyl-addition polynorbornenes provide one of the most suitable polymer backbone structures due to their excellent chemical and mechanical stability. Anion exchange vinyl-addition polynorbornenes were successfully synthesized and the effect of the quaternary ammonium pendant length and incorporation of hydrophobic groups on membrane performance was studied in an aqueous environment. The membrane with a propyl quaternary ammonium tether (QPN) demonstrated the best combination of high hydroxide conductivity (109 mS/cm in water at 80 °C) with moderate water uptake (71%). Conductivity and water uptake decreases with increasing incorporation of hydrophobic hexyl side chains. The QPN membrane was selected for further study in a non-aqueous environment for potential application in a non-aqueous flow battery. The QPN membrane equilibrated in a 0.5 m tetraethylammonium tetrafluoroborate in acetonitrile solution exhibited an uptake of 48% and conductivity of 3.2 mS/cm. The robust, high-performance membranes synthesized here demonstrate the potential for use in a variety of aqueous and non-aqueous applications.

Introduction

To meet the growing demands for global decarbonization, developments in next-generation energy storage and conversion are necessary. Fuel cells are an attractive technology for small-scale electricity generation, such as the energy source for heavy duty transportation applications. Anion exchange membrane fuel cells (AEMFC) are of interest as a cost-effective alternative to traditional proton exchange membrane fuel cells (PEMFC). The use of an alkaline electrolyte enables the incorporation of a wider range of stable, low cost materials and components, including platinum-free catalysts and inexpensive corrosion resistant bipolar plates.[203-205] A membrane for an AEMFC needs to be mechanically strong, having excellent hydroxide (OH^-) conductivity but limited swelling, and be stable for long term operation in an alkaline environment at temperatures of 80°C or higher.[206] Over the last several years, considerable progress in identifying polymer backbones and tethered cations that offer increased stability for AEMFC has been made. Despite their mechanical robustness, various studies found out that polymer backbones consisting of aryl ether linkages degrade quickly under basic conditions.[49, 207-210] Anion exchange membranes (AEMs) with the best alkaline stability are those consisting of aliphatic or aromatic backbones.[77, 87, 211, 212]

In addition to AEMFCs, AEMs are a key competent in many aqueous and non-aqueous flow batteries. Redox flow batteries (RFBs) are promising technologies for long-duration, large-scale energy storage applications due to their modular design and ability to decouple energy and

power. Non-aqueous redox flow batteries (NARFBs) show great potential as next-generation RFBs due to their flexible material selection and wide operating voltage window. A membrane for a NARFB must provide high mechanical strength, high ionic conductivity and selectivity, and excellent chemical and electrochemical stability.[29] AEMs are employed for NARFBs when the anion is utilized as the charge carrier. Commercially available AEMs that were designed for aqueous applications are often utilized for NARFBs, but these membranes lack the chemical and mechanical stability in non-aqueous electrolytes.[36, 213]

Vinyl-addition polynorbornenes feature a saturated aliphatic backbone that exhibits a high glass transition temperature and excellent mechanical robustness. Vinyl-addition polynorbornenes also offer excellent chemical stability and have been studied for use in both PEMFCs and AEMFCs, but not in non-aqueous systems. The synthesis of PEMs from vinyl-addition norbornenes has been reported, but the membranes are limited to low IEC values (<1.1 meq/g) due to solubility issues, and thus, the performance of these membranes has been poor.[214-216] On the other hand, due to the ability to quaternize the membrane form of polynorbornene using amine compounds, such as trimethylamine, AEMs have been synthesized that demonstrate excellent hydroxide conductivity and alkaline stability. Shelhort et al. investigated the influence of the number of blocks for poly(trimethylamine butylnorbornene-*b*-hexylnorbornene) copolymers. The authors found that a tetrablock copolymer had the highest conductivity (103 mS/cm at 80 °C) but also the highest water uptake (85%). Furthermore, membranes with high IEC values have been fabricated as poly(trimethylamine propylnorbornene-*b*-butylnorbornene) tetrablock copolymers with the assistance of crosslinking to control water uptake.[77] Membranes with an exceptionally high IEC of 3.4 meq/g demonstrated a conductivity of 167 mS/cm in water at 80 °C with 10 mol% of crosslinking and 53% water uptake. These studies demonstrate the great potential of vinyl-addition polynorbornenes for use as AEMFC membranes, though these studies only utilized a block copolymer with a single quaternary ammonium alkyl tether length and hydrophobic norbornene blocks (butyl or hexyl substituted norbornene).[77, 217, 218]

This study aims to elucidate the impact of the quaternary ammonium tether length and the ratio of hydrophobic norbornene to unsubstituted norbornene on membrane performance for an AEMFC application. The optimal quaternary ammonium tether length can differ for different backbone chemistries as the hydration and flexibility of the cation differ between polymer systems. Thus, the impact of the quaternized ammonium alkyl tether length is unknown for vinyl-addition polynorbornenes. Furthermore, the optimal ratio of hydrophobic norbornene to unsubstituted norbornene has not been previously considered for vinyl-addition polynorbornenes and needs to be elucidated to design membranes with the desired performance for specific applications. From this study in an aqueous system, the best performing membrane was investigated for use in a non-aqueous flow battery system. The ionic conductivity and solvent uptake of the AEM were evaluated in several organic solvents of various polarities. This study

demonstrates that vinyl-addition polynorbornenes are robust high performance membranes suitable for a variety of aqueous and non-aqueous applications.

Experimental

Materials

Dichloromethane (DCM) for polymerizations was obtained from a PureSolv solvent purification system and stored over molecular sieves. Norbornene was made into a 4 M solution in DCM and stored in the glovebox over molecular sieves. All monomers were purified and stored in the glovebox over molecular sieves. Tetraethylammonium tetrafluoroborate ($TEABF_4$) was dried at 65 °C under vacuum overnight then stored in the glovebox. The solvents propylene carbonate (PC) and tetraethylene glycol dimethyl ether (TEGDME) were stored in the glovebox over molecular sieves. [$NiBr_2$(dme)] was purchased from Strem Chemical. All other reagents and solvents were purchased from Sigma Aldrich, Acros Organics, Fisher Scientific, or TCI America and used as received.

Small Molecule Synthesis

Synthesis of nickel catalyst. The catalyst *trans*-[$Ni(C_6F_5)_2(SbPh_3)_2$] was synthesized following a literature procedure with slight modification.[219] Briefly, *n*-butyllithium (8.1 ml, 1.6 M solution in hexane, 12.96 mmol) was added dropwise to a solution of bromopentafluorobenzene (3.2 g, 12.96 mmol) in dry/degassed diethyl ether (60 ml) at -83°C and stirred for 1 hour. Then [$NiBr_2$(dme)] (2.0g, 6.48 mmol, 40 ml DEE) was cooled to -83°C and the bromopentafluorobenzene and $SbPh_3$ (5.0337 g, 14.26 mmol, 20 ml DEE) solutions were added sequentially via cannula transfer. The mixture was stirred overnight and slowly warmed to room temperature. The DEE was removed by rotary evaporation, and the residue was extracted using chloroform (100 ml). The filtrate was evaporated to ~5 ml before ethanol (40mL) was added to precipitate the product. The catalyst was collected via vacuum filtration and dried in vacuo to yield a mustard-yellow powder (4.0 g, 56% yield).

Synthesis of 5-bromomethyl-2-norbornene (BMN). The synthesis of bromomethyl norbornene was carried out following a literature procedure.[220] Allyl bromide (21.0 g, 173.6 mmol), dicyclopentadiene (11.5 g, 86.8 mmol), and hydroquinone (0.1 g) were added to a 150 ml pressure vessel and heated at 180 °C for 15 h. The product was purified by sequential distillations (4 torr, 100 °C) to yield 14.0 g of product (45% yield).

Synthesis of 5-(3-bromopropyl) -2-norbornene (BPN). Dicyclopentadiene (11.09 g, 83.9 mmol), 5-bromopentene (37.5 g, 251.6 mmol), and hydroquinone (0.4g) were added to a 150 ml

pressure vessel, then heated at 200 °C for 72 h. The product was purified by sequential distillations (1.5 torr, 120 °C) to yield 13.1 g of product (36% yield).

Synthesis of 5-(6-bromohexyl)-2-norbornene (BHN). Dicyclopentadiene (13.0 g, 98.1 mmol) and 8-bromooctene (37.5 g, 196.2 mmol) were added to a 150 ml pressure vessel, then heated at 210 °C for 72 h. The product was purified by distillation under reduced pressure (2.0 torr, 170 °C), then by column chromatography (CombiFlash,) using 4:1 hexanes/ethyl acetate to yield 11.5 g of product (11% yield).

Synthesis of 5-*n*-hexyl-2-norbornene (HN). Dicyclopentadiene (15.0 g, 113.5 mmol) and 1-octene (38.2 g, 340.5 mmol) were added to a 150 ml pressure vessel, then heated at 200 °C for 48 h. The product was purified by sequential distillations (1.85 torr, 110 °C) to yield 14.0 g of product (32% yield).

Polymer Synthesis

All polymerizations were carried out in an Ar filled glovebox using a similar procedure, with the ratio of monomers in the feed solution adjusted to obtain the desired polymer composition. The synthesis of BPN is provided as a representative polymerization. The catalyst *trans*-[$Ni(C_6F_5)_2(SbPh_3)_2$] (36.8 mg, 0.033 mmol) and 12 ml DCM were added to a dry 100 ml round bottom flask. A solution of BPN (0.554 g, 2.57 mmol), norbornene (0.699 g, 7.42 mmol), and 3 ml DCM were then injected into the catalyst solution. The reaction mixture was stirred for 15 min, diluted with chloroform, and precipitated into methanol to yield 1.20 g of polymer (95% yield).

Membranes were cast onto a glass plate from a ~4 wt% chloroform solution using an adjustable doctor blade, dried, and placed under vacuum to remove any residual solvent. Membranes were released from the glass plate by immersion in water to obtain free-standing membranes with a thickness of ~20 µm. Membranes were then immersed in a 45 wt% aqueous trimethylamine solution for 48 h at room temperature. The ionic membranes were then washed with deionized water (DI) and stored under ambient conditions until use. Polymers in ionic form are denoted as QXN, where X is the trimethylamine tether length (ie., poly(trimethylamine propylnorbornene-*r*-norbornene, QPN). Polymers containing the hydrophobic HN monomer are denoted as HNX, where X is the molar ratio of HN in the terpolymer (ie., poly(trimethylamine propylnorbornene-*r*-hexylnorbornene-*r*-norbornene, QPN-HN5). Before any characterizations were performed in hydroxide form, membranes were hydrated, soaked in an excess of NaOH overnight, and rinsed with nitrogen purged deionized water to limit carbonate formation.

Characterizations

Nuclear magnetic resonance (NMR) analysis was performed using a Bruker Avance III 400 Hz spectrometer. ^{1}H NMR spectra for the brominated polymers were collected in chloroform-*d*. Molecular weights of polynorbornene were determined using a Malvern Viscotek 350B size exclusion chromatography (SEC) with trichlorobenzene as the eluant at 150 °C against polystyrene standards.

The storage moduli of the membranes were determined by dynamic mechanical analysis (DMA) at an operating frequency of 1 Hz and an amplitude of 10 μm using a TA Instruments DMA850. For dry measurements, samples in $^{-}$OH form were heated from 16 to 130 °C at a rate of 3 °C/min under nitrogen. The storage moduli of the membranes were also measured in Cl^{-} form at 80% relative humidity at a heating rate of 2 °C from 25 to 80 °C. For tensile measurements, the membranes in $^{-}$OH form were elongated at a rate of 10 mm/min under ambient conditions until break using an Instron 3343 universal tensile meter. Reported tensile properties are an average of at least 3 samples.

The ion exchange capacity (IEC) of the ionic membranes were determined using acid-base titration. A piece of membrane in $^{-}$OH form was placed in 24 ml of 0.01 N HCl for 24 h. The HCl solution was then decanted, and the membrane rinsed with deionized water to extract all the HCl from the membrane. The solution was then titrated to a pH 7 using a standardized 0.005 N NaOH solution and phenolphthalein indicator. The membrane in Cl^{-} from was dried under vacuum at 60 °C for 24 h to obtain the dry mass of the membrane. The IEC was calculated using the following equation:

$$IEC = \frac{V_{HCl}C_{HCl} - V_{NaOH}C_{NaOH}}{M_d} \quad (8)$$

where V is the volume of HCl and NaOH, C is the concentration of HCl and NaOH utilized, and m_d is the dry mass of the membrane.

The water uptake (WU) of the membranes was carried out in $^{-}$OH form using the following equation:

$$WU(\%) = \frac{M_w - M_d}{M_d} \times 100 \quad (9)$$

where m_w is the mass of the wet membrane and m_d is the mass of the dry membrane. The mass of the wet membrane was recorded, the membrane was converted to Cl^{-} from by soaking in a 1 M NaCl solution for several hours, rinsed with DI water, and dried under vacuum at 60 °C for 24 h. The swelling ratio of the membranes was determined in $^{-}$OH form using a piece of membrane with dry dimensions of ~1×3 cm. The length of the membrane was recorded wet and after drying under vacuum at 60 °C for 24 h. The swelling ratio was determined using

$$SR(\%) = \frac{L_w - L_d}{L_d} \quad (10)$$

where L_w is the wet length and L_d is the dry length of the membranes.

The hydration number (λ) of the membranes was determined using

$$\lambda = \frac{1000 \times WU}{IEC \times 18} \quad (11)$$

where IEC and WU are calculated as above, and 18 is the molecular mass of water.
The in plane conductivity of the membranes was determined by electrochemical impedance spectroscopy using a Biologic VSP potentiostat and a 2-probe conductivity cell. The wet membrane (~1.5 × 3.0 × 0.004 cm) in $^{-}$OH form, was quickly loaded into the conductivity cell and placed in a Nalgene bottle containing nitrogen purged DI water. The impedance was measured from 25 – 80 °C over a frequency range of 10^6 - 100 Hz using a 10 mV AC signal. The resistance of all samples was determined from the high frequency intercept of the real axis, with the conductivity determined using:

$$\sigma = \frac{L}{RWt} \quad (12)$$

where L is the length between electrodes (1.65 cm), R the resistance, W the membrane width, and t the membrane thickness.

For non-aqueous characterizations, the QPN membrane was exchanged to BF_4^- form by soaking in a 0.5 M aqueous $LiBF_4$ solution for 24 hours with the solution changed 3 times. The membrane was washed well with deionized water, dried at 65 °C under vacuum overnight, and transferred into an argon filled glovebox. Pieces of the membrane were soaked in the various electrolyte solutions for 3 days before measurements. Electrolyte uptake was determined using Equation 9. Through plane conductivity measurements were performed by electrochemical impedance spectroscopy. Samples were sealed between two stainless-steel blocking electrodes, and the impedance measured at 25 °C using a frequency range of 1 MHz - 1 Hz and a 6 mV AC signal. The resistance was recorded from the high frequency intercept of the real axis. The conductivity was calculated using:

$$\sigma = \frac{t}{RA} \quad (13)$$

where A is the membrane area.

Results and Discussion

Polymer Synthesis

Vinyl-addition polynorbornenes are an excellent choice for use in a variety of electrochemical applications. Due to the cyclic, fully aliphatic backbone structure, vinyl-addition polynorbornenes have excellent chemical, electrochemical, and thermal stability. Three types of brominated monomers were synthesized for this work, with alkyl tether lengths of 1, 3, and 6 carbon atoms (Figure 31). In addition, a hydrophobic monomer was synthesized with an *n*-hexyl sidechain. All the monomers were synthesized by a high-temperature Diels-Alder reaction

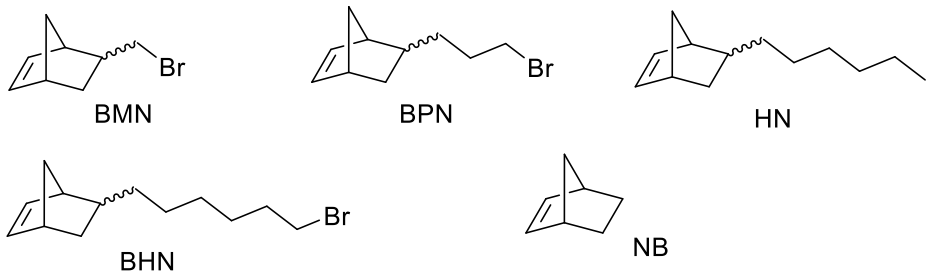

Figure 31. Schematic of monomers synthesized and norbornene.

between the corresponding vinyl compound and the in-situ formation of cyclopentadiene. The monomers were purified by subsequent distillations, except for the BHN monomer. A mixture of the BHN monomer and unreacted dicyclopentadiene were distilled from the vinyl compound and higher-order norbornene derivatives, then separated by column chromatography. The catalyst selected for the polymerizations demonstrates superior functional group tolerance and the ability to yield high molecular weight polymers. The catalyst, *trans*-[$Ni(C_6F_5)_2(SbPh_3)_2$], was synthesized in-house following a published procedure.[219] The copolymerization of a functionalized norbornene with norbornene can produce copolymers with very high molecular weights, to such a degree that they become insoluble in common organic solvents. To fabricate membranes with excellent mechanical robustness, polymers with molecular weights of >100 kg/mol are desirable. Thus, the molecular weight (M_n) of the various compositions was controlled by utilizing a fixed catalyst to monomer ratio of 1:300, varying the reaction solution concentration, and the reaction time (Table 8). M_n of all polymers is above the target value of 100 kg/mol, as determined against polystyrene standards. Polymers were synthesized as random copolymers, with a quaternized trimethylammonium (Br^-) ion exchange capacity of ~1.8 meq/g, and excellent yields of ≥ 95%. Copolymers were synthesized by utilizing norbornene (NB) and an alkyl bromide norbornene, BMN, BPN, or BHN to make polymers PBMN, PBPN, and PBHN (Figure 32a). The terpolymers were synthesized using NB, BPN, and HN. The molar ratio of HN was increased from 5 – 30 mol% to determine the impact of increasing hydrophobicity on membrane properties (Figure 32b) to make polymers PBPN-HN5, PBPN-HN15, and PBPN-HN30. Representative NMR spectra of monomers and polymers are in the appendix (Figures 38-45).

A heterogeneous reaction method was utilized for the fabrication of the AEMs reported here. Free-standing membranes were obtained by casting polynorbornene polymers from a ~4 wt% chloroform solution onto a glass plate. After drying to remove any residual solvent, membranes were removed from the glass plate and immersed in a 45 wt% aqueous trimethylamine solution for 48 h. The ionic membranes with a Br^- counter-ion were then washed with deionized water (DI) and stored under ambient conditions until use. Conversion to ionic form was confirmed by acid-base titration due to insolubility of the ionic polymers in common NMR solvents. All membranes, except for QMN, had a titrated IEC of 1.6-1.7 meq/g. The titrated IEC is slightly lower than expected from theoretical IEC values likely due to incomplete exchange of the Br^- counter-ion to ^-OH form. When select samples were heated at 80 °C in 1 M NaOH for further testing, their ^-OH conductivity increased by ~8%. In addition, a previous report of a polynorbornene-based AEM utilized an elevated temperature to exchange their membranes to ^-OH form. Minimal conversion was achieved for the QMN polymer despite extending the reaction time, increasing the temperature (1 week at 80°C), and the addition of a polar aprotic solvent to the aqueous TMA solution. The poor conversion is likely due to steric hindrance and tight packing of the polymer chains.

Table 8. Synthetic data for brominated polynorbornenes used for the fabrication of AEMs.

Sample	Reaction Time (h)	Feed Composition NB:BxN:HNB[a]	Polymer Composition NB:BxN:HNB[b]	Molecular Weight, M_n[d] (g/mol)	Dispersity (*Đ*)[c]
PBMN	3	74:26:0	72:28:0	n/a	n/a
PBPN	0.25	74:26:0	76:24:0	3,961,000	2.83
PBHN	4	72:28:0	71:29:0	838,000	2.46
PBP-HN5	3	71:24:5	60:26:14	483,000	2.94
PBP-HN15	3	60:25:15	53:26:21	169,000	2.56
PBP-HN30	3	42:28:30	25:33:42	229,000	2.24

[a]Molar ratio of monomers, x refers to alkyl bromide chain length. [b]Molar ratio determined by ^{1}H NMR spectroscopy. [c]Theortical IEC determined from ^{1}H NMR. [d]Determined by SEC against polystyrene standards with trichlorobenzene as the eluent.

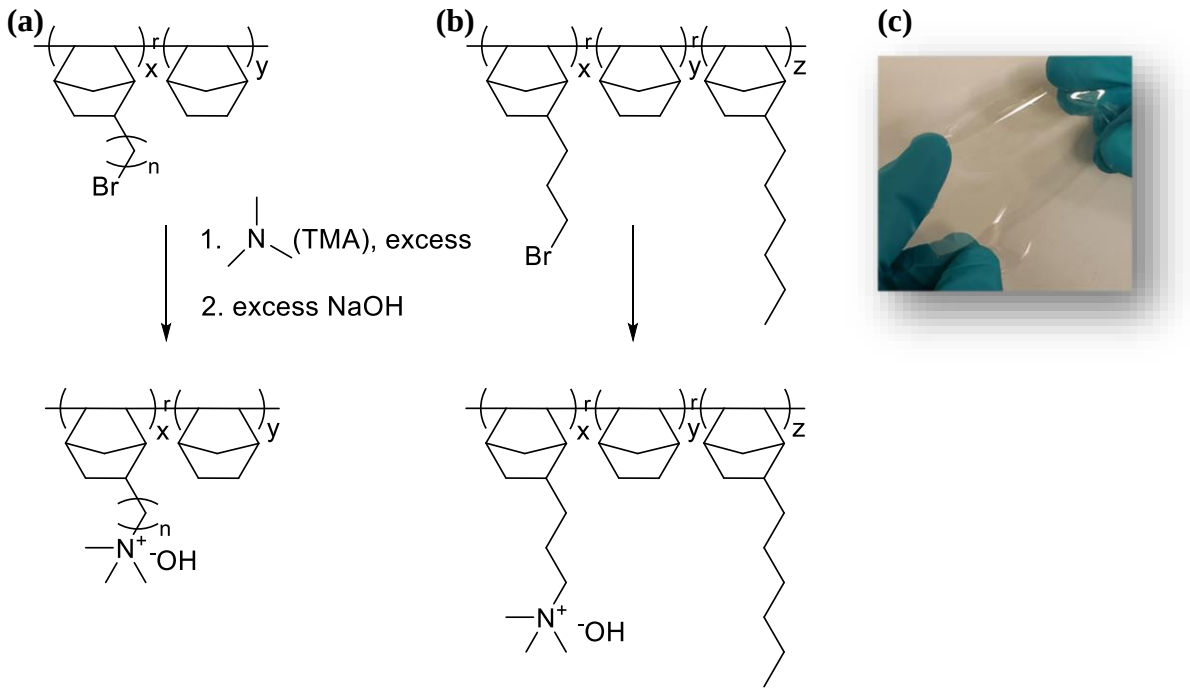

Figure 32. Synthesis scheme of norbornene anion exchange membranes. (a) Copolymers where the alkyl chain length was varied, *n= 1,3 and 6* to yield quaternized polymers QMN, QPN and QHN. (b) Terpolymers where the molar ratio of *z* (hexyl norbornene) was varied to yield quaternized polymers QP-HN5, QP-HN15, and QP-HN30. (c) Image of PBPN membrane.

Mechanical Properties

The mechanical properties of the membranes were evaluated by DMA and tensile measurements. The storage moduli (E') and loss moduli (E") were probed under dry conditions (in $^{-}$OH from) and at 80% relative humidity (in Cl^{-} form). The storage modulus of the QPN and QHN membranes remains at ~1 GPa over a wide temperature range (Figure 33a). As expected, no indication of a thermal transition occurs within the temperature range measured (15-130 °C), as the T_g of polynorbornene is ~300 °C. The storage modulus of the QHN membrane is slightly lower than the QPN membrane, likely due to a decrease in rigidity of the backbone with the long alkyl tether. A similar decrease in E' was observed for a poly(arylene ether sulfone ketone) with an increase in alkyl chain tether length.[221] At 80% RH, E' is reduced to 0.52 and 0.72 GPa at 30 °C and continues to decrease to 0.35 and 0.48 GPa at 80 °C for the QHN and QPN membranes, respectively (Figure 33b). This slight decrease in E' with increased temperature is presumably due to increased water uptake by the membranes at a higher temperature. The high temperature mechanical stability of these membranes demonstrates potential applications in high temperature fuel cells operating at 80-120 °C. Stress-strain curves of the membranes were obtained in a dry and wet state in $^{-}$OH form. The QPN and QHN membranes demonstrate an excellent maximum tensile stress of ≥25 MPa when dry, with a reasonable elongation (Figure 34). Having excellent mechanical properties in a dry state allows for easy fabrication of the membrane electrode assembly and incorporation into roll-to-roll manufacturing. In the wet state, the membranes become more flexible due to the plasticizing effect of water, with a maximum tensile stress of 10 and 15 MPa and elongation of 60 and 45% for the QHN and QPN membranes, respectively. Even with this decrease of mechanical properties in a wet state, the membranes exhibit high robustness for use in an operating fuel cell. Furthermore, the high mechanical strength combined with reasonable elasticity enables thin (<15 μm) membranes to be fabricated. A thin membrane is of great importance to reduce the area specific resistance of the membrane and improve water transport across the fuel cell.[222]

Aqueous Performance

The performance of these membranes was first evaluated in an aqueous environment for use in an alkaline fuel cell. Previous studies with vinyl-addition norbornene-based AEMs utilized a block copolymer with a single quaternary ammonium alkyl tether length and hydrophobic norbornene blocks (butyl or hexyl substituted norbornene).[77, 217, 218] The optimal tether length of the quaternary ammonium groups can differ for different backbone chemistries as the hydration and flexibility of the cation differs between polymer systems. Thus, the impact of the quaternized ammonium alkyl tether length is unknown for this system. Furthermore, the optimal ratio of hydrophobic norbornene to unsubstituted norbornene has not been previously considered for vinyl-addition norbornenes and needs to be elucidated to design membranes with the desired performance for specific applications.

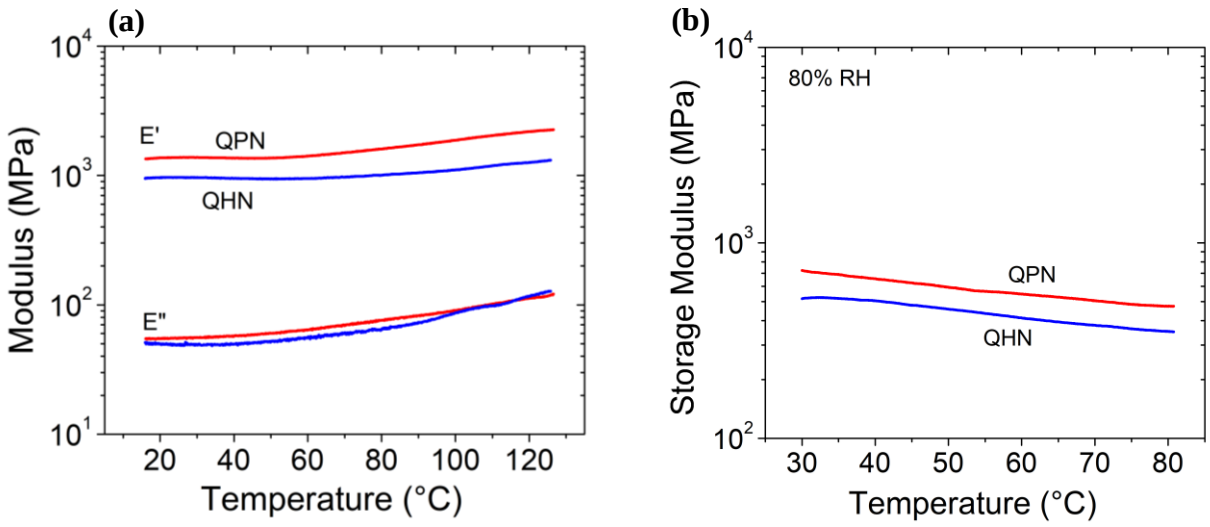

Figure 33. (a) Modulus of dry polynorbornene membranes in $^{-}$OH form. (b) Storage modulus of polynorbornene membranes at 80% relative humidity in Cl^{-} form.

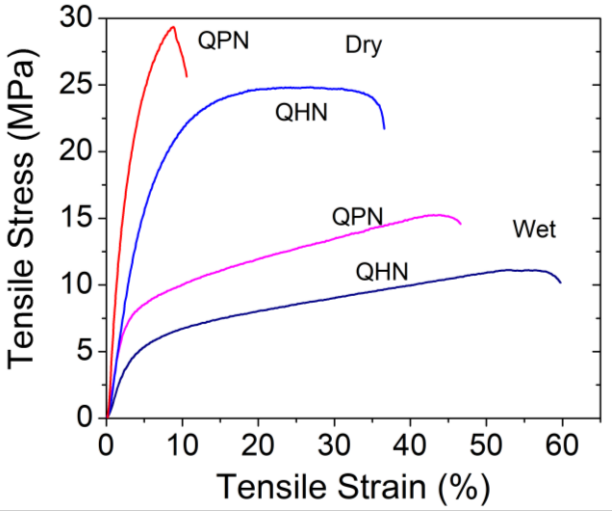

Figure 34. Tensile properties of dry and wet polynorbornene membranes in $^{-}$OH form.

Water uptake and swelling ratio of these membranes were measured in water at room temperature. The sample with the longer tether, QHN, exhibits a higher water uptake than the QPN sample (Figure 35a). Often, a change in water uptake can be attributed to changes in polymer morphology due to phase separation between the hydrophilic ionic domains and the hydrophobic domains. No phase separation is observed for these membranes in their dry state (Figure 36). The differences in water uptake between the QPN and QHN samples may be in part due to the significantly higher M_n of the QPN sample (3961 kDa) compared to the QHN membrane (838 kDa). An increase in M_n increases chain engagement, reducing the mobility of the polymer chains and their ability to swell. Furthermore, a decrease in water uptake with higher molecular weight occurred in a similar polymer system.[218] In addition, the length of the tether is shown to affect water uptake in AEMs. In a study by Mahmoud et al., room temperature water uptake increased significantly when the tether length was greater than 3 carbon atoms.[223] The addition of hydrophobic groups decreases water uptake from 71% to 63% for the QPN and QP-HN5 samples, respectively (Figure 35a). A further reduction in water uptake is observed for the QP-HN15 sample, though continued addition of hydrophobic groups exhibited little change in water uptake.

The swelling ratio is related to the stiffness of the polymer backbone and the amount of water uptake. These samples demonstrate a reasonable swelling ratio with the highest swelling ratio occurring for QHN at 28% and the lowest for QP-HN30 at 16% (Figure 35a). For membranes, light crosslinking can be employed if the water uptake and swelling ratio are too large for the desired application. Lamda (λ) is a measure of the number of water molecules per quaternary ammonium group. As expected, λ follows the same trend as water uptake for the membranes, with the highest occurring with the QHN (($\lambda = 29$) and the lowest the QP-HN30 sample ($\lambda = 18$). The membrane demonstrating the highest hydroxide conductivity is QPN, having a propyl tether length copolymerized with norbornene. The conductivity of QPN membrane reaches almost 110 mS/cm at 80 °C in water (Figure 35b). In comparison, a tetrablock copolymer membrane with the same IEC exhibits a conductivity of ~100 mS/cm with a water uptake of 85%.[217] The QHN membrane shows a lower conductivity but higher water uptake than the QPN membrane. This is counter to the trend observed where conductivity generally increases with water uptake. Thus, it appears that the 3 carbon tether length is optimal for this system. In addition, Mahmoud et al. found that a 3 carbon tether exhibited the lowest water uptake and highest conductivity in water at 60 °C for a fluorinated ethylene-benzene copolymer.[223] The conductivity of the samples incorporating the hydrophobic HN norbornene exhibit a decrease in hydroxide conductivity that is directly related to a reduction in water uptake.

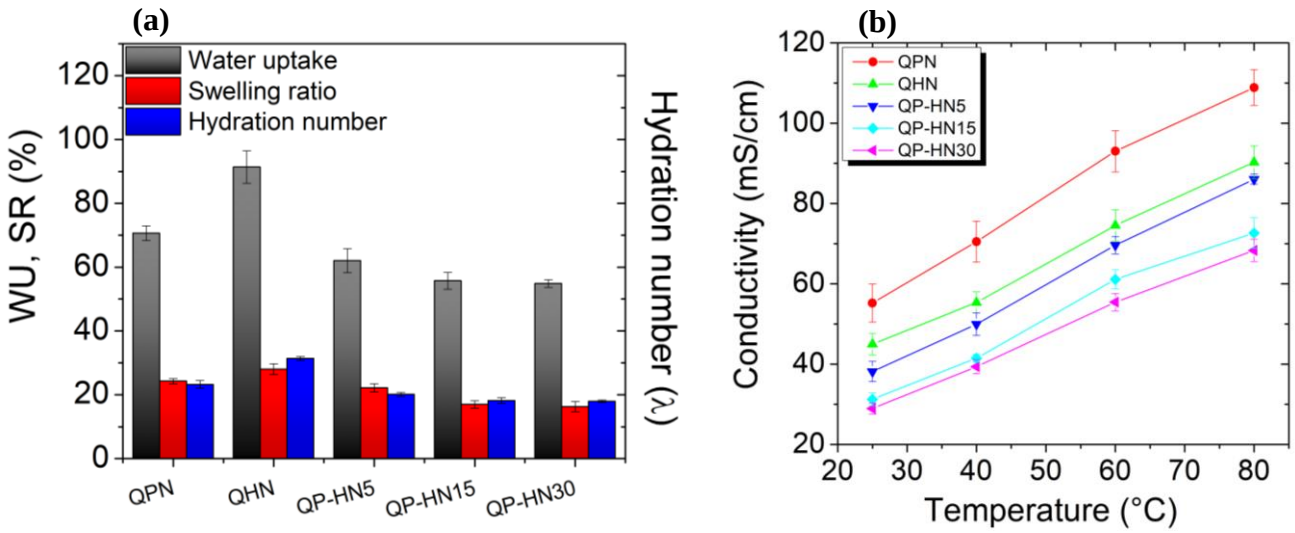

Figure 35. (a) Water uptake, swelling ratio, and hydration number of polynorbornene membranes, measured in water at room temperature in $^{-}$OH form. (b) $^{-}$OH conductivity of membranes in water. Error bars are the standard deviation of at least 3 samples.

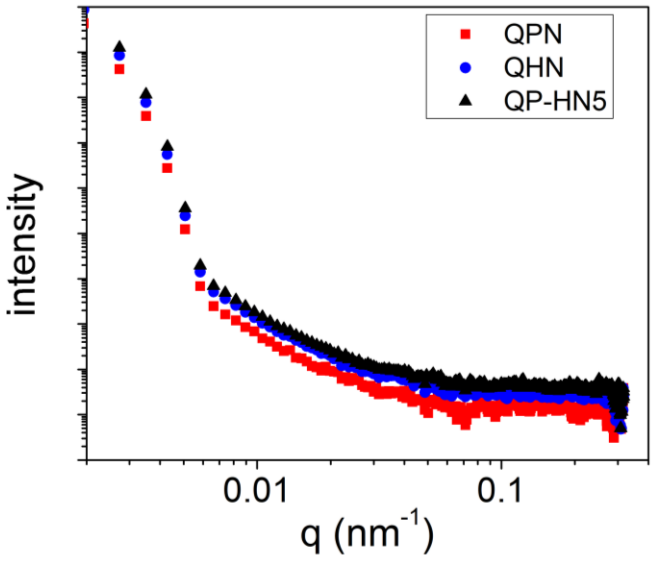

Figure 36. SAXS profiles of polynorbornene membranes in $^{-}$OH form. Profiles are offset for ease of viewing.

Non-Aqueous Performance

The best performing membrane from the aqueous study, QPN, was selected for further study as a candidate for non-aqueous systems. The membrane was exchanged to BF_4^- counter-ion form in an aqueous solution before being dried and transferred to the glovebox for the non-aqueous study. The selected solvents were propylene carbonate (PC), acetonitrile (MeCN), and tetraethylene glycol dimethyl ether (TEGDME) and represent a range of dielectric constants. The salt was tetraethylammonium tetrafluoroborate ($TEABF_4$), which is commonly used in non-aqueous flow battery studies utilizing an anion exchange membrane.[38, 41, 72] Pieces of membrane were immersed in the various electrolyte solutions for at least 24h to ensure complete equilibration of the membrane.

Membrane uptake in the neat solvents varies significantly, following the trend of solvent dielectric constant (Figure 37). In the high dielectric constant solvent PC, membrane uptake reaches 4500%, while the uptake decreases to <100% in the low dielectric solvent, TEGDME. It should be noted that the membranes soaked in PC maintained a solid form, though soft, and were able to be carefully handled. This finding attests to the superior mechanical properties of vinyl-addition polynorbornenes. The higher uptake in PC can be partially attributed to the relatively high IEC of these membranes (1.8 meq/g) compared to previous studies utilizing AEM membranes in PC (<1.3 meq/g).[41, 66, 72] Furthermore, membrane IEC is shown to have more of an impact on membrane uptake in a high dielectric solvent than a low dielectric solvent.[50] Even so, membrane IEC does not account for the substantial uptake of PC by the membrane and warrants further investigation. As seen in Figure 37, membrane uptake decreases with increasing electrolyte salt concentration for both PC and MeCN. A similar trend was observed in the previous chapter for the cation exchange membrane in PC. In addition, a decrease in membrane uptake with an increase in salt concentration is commonly observed in aqueous solutions.[54, 173, 194] Membrane uptake measurements were not performed as a function of electrolyte concentration in TEGDME due to the insolubility of the salt in TEGDME. From uptake measurements, it was determined that MeCN is the most suitable solvent for this polymer system and thus selected for conductivity measurements.

The room temperature ionic conductivity of the QPN membrane with the BF_4^- counter-ion was measured in MeCN and a 0.5 m concentration of the $TEABF_4$ salt in MeCN. The single-ion conductivity of these membranes reaches 1.05 ± 0.17 mS/cm, while the conductivity is 3.2 ± 0.11 mS/cm in 0.5 m $TEABF_4$ in MeCN. The conductivity of the membrane only moderately increased with the addition of an electrolyte solution, suggesting that a limited amount of salt was absorbed into the membrane. These conductivity values are similar to reported values for the quaternized trimethylammonium functionalized AEM, Neosepta AHA, in a 0.1 M $TEABF_4$ in MeCN electrolyte (0.53 - 5.27 mS/cm).[40, 41, 78] Neosepta AHA is a thick reinforced membrane

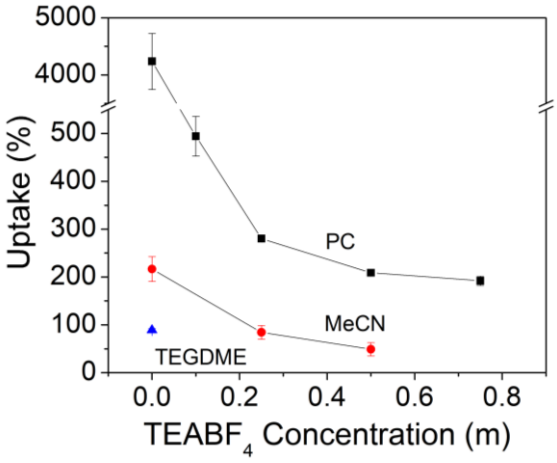

Figure 37. QPN membrane uptake as a function of electrolyte salt concentation in various solvents. PC=propylene carbonate, MeCN=acetonitrile, TEGDME=tetraethylene glycol dimethyl ether. Error bars are the standard deviation of at least 3 samples.

(220 µm) consisting of a crosslinked styrene-divinylbenzene backbone with an IEC of 1.39 meq /g. While the ionic conductivity of Neosepta AHA is competitive with that of the QPN membrane, the thickness of the membrane leads to high ASR values (4.1 to 41 Ω cm^2), making it unsuitable for use in high power NARFBs. The QPN membrane can be fabricated as thin as 20 µm without a support layer, providing ASR values as low as 0.62 Ω cm^2.

Conclusions

A series of vinyl-addition polynorbornene AEMs were synthesized as random copolymers containing various quaternary ammonium pendant lengths and ratios of hydrophobic moieties. The membranes are mechanically robust with a tensile strength >25 MPa and storage modulus in the GPa range. For an AEMFC application, the membranes demonstrate excellent hydroxide conductivity (109 mS/cm in water at 80 °C) with moderate water uptake (71%). The propyl pendant length provides higher conductivity with lower water uptake than the hexyl pendant length. The incorporation of 5 mol% of a hydrophobic monomer significantly decreases water uptake and hydroxide conductivity. The continued addition of the hydrophobic monomer to 30 mol% exhibits only a small change in water uptake and hydroxide conductivity. In addition to demonstrating excellent performance, these results provide a method to selectively control water uptake without the use of crosslinking for AEMFC applications. Furthermore, the potential application of these membranes for a non-aqueous flow battery was demonstrated. In an acetonitrile-based electrolyte solution, the membranes exhibit an ionic conductivity of 3.2 mS/cm at 20 °C with an uptake of 49%. This study demonstrates the versatility of vinyl-addition polynorbornenes for a variety of aqueous and non-aqueous electrochemical applications.

Appendix

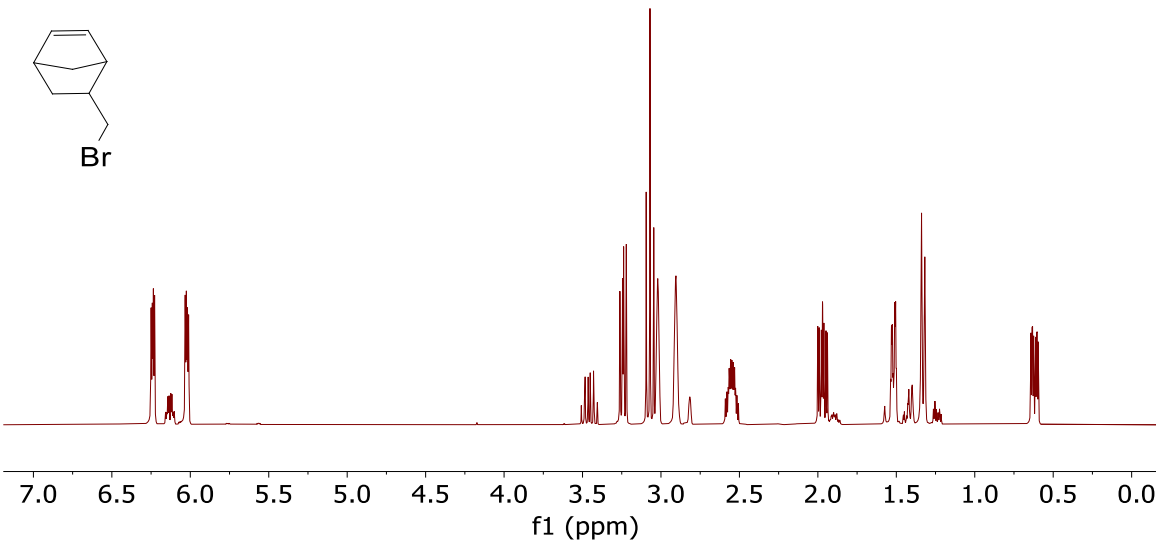

Figure 38. ^{1}H NMR spectra of 5-bromomethyl-2-norbornene in $CDCl_3$.

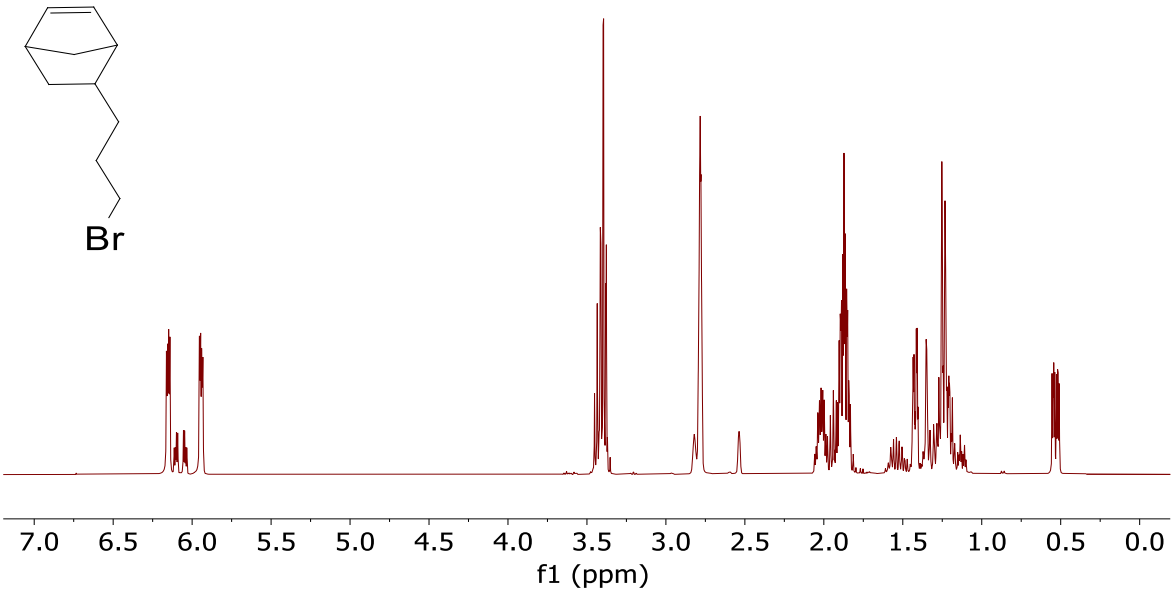

Figure 39. ^{1}H NMR spectra of 5-bromopropyl-2-norbornene in $CDCl_3$.

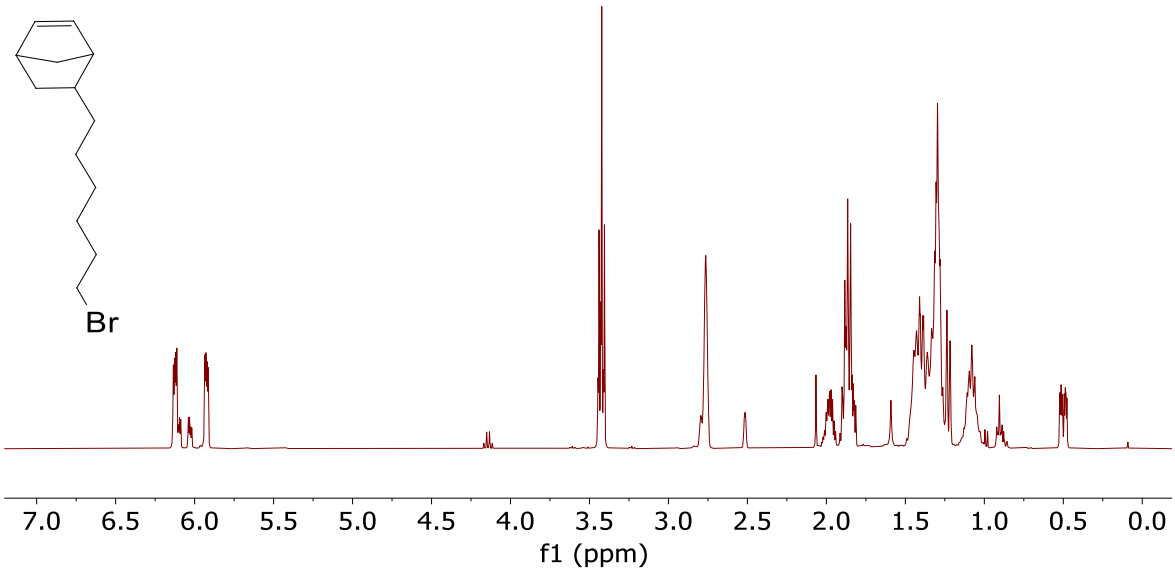

Figure 40. ^{1}H NMR spectra of 5-bromohexyl-2-norbornene in $CDCl_3$.

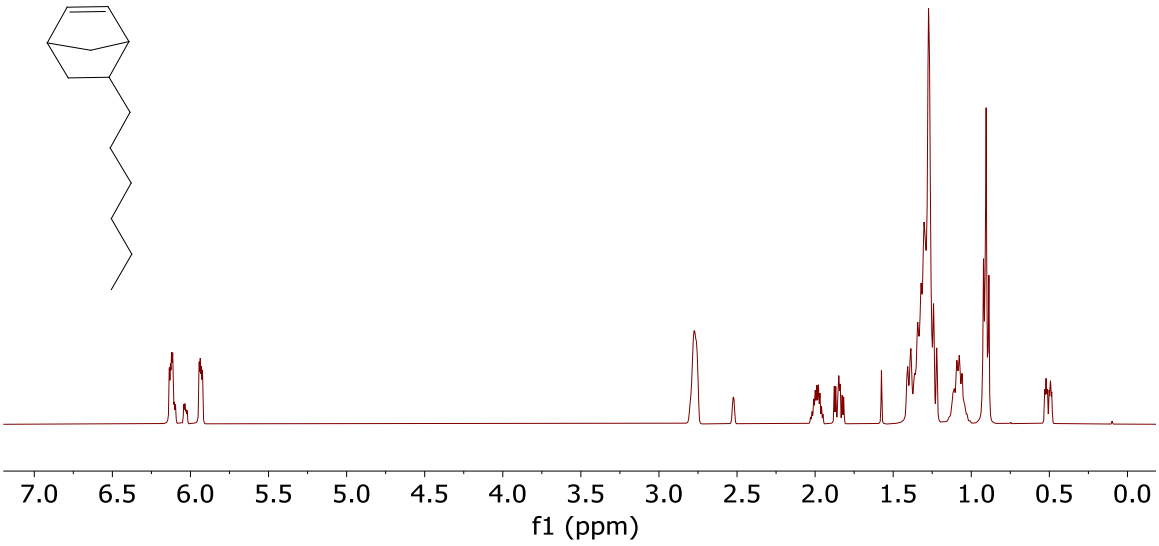

Figure 41. ^{1}H NMR spectra of 5-hexyl-2-norbornene in $CDCl_3$.

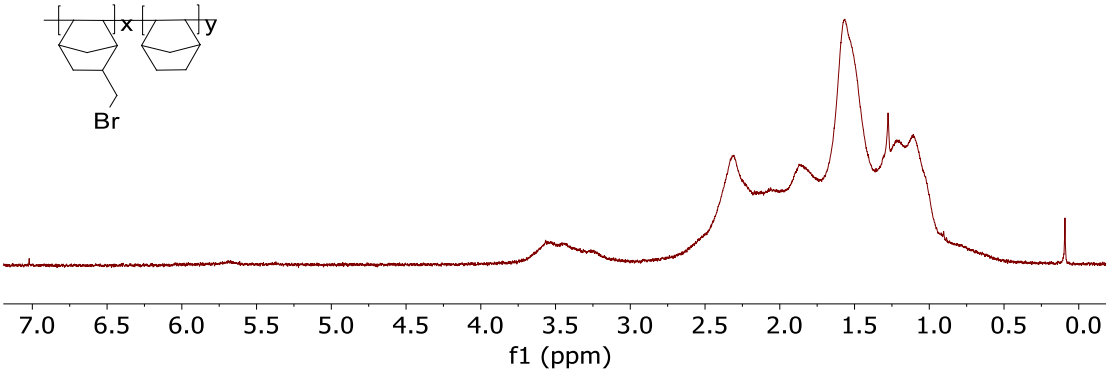

Figure 42. ^{1}H NMR spectra of bromomethylnorbornene-norbornene copolymer (BMN) in $CDCl_3$.

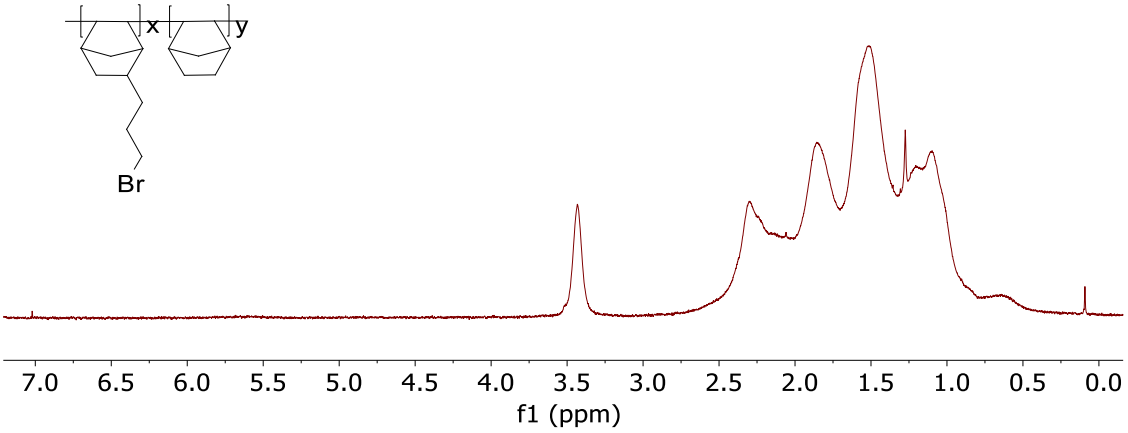

Figure 43. ^{1}H NMR spectra of bromopropylnorbornene-norbornene copolymer (BPN) in $CDCl_3$

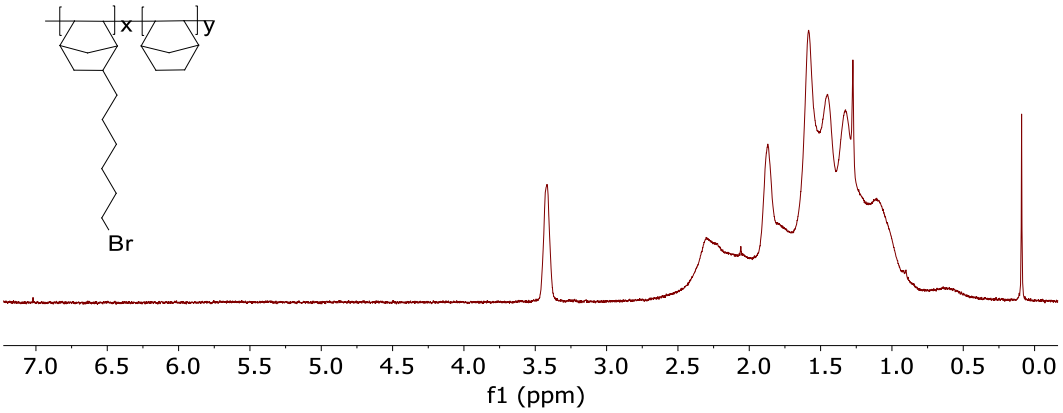

Figure 44. ^{1}H NMR spectra of bromohexylnorbornene-norbornene copolymer (BHN) in $CDCl_3$

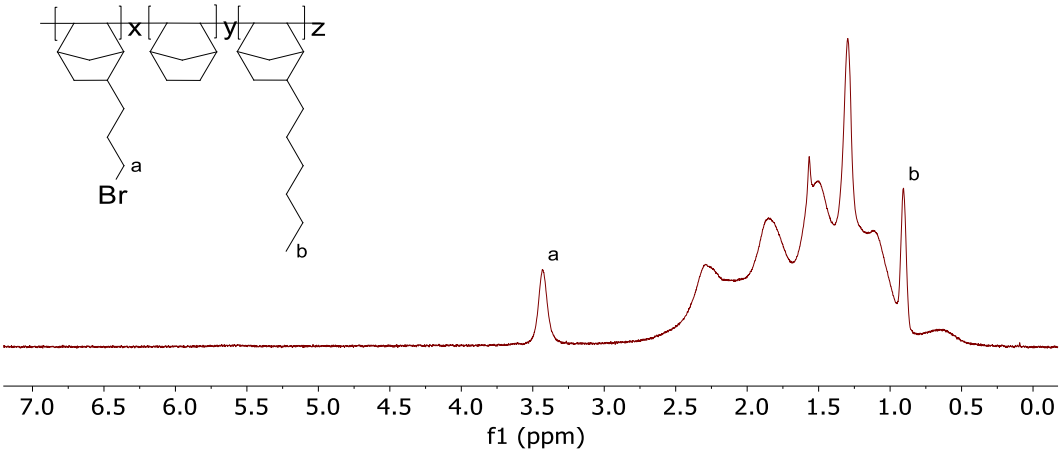

Figure 45. Representative ^{1}H NMR spectra of bromopropylnorbornene-hexylnorbornene-norbornene terpolymer (BP-HN) in $CDCl_3$.

CONCLUSION

To further advance LDES technologies, high performance membranes and a greater understanding of membrane properties in non-aqueous electrolytes is needed. In this dissertation, several new polymeric materials were synthesized, and a systematic evaluation of membrane properties were undertaken to unravel the structure property relationships in a non-aqueous environment. A crosslinked poly(ethylene oxide), (PEO) membrane was fabricated to improve upon the mechanical properties of linear PEO and to reduce PEO crystallization. The plasticized crosslinked membranes demonstrate almost an order of magnitude increase in conductivity at 20 °C compared to linear PEO (2×10^{-4} vs. 4.5×10^{-5} S/cm), just slightly lower than that of a TEGDME-based liquid electrolyte (1×10^{-3} S/cm). Furthermore, the membranes are mechanically robust and stable over a wide temperature range (-20 to 180 °C), while linear PEO becomes a viscous liquid once above the crystalline melting point of 60 °C. The membranes are sufficiently robust to resist short-circuit by sodium dendrites over the course of 180 hours when cycled in a Na metal symmetric cell, and have a Na^+ transference number of 0.58 as dry membranes and 0.31 as plasticized membranes at 40°C. To determine the influence of a Lewis basic functional group on membrane transport properties, a crosslinked PEO/poly(ethyleneimine), (PEI) membrane was synthesized. The membranes were synthesized via a single-step procedure utilizing branched PEI and epoxide terminated PEO with varying amine NH to epoxide ratios. The amine functional group in the PEI-PEO crosslinked matrix provides Lewis basic and hydrogen bonding characteristics that facilitates the dissolution of lithium salt to a greater extent than the crosslinked PEO matrix. In addition, this Lewis basic group enables improved conductivity (1.8×10^{-5} S/cm at 30 °C) and cation transport number (0.76), values significantly higher than dry polymer electrolytes utilizing linear PEO (1.5×10^{-6} S/cm at 30 °C and 0.2-0.5). Furthermore, the highly conductive membranes demonstrate reasonable cycling in a lithium metal full cell under harsh conditions (75 °C).

Then the performance on a cation exchange membrane was evaluated in various electrolyte solutions. The facile modification of a commercially available sulfonated penta-block copolymer, Nexar, to TFSI form significantly improves membrane conductivity, over two orders of magnitude. Membrane conductivity further increases to 7.2×10^{-5} S/cm and 1.4×10^{-4} S/cm at 25 °C when equilibrated in a 0.5 M NaTf TEGDME or PC-based electrolyte, respectively. Importantly, a high cation transport number (>0.75) was maintained across the concertation range for PC and at low salt concentrations for TEGDME. This study provides insights into the factors that govern membrane properties in non-aqueous electrolytes for improved device performance. Moreover, it is demonstrated that plasticization of a CEM with an electrolyte solution is an effective method to improve membrane performance, providing a new design system for Li and Na-ion batteries. Lastly, we have demonstrated the synthesis of a vinyl-addition polynorbornene anion exchange membrane. The membranes are mechanically robust,

with a tensile modulus of over 25 MPa and a GPa range storage modulus, demonstrating potential use in high temperature electrochemical applications. Furthermore, the membrane with a 3 carbon quaternary ammonium tether length demonstrates excellent aqueous performance, reaching a hydroxide conductivity of 109 mS/cm at 80 °C in water, with reasonable water uptake (71%). In the non-aqueous electrolyte solution of 0.5 m $TEABF_4$ in MeCN, the same membrane exhibits a conductivity of 3.2 mS/cm and an uptake of 49%.

The performance of polymer electrolytes for both solid-state and redox flow batteries still requires significant improvement before the wide-spread adoption of these technologies is realized. For salt-in-polymer electrolytes, the addition of inorganic fillers to the crosslinked network provides a route to significantly improve the mechanical properties of the membranes. Furthermore, the addition of a conductive ceramic particles may be a route to improve cation transport of the membranes, similar to the effect of a tethered anion within the membrane. The concept of adding a salt to a single-ion conducting membrane has the potential to significantly impact the solid-state battery field. Thus, this concept warrants further investigation, including device performance in Li and Na-based batteries.

For non-aqueous flow batteries, systematic studies of polymer-electrolyte interactions and its influence on ion transport and crossover is needed to improve membrane performance. Within this, the impact of different tethered anions and cations needs to be investigated to determine the role of the tethered ion on ionic conductivity and crossover in various electrolyte solutions. For example, does a delocalized negative charge on the anion improve the cation transport in addition to conductivity in non-aqueous electrolytes? Does a delocalized charge have an impact of redox species permeability? Furthermore, the impact of polymer architecture, polarity, and IEC on membrane conductivity and device performance needs to be further investigated to provide design parameters for future membrane development. This dissertation provides insight into ion-transport through polymeric membranes in non-aqueous solutions that may aid in the design of high performance membranes for a variety of electrochemical applications and provides an avenue for the significant advancement of Li-ion and non-aqueous flow batteries.

REFERENCES

1. Veum, K.; Bauknecht, D., How to reach the EU renewables target by 2030? An analysis of the governance framework. *Energy Policy* **2019,** *127*, 299-307.
2. Wang, T.; Jiang, Z.; Zhao, B.; Gu, Y.; Liou, K.-N.; Kalandiyur, N.; Zhang, D.; Zhu, Y., Health co-benefits of achieving sustainable net-zero greenhouse gas emissions in California. *Nature Sustainability* **2020**, 1-9.
3. Albertus, P.; Manser, J. S.; Litzelman, S., Long-duration electricity storage applications, economics, and technologies. *Joule* **2020,** *4* (1), 21-32.
4. Long Duration Storage Shot: An Introduction. *https://www.energy.gov/sites/default/files/2021-07/Storage%20shot%20fact%20sheet_071321_%20final.pdf* **2021**, Last accessed Nov 8 2021.
5. Pozyczka, K.; Marzantowicz, M.; Dygas, J. R.; Krok, F., Ionic Conductivity and Lithium Transference Number of Poly(ethylene oxide):LiTFSI System. *Electrochim Acta* **2017,** *227*, 127-135.
6. Song, J., Wang, YY, Wan, CC, A review of gel-type polymer electrolytes for lithium-ion batteries. *J Power Sources* **1998,** *77*, 183-197.
7. Bouchet, R.; Maria, S.; Meziane, R.; Aboulaich, A.; Lienafa, L.; Bonnet, J.-P.; Phan, T. N.; Bertin, D.; Gigmes, D.; Devaux, D., Single-ion BAB triblock copolymers as highly efficient electrolytes for lithium-metal batteries. *Nat Mater* **2013,** *12* (5), 452.
8. Dou, S.; Zhang, S.; Klein, R. J.; Runt, J.; Colby, R. H., Synthesis and characterization of poly (ethylene glycol)-based single-ion conductors. *Chemistry of Materials* **2006,** *18* (18), 4288-4295.
9. Li, J.; Zhu, H.; Wang, X.; Armand, M.; MacFarlane, D. R.; Forsyth, M., Synthesis of Sodium Poly [4-styrenesulfonyl (trifluoromethylsulfonyl) imide]-co-ethylacrylate] Solid Polymer Electrolytes. *Electrochim Acta* **2015,** *175*, 232-239.
10. Li, Z.; Lu, W.; Zhang, N.; Pan, Q.; Chen, Y.; Xu, G.; Zeng, D.; Zhang, Y.; Cai, W.; Yang, M., Single ion conducting lithium sulfur polymer batteries with improved safety and stability. *J Mater Chem A* **2018,** *6* (29), 14330-14338.
11. Nguyen, H.-D.; Kim, G.-T.; Shi, J.; Paillard, E.; Judeinstein, P.; Lyonnard, S.; Bresser, D.; Iojoiu, C., Nanostructured multi-block copolymer single-ion conductors for safer high-performance lithium batteries. *Energ Environ Sci* **2018,** *11* (11), 3298-3309.
12. Pan, Q.; Li, Z.; Zhang, W.; Zeng, D.; Sun, Y.; Cheng, H., Single ion conducting sodium ion batteries enabled by a sodium ion exchanged poly (bis (4-carbonyl benzene sulfonyl) imide-co-2, 5-diamino benzesulfonic acid) polymer electrolyte. *Solid State Ionics* **2017,** *300*, 60-66.
13. Barpanda, P.; Oyama, G.; Nishimura, S.; Chung, S. C.; Yamada, A., A 3.8-V earth-abundant sodium battery electrode. *Nat Commun* **2014,** *5*, 4358-4366.
14. Leung, P.; Shah, A.; Sanz, L.; Flox, C.; Morante, J.; Xu, Q.; Mohamed, M.; de León, C. P.; Walsh, F., Recent developments in organic redox flow batteries: a critical review. *J Power Sources* **2017,** *360*, 243-283.
15. Chen, R., Toward High-Voltage, Energy-Dense, and Durable Aqueous Organic Redox Flow Batteries: Role of the Supporting Electrolytes. *Chemelectrochem* **2019,** *6* (3), 603-612.

16. Gong, K.; Fang, Q.; Gu, S.; Li, S. F. Y.; Yan, Y., Nonaqueous redox-flow batteries: organic solvents, supporting electrolytes, and redox pairs. *Energ Environ Sci* **2015,** *8* (12), 3515-3530.
17. Small, L. J.; Pratt, H. D.; Fujimoto, C. H.; Anderson, T. M., Diels Alder polyphenylene anion exchange membrane for nonaqueous redox flow batteries. *J Electrochem Soc* **2016,** *163* (1), A5106-A5111.
18. Berthier, C.; Gorecki, W.; Minier, M.; Armand, M. B.; Chabagno, J. M.; Rigaud, P., Microscopic Investigation of Ionic-Conductivity in Alkali-Metal Salts Poly(Ethylene Oxide) Adducts. *Solid State Ionics* **1983,** *11* (1), 91-95.
19. Papke, B. L.; Ratner, M. A.; Shriver, D. F., Vibrational Spectroscopy and Structure of Polymer Electrolytes, Poly(Ethylene Oxide) Complexes of Alkali-Metal Salts. *J Phys Chem Solids* **1981,** *42* (6), 493-500.
20. Petersen, G.; Jacobsson, P.; Torell, L. M., A Raman-Study of Ion Polymer and Ion Ion Interactions in Low-Molecular-Weight Polyether-Licf3so3 Complexes. *Electrochim Acta* **1992,** *37* (9), 1495-1497.
21. Hashmi, S. A.; Chandra, S., Experimental Investigations on a Sodium-Ion-Conducting Polymer Electrolyte Based on Poly(Ethylene Oxide)Complexed with Napf6. *Mat Sci Eng B-Solid* **1995,** *34* (1), 18-26.
22. Moreno, J. S.; Armand, M.; Berman, M. B.; Greenbaum, S. G.; Scrosati, B.; Panero, S., Composite PEOn:NaTFSI polymer electrolyte: Preparation, thermal and electrochemical characterization. *J Power Sources* **2014,** *248*, 695-702.
23. Rao, S. S.; Reddy, M. J.; Reddy, K. N.; Rao, U. V. S., A New Na+ Ion Conducting Polymer Electrolyte Based on (Peo+Nayf4) and Its Use as a Electrochemical-Cell. *Solid State Ionics* **1994,** *74* (3-4), 225-228.
24. Hallinan, D. T.; Balsara, N. P., Polymer Electrolytes. *Annu Rev Mater Res* **2013,** *43*, 503-525.
25. Thaller, L. H., Electrically rechargeable redox flow cell. Google Patents: 1976.
26. Sum, E.; Skyllas-Kazacos, M., A study of the V (II)/V (III) redox couple for redox flow cell applications. *J Power Sources* **1985,** *15* (2-3), 179-190.
27. Self, E. C.; Delnick, F. M.; Ruther, R. E.; Allu, S.; Nanda, J., High-Capacity Organic Radical Mediated Phosphorus Anode for Sodium-Based Redox Flow Batteries. *ACS Energy Lett* **2019,** *4* (11), 2593-2600.
28. Akhil, A. A.; Huff, G.; Currier, A. B.; Kaun, B. C.; Rastler, D. M.; Chen, S. B.; Cotter, A. L.; Bradshaw, D. T.; Gauntlett, W. D. *DOE/EPRI Electricity Storage Handbook in Collaboration with NRECA*; 2015.
29. Shin, S.-H.; Yun, S.-H.; Moon, S.-H., A review of current developments in non-aqueous redox flow batteries: characterization of their membranes for design perspective. *RSC Adv* **2013,** *3* (24), 9095-9116.
30. Darling, R.; Gallagher, K.; Xie, W.; Su, L.; Brushett, F., Transport property requirements for flow battery separators. *J Electrochem Soc* **2015,** *163* (1), A5029-A5040.
31. Chen, L.; Venkatram, S.; Kim, C.; Batra, R.; Chandrasekaran, A.; Ramprasad, R., Electrochemical stability window of polymeric electrolytes. *Chemistry of Materials* **2019,** *31* (12), 4598-4604.

32. Park, H. B.; Kamcev, J.; Robeson, L. M.; Elimelech, M.; Freeman, B. D., Maximizing the right stuff: The trade-off between membrane permeability and selectivity. *Science* **2017,** *356* (6343), 1137-1147.
33. Florjańczyk, Z.; Zygadło-Monikowska, E.; Affek, A.; Tomaszewska, A.; Łasińska, A.; Marzantowicz, M.; Dygas, J.; Krok, F., Polymer electrolytes based on acrylonitrile–butyl acrylate copolymers and lithium bis (trifluoromethanesulfone) imide. *Solid State Ionics* **2005,** *176* (25-28), 2123-2128.
34. Matsumoto, M.; Uno, T.; Kubo, M.; Itoh, T., Polymer electrolytes based on polycarbonates and their electrochemical and thermal properties. *Ionics* **2013,** *19* (4), 615-622.
35. Park, C. H.; Sun, Y.-K.; Kim, D.-W., Blended polymer electrolytes based on poly (lithium 4-styrene sulfonate) for the rechargeable lithium polymer batteries. *Electrochim Acta* **2004,** *50* (2-3), 375-378.
36. Kim, J.-H.; Ryu, S.; Maurya, S.; Lee, J.-Y.; Sung, K.-W.; Lee, J.-S.; Moon, S.-H., Fabrication of a composite anion exchange membrane with aligned ion channels for a high-performance non-aqueous vanadium redox flow battery. *RSC Adv* **2020,** *10* (9), 5010-5025.
37. Cho, E.; Won, J., Novel composite membrane coated with a poly (diallyldimethylammonium chloride)/urushi semi-interpenetrating polymer network for non-aqueous redox flow battery application. *J Power Sources* **2016,** *335*, 12-19.
38. Maurya, S.; Shin, S.-H.; Sung, K.-W.; Moon, S.-H., Anion exchange membrane prepared from simultaneous polymerization and quaternization of 4-vinyl pyridine for non-aqueous vanadium redox flow battery applications. *J Power Sources* **2014,** *255*, 325-334.
39. Tung, S.; Fisher, S. L.; Kotov, N. A.; Thompson, L. T., Nanoporous aramid nanofibre separators for nonaqueous redox flow batteries. *Nat Commun* **2018,** *9* (1), 1-9.
40. Bang, H. S.; Kim, D.; Hwang, S. S.; Won, J., Surface-modified porous membranes with electrospun Nafion/PVA fibres for non-aqueous redox flow battery. *J Membrane Sci* **2016,** *514*, 186-194.
41. Shin, S.-H.; Kim, Y.; Yun, S.-H.; Maurya, S.; Moon, S.-H., Influence of membrane structure on the operating current densities of non-aqueous redox flow batteries: Organic–inorganic composite membranes based on a semi-interpenetrating polymer network. *J Power Sources* **2015,** *296*, 245-254.
42. Gebel, G.; Aldebert, P.; Pineri, M., Swelling study of perfluorosulphonated ionomer membranes. *Polymer* **1993,** *34* (2), 333-339.
43. Doyle, M.; Lewittes, M. E.; Roelofs, M. G.; Perusich, S. A.; Lowrey, R. E., Relationship between ionic conductivity of perfluorinated ionomeric membranes and nonaqueous solvent properties. *J Membrane Sci* **2001,** *184* (2), 257-273.
44. Lee, W.-H.; Park, E. J.; Han, J.; Shin, D. W.; Kim, Y. S.; Bae, C., Poly (terphenylene) anion exchange membranes: the effect of backbone structure on morphology and membrane property. *ACS Macro Lett* **2017,** *6* (5), 566-570.
45. Chen, W. T.; Mandal, M.; Huang, G.; Wu, X. M.; He, G. H.; Kohl, P. A., Highly Conducting Anion-Exchange Membranes Based on Cross-Linked Poly(norbornene): Ring Opening Metathesis Polymerization. *ACS Appl Energ Mater* **2019,** *2* (4), 2458-2468.
46. Jeon, J. Y.; Park, S.; Han, J.; Maurya, S.; Mohanty, A. D.; Tian, D.; Saikia, N.; Hickner, M. A.; Ryu, C. Y.; Tuckerman, M. E.; Paddison, S. J.; Kim, Y. S.; Bae, C., Synthesis of Aromatic

Anion Exchange Membranes by Friedel-Crafts Bromoalkylation and Cross-Linking of Polystyrene Block Copolymers. *Macromolecules* **2019,** *52* (5), 2139-2147.
47. Matsushita, S.; Kim, J.-D., Organic solvent-free preparation of electrolyte membranes with high proton conductivity using aromatic hydrocarbon polymers and small cross-linker molecules. *Solid State Ionics* **2018,** *316*, 102-109.
48. Han, J.; Kim, K.; Kim, J.; Kim, S.; Choi, S.-W.; Lee, H.; Kim, J.-j.; Kim, T.-H.; Sung, Y.-E.; Lee, J.-C., Cross-linked highly sulfonated poly (arylene ether sulfone) membranes prepared by in-situ casting and thiol-ene click reaction for fuel cell application. *J Membrane Sci* **2019,** *579*, 70-78.
49. Shukla, G.; Shahi, V. K., Poly(arylene ether ketone) Copolymer Grafted with Amine Groups Containing a Long Alkyl Chain by Chloroacetylation for Improved Alkaline Stability and Conductivity of Anion Exchange Membrane. *ACS Appl Energ Mater* **2018,** *1* (3), 1175-1182.
50. Doyle, M.; Lewittes, M. E.; Roelofs, M. G.; Perusich, S. A., Ionic conductivity of nonaqueous solvent-swollen ionomer membranes based on fluorosulfonate, fluorocarboxylate, and sulfonate fixed ion groups. *J Phy Chem B* **2001,** *105* (39), 9387-9394.
51. Kraytsberg, A.; Ein-Eli, Y., Review of advanced materials for proton exchange membrane fuel cells. *Energ Fuels* **2014,** *28* (12), 7303-7330.
52. Weiss, R.; Fitzgerald, J.; Kim, D., Viscoelastic behavior of plasticized sulfonated polystyrene ionomers. *Macromolecules* **1991,** *24* (5), 1064-1070.
53. Li, Y.; Sniekers, J.; Malaquias, J. C.; Van Goethem, C.; Binnemans, K.; Fransaer, J.; Vankelecom, I. F., Crosslinked anion exchange membranes prepared from poly (phenylene oxide)(PPO) for non-aqueous redox flow batteries. *J Power Sources* **2018,** *378*, 338-344.
54. Stenina, I.; Sistat, P.; Rebrov, A.; Pourcelly, G.; Yaroslavtsev, A., Ion mobility in Nafion-117 membranes. *Desalination* **2004,** *170* (1), 49-58.
55. Sachan, S.; Ray, C. A.; Perusich, S. A., Lithium ion transport through nonaqueous perfluoroionomeric membranes. *Polymer Eng Sci* **2002,** *42* (7), 1469-1480.
56. Sanginov, E.; Evshchik, E. Y.; Kayumov, R.; Dobrovol'skii, Y. A., Lithium-ion conductivity of the Nafion membrane swollen in organic solvents. *Russian J Electrochem* **2015,** *51* (10), 986-990.
57. Duan, Q.; Wang, H.; Benziger, J., Transport of liquid water through Nafion membranes. *J Membrane Sci* **2012,** *392*, 88-94.
58. Schmidt-Rohr, K.; Chen, Q., Parallel cylindrical water nanochannels in Nafion fuel-cell membranes. *Nat Mater* **2008,** *7* (1), 75-83.
59. Su, L.; Darling, R. M.; Gallagher, K. G.; Xie, W.; Thelen, J. L.; Badel, A. F.; Barton, J. L.; Cheng, K. J.; Balsara, N. P.; Moore, J. S., An investigation of the ionic conductivity and species crossover of lithiated nafion 117 in nonaqueous electrolytes. *J Electrochem Soc* **2016,** *163* (1), A5253-A5262.
60. Escalante-García, I. L.; Wainright, J. S.; Thompson, L. T.; Savinell, R. F., Performance of a non-aqueous vanadium acetylacetonate prototype redox flow battery: examination of separators and capacity decay. *J Electrochem Soc* **2014,** *162* (3), A363-A373.
61. Elmore, C. T.; Seidler, M. E.; Ford, H. O.; Merrill, L. C.; Upadhyay, S. P.; Schneider, W. F.; Schaefer, J. L., Ion transport in solvent-free, crosslinked, single-ion conducting polymer electrolytes for post-lithium ion batteries. *Batteries* **2018,** *4* (2), 28-45.

62. Lou, K., Characterization Techniques and Cation Exchange Membrane for Non-aqueous Redox Flow Battery. *Doctorate thesis* **2021,** *University of Tennessee*.
63. Jing, M.; Wei, Z.; Su, W.; He, H.; Fan, X.; Qin, Y.; Liu, J.; Yan, C., Improved electrochemical performance for vanadium flow battery by optimizing the concentration of the electrolyte. *J Power Sources* **2016,** *324*, 215-223.
64. Tang, Z.; Lawton, J. S.; Sun, C.-N.; Chen, J.; Bright, M. I.; Jones, A. M.; Papandrew, A. B.; Fujimoto, C. H.; Zawodzinski, T. A., Characterization of sulfonated Diels-Alder poly (phenylene) membranes for electrolyte separators in vanadium redox flow batteries. *J Electrochem Soc* **2014,** *161* (12), A1860-A1868.
65. McCormack, P. M.; Luo, H.; Geise, G. M.; Koenig Jr, G. M., Conductivity, permeability, and stability properties of chemically tailored poly (phenylene oxide) membranes for Li+ conductive non-aqueous redox flow battery separators. *J Power Sources* **2020,** *460*, 228107-228117.
66. Kim, D.-H.; Seo, S.-J.; Lee, M.-J.; Park, J.-S.; Moon, S.-H.; Kang, Y. S.; Choi, Y.-W.; Kang, M.-S., Pore-filled anion-exchange membranes for non-aqueous redox flow batteries with dual-metal-complex redox shuttles. *J Membrane Sci* **2014,** *454*, 44-50.
67. Kamcev, J.; Paul, D. R.; Manning, G. S.; Freeman, B. D., Accounting for frame of reference and thermodynamic non-idealities when calculating salt diffusion coefficients in ion exchange membranes. *J Membrane Sci* **2017,** *537*, 396-406.
68. Seo, S.-J.; Kim, B.-C.; Sung, K.-W.; Shim, J.; Jeon, J.-D.; Shin, K.-H.; Shin, S.-H.; Yun, S.-H.; Lee, J.-Y.; Moon, S.-H., Electrochemical properties of pore-filled anion exchange membranes and their ionic transport phenomena for vanadium redox flow battery applications. *J Membrane Sci* **2013,** *428*, 17-23.
69. Chai, J.; Lashgari, A.; Cao, Z.; Williams, C. K.; Wang, X.; Dong, J.; Jiang, J. J., PEGylation-Enabled Extended Cyclability of a Non-aqueous Redox Flow Battery. *ACS Appl Mater Inter* **2020,** *12* (13), 15262-15270.
70. Mushtaq, K.; Lagarteira, T.; Zaidi, A. A.; Mendes, A., In-situ crossover diagnostics to assess membrane efficacy for non-aqueous redox flow battery. *J Energy Stor* **2021,** *40*, 102713-102723.
71. McCormack, P. M.; Koenig Jr, G. M.; Geise, G. M., Thermodynamic Interactions as a Descriptor of Cross-Over in Nonaqueous Redox Flow Battery Membranes. *ACS Appl Mater Inter* **2021,** *13* (41), 49331-49339.
72. Kim, D.; Song, J.; Won, J., Structural effects of anion exchange composite membranes in non-aqueous redox flow batteries. *J Membrane Sci* **2018,** *564*, 523-531.
73. Maier, G.; Meier-Haack, J., Sulfonated aromatic polymers for fuel cell membranes. *Fuel cells II* **2008**, (Springer).
74. Lehmann, M. L.; Yang, G.; Gilmer, D.; Han, K. S.; Self, E. C.; Ruther, R. E.; Ge, S.; Li, B.; Murugesan, V.; Sokolov, A. P.; Delnick, F. M.; Nanda, J.; Saito, T., Tailored Crosslinking of Poly (Ethylene Oxide) Enables Mechanical Robustness and Improved Sodium-Ion Conductivity. *Energy Stor Mater* **2019,** *21*, 85-96.
75. Hallinan Jr, D. T.; Mullin, S. A.; Stone, G. M.; Balsara, N. P., Lithium metal stability in batteries with block copolymer electrolytes. *J Electrochem Soc* **2013,** *160* (3), A464-A470.

76. Truong, P. V.; Shingleton, S.; Kammoun, M.; Black, R. L.; Charendoff, M.; Willis, C.; Ardebili, H.; Stein, G. E., Structure and properties of sulfonated pentablock terpolymer films as a function of wet–dry cycles. *Macromolecules* **2018,** *51* (6), 2203-2215.
77. Mandal, M.; Huang, G.; Kohl, P. A., Highly Conductive Anion-Exchange Membranes Based on Cross-Linked Poly(norbornene): Vinyl Addition Polymerization. *ACS Appl Energ Mater* **2019,** *2* (4), 2447-2457.
78. Jung, J.; Won, J.; Hwang, S. S., Highly selective composite membranes using ladder-like structured polysilsesquioxane for a non-aqueous redox flow battery. *J Membrane Sci* **2020,** *595*, 117520-117530.
79. Wang, T.; Wang, X.; Pendse, A.; Gao, Y.; Wang, K.; Bae, C.; Kim, S., High-efficient multifunctional electrochemical membrane for lithium polysulfide redox flow batteries. *J Membrane Sci* **2021**, 119539-119548.
80. Kalnaus, S.; Wang, Y.; Turner, J. A., Mechanical behavior and failure mechanisms of Li-ion battery separators. *J Power Sources* **2017,** *348*, 255-263.
81. Bamgbopa, M. O.; Shao-Horn, Y.; Almheiri, S., The potential of non-aqueous redox flow batteries as fast-charging capable energy storage solutions: demonstration with an iron–chromium acetylacetonate chemistry. *J Mater Chem A* **2017,** *5* (26), 13457-13468.
82. Chen, X. C.; Zhang, Y.; Merrill, L. C.; Soulen, C.; Lehmann, M. L.; Schaefer, J. L.; Du, Z.; Saito, T.; Dudney, N. J., Gel composite electrolyte–an effective way to utilize ceramic fillers in lithium batteries. *J Mater Chem A* **2021,** *9* (10), 6555-6566.
83. Darling, R. M.; Gallagher, K. G.; Kowalski, J. A.; Ha, S.; Brushett, F. R., Pathways to low-cost electrochemical energy storage: a comparison of aqueous and nonaqueous flow batteries. *Energ Environ Sci* **2014,** *7* (11), 3459-3477.
84. Dmello, R.; Milshtein, J. D.; Brushett, F. R.; Smith, K. C., Cost-driven materials selection criteria for redox flow battery electrolytes. *J Power Sources* **2016,** *330*, 261-272.
85. Crawford, A.; Thomsen, E.; Reed, D.; Stephenson, D.; Sprenkle, V.; Liu, J.; Viswanathan, V., Development and validation of chemistry agnostic flow battery cost performance model and application to nonaqueous electrolyte systems. *International Journal of Energy Research* **2016,** *40* (12), 1611-1623.
86. Park, E. J.; Kim, Y. S., Quaternized aryl ether-free polyaromatics for alkaline membrane fuel cells: synthesis, properties, and performance - a topical review. *J Mater Chem A* **2018,** *6* (32), 15456-15477.
87. Wang, J. H.; Zhao, Y.; Setzler, B. P.; Rojas-Carbonell, S.; Ben Yehuda, C.; Amel, A.; Page, M.; Wang, L.; Hu, K.; Shi, L.; Gottesfeld, S.; Xu, B. J.; Yan, Y. S., Poly(aryl piperidinium) membranes and ionomers for hydroxide exchange membrane fuel cells. *Nat Energy* **2019,** *4* (5), 392-398.
88. Bai, H.; Peng, H.; Xiang, Y.; Zhang, J.; Wang, H.; Lu, S.; Zhuang, L., Poly (arylene piperidine) s with phosphoric acid doping as high temperature polymer electrolyte membrane for durable, high-performance fuel cells. *J Power Sources* **2019,** *443*, 227219-227228.
89. Sun, C.-N.; Mench, M.; Zawodzinski, T., High performance redox flow batteries: an analysis of the upper performance limits of flow batteries using non-aqueous solvents. *Electrochim Acta* **2017,** *237*, 199-206.
90. Gong, S. J.; Kim, D.; Cho, E.; Hwang, S. S.; Won, J., A chitosan/urushi anion exchange membrane for a non–aqueous redox flow battery. *ChemistrySelect* **2017,** *2* (5), 1843-1849.

91. Li, Y. M.; Lu, Y. X.; Zhao, C. L.; Hu, Y. S.; Titirici, M. M.; Li, H.; Huang, X. J.; Chen, L. Q., Recent advances of electrode materials for low-cost sodium-ion batteries towards practical application for grid energy storage. *Energy Storage Mater* **2017,** *7*, 130-151.
92. Goodenough, J. B., Energy storage materials: A perspective. *Energy Storage Mater* **2015,** *1*, 158-161.
93. Che, H. Y.; Chen, S. L.; Xie, Y. Y.; Wang, H.; Amine, K.; Liao, X. Z.; Ma, Z. F., Electrolyte design strategies and research progress for room-temperature sodium-ion batteries. *Energ Environ Sci* **2017,** *10* (5), 1075-1101.
94. Palomares, V.; Serras, P.; Villaluenga, I.; Hueso, K. B.; Carretero-Gonzalez, J.; Rojo, T., Na-ion batteries, recent advances and present challenges to become low cost energy storage systems. *Energ Environ Sci* **2012,** *5* (3), 5884-5901.
95. Wang, Q. S.; Ping, P.; Zhao, X. J.; Chu, G. Q.; Sun, J. H.; Chen, C. H., Thermal runaway caused fire and explosion of lithium ion battery. *J Power Sources* **2012,** *208*, 210-224.
96. Carbone, L.; Gobet, M.; Peng, J.; Devany, M.; Scrosati, B.; Greenbaum, S.; Hassoun, J., Comparative Study of Ether-Based Electrolytes for Application in Lithium-Sulfur Battery. *ACS Appl Mater Inter* **2015,** *7* (25), 13859-13865.
97. Chandrasekaran, R.; Mangani, I. R.; Vasanthi, R.; Selladurai, S., Conductivity Studies on PEO:NaClO3 Electrolyte System With Different Plasticizers. *Ionics* **2001,** *7* (1-2), 94-100.
98. Pradhan, D. K.; Samantaray, B. K.; Choudhary, R. N. P.; Karan, N. K.; Thomas, R.; Katiyar, R. S., Effect of plasticizer on structural and electrical properties of nanocomposite solid polymer electrolytes. *Ionics* **2011,** *17* (2), 127-134.
99. Ruther, R. E.; Yang, G.; Delnick, F. M.; Tang, Z. J.; Lehmann, M. L.; Saito, T.; Meng, Y. J.; Zawodzinski, T. A. J.; Nanda, J., Mechanically Robust, Sodium-Ion Conducting Membranes for Nonaqueous Redox Flow Batteries. *ACS Energy Lett* **2018,** *3* (7), 1640-1647.
100. Khurana, R.; Schaefer, J. L.; Archer, L. A.; Coates, G. W., Suppression of Lithium Dendrite Growth Using Cross-Linked Polyethylene/Poly(ethylene oxide) Electrolytes: A New Approach for Practical Lithium-Metal Polymer Batteries. *J Am Chem Soc* **2014,** *136* (20), 7395-7402.
101. Luo, D.; Li, Y.; Yang, M. J., Crosslinked poly(acrylonitrile-glycidyl methacrylate) as a novel gel polymer electrolyte. *Mater Chem Phys* **2011,** *125* (1-2), 231-235.
102. Porcarelli, L.; Gerbaldi, C.; Bella, F.; Nair, J. R., Super Soft All-Ethylene Oxide Polymer Electrolyte for Safe All-Solid Lithium Batteries. *Sci Rep-Uk* **2016,** *6*, 1-14.
103. Chaudoy, V.; Van, F. T.; Deschamps, M.; Ghamouss, F., Ionic liquids in a poly ethylene oxide cross-linked gel polymer as an electrolyte for electrical double layer capacitor. *Journal of Power Sources* **2017,** *342*, 872-878.
104. Tsao, C.-H.; Hsiao, Y.-H.; Hsu, C.-H.; Kuo, P.-L., Stable lithium deposition generated from ceramic-cross-linked gel polymer electrolytes for lithium anode. *ACS applied materials & interfaces* **2016,** *8* (24), 15216-15224.
105. Lenest, J. F.; Callens, S.; Gandini, A.; Armand, M., A New Polymer Network for Ionic-Conduction. *Electrochim Acta* **1992,** *37* (9), 1585-1588.
106. Sun, X. G.; Reeder, C. L.; Kerr, J. B., Synthesis and characterization of network type single ion conductors. *Macromolecules* **2004,** *37* (6), 2219-2227.

107. Watanabe, M.; Nishimoto, A., Effects of Network Structures and Incorporated Salt Species on Electrochemical Properties of Polyether-Based Polymer Electrolytes. *Solid State Ionics* **1995,** *79*, 306-312.
108. Aihara, Y.; Kuratomi, J.; Bando, T.; Iguchi, T.; Yoshida, H.; Ono, T.; Kuwana, K., Investigation on solvent-free solid polymer electrolytes for advanced lithium batteries and their performance. *J Power Sources* **2003,** *114* (1), 96-104.
109. Gao, H. C.; Zhou, W. D.; Park, K.; Goodenough, J. B., A Sodium-Ion Battery with a Low-Cost Cross-Linked Gel-Polymer Electrolyte. *Adv Energy Mater* **2016,** *6* (18), 1-8.
110. Colo, F.; Bella, F.; Nair, J. R.; Gerbaldi, C., Light-cured polymer electrolytes for safe, low-cost and sustainable sodium-ion batteries. *J Power Sources* **2017,** *365*, 293-302.
111. Bella, F.; Colo, F.; Nair, J. R.; Gerbaldi, C., Photopolymer Electrolytes for Sustainable, Upscalable, Safe, and Ambient-Temperature Sodium-Ion Secondary Batteries. *ChemSusChem* **2015,** *8* (21), 3668-3676.
112. Seh, Z. W.; Sun, J.; Sun, Y. M.; Cui, Y., A Highly Reversible Room-Temperature Sodium Metal Anode. *ACS Central Sci* **2015,** *1* (8), 449-455.
113. Nogueira, V. C., Longo, C., Nogueira, A.F., Solid-state dye-sensitized solar cell: improved performance and stability using a plasticized polymer electrolyte. *Journal of Photochemistry and Photobiology A: Chemistry* **2006,** *181*, 226-232.
114. Carper, W. R.; Keller, C. E., Direct Determination of NMR Correlation Times from Spin−Lattice and Spin−Spin Relaxation Times. *The Journal of Physical Chemistry A* **1997,** *101* (18), 3246-3250.
115. Carper, W. R.; Mains, G. J.; Piersma, B. J.; Mansfield, S. L.; Larive, C. K., 13C NMR Relaxation and 1H Diffusion (DOSY) Studies of an Acidic Chloroaluminate Melt. *The Journal of Physical Chemistry* **1996,** *100* (12), 4724-4728.
116. Shannon, R., Revised effective ionic radii and systematic studies of interatomic distances in halides and chalcogenides. *Acta Crystallographica Section A* **1976,** *32* (5), 751-767.
117. Johansson, P., Electronic structure calculations on lithium battery electrolyte salts. *Phys. Chem. Chem. Phys.* **2007,** *9* (12), 1493-1498.
118. He, R. X.; Kyu, T., Effect of Plasticization on Ionic Conductivity Enhancement in Relation to Glass Transition Temperature of Crosslinked Polymer Electrolyte Membranes. *Macromolecules* **2016,** *49* (15), 5637-5648.
119. Kriz, J.; Abbrent, S.; Dybal, J.; Kurkova, D.; Lindgren, J.; Tegenfeldt, J.; Wendsjo, A., Nature and dynamics of lithium ion coordination in oligo(ethylene glycol) dimethacrylate-solvent systems: NMR, Raman, and quantum mechanical study. *J Phys Chem A* **1999,** *103* (42), 8505-8515.
120. Kim, J. K.; Lim, Y. J.; Kim, H.; Cho, G. B.; Kim, Y., A hybrid solid electrolyte for flexible solid-state sodium batteries. *Energ Environ Sci* **2015,** *8* (12), 3589-3596.
121. Hallinan, D. T.; Villaluenga, I.; Balsara, N. P., Polymer and composite electrolytes. *MRS Bull* **2018,** *43* (10), 759-767.
122. Paranjape, N.; Mandadapu, P. C.; Wu, G.; Lin, H. Q., Highly-branched cross-linked poly(ethylene oxide) with enhanced ionic conductivity. *Polymer* **2017,** *111*, 1-8.
123. Thiam, A.; Antonelli, C.; Iojoiu, C.; Alloin, F.; Sanchez, J. Y., Optimizing ionic conduction of poly(oxyethylene) electrolytes through controlling the cross-link density. *Electrochim Acta* **2017,** *240*, 307-315.

124. Zheng, Q.; Ma, L.; Khurana, R.; Archer, L. A.; Coates, G. W., Structure-property study of cross-linked hydrocarbon/poly(ethylene oxide) electrolytes with superior conductivity and dendrite resistance. *Chem Sci* **2016,** *7* (11), 6832-6838.
125. Pradhan, D. K.; Samantaray, B. K.; Choudhary, R. N. P.; Thakur, A. K., Effect of plasticizer on structure - property relationship in composite polymer electrolytes. *J Power Sources* **2005,** *139* (1-2), 384-393.
126. Ma, Q.; Liu, J. J.; Qi, X. G.; Rong, X. H.; Shao, Y. J.; Feng, W. F.; Nie, J.; Hu, Y. S.; Li, H.; Huang, X. J.; Chen, L. Q.; Zhou, Z. B., A new Na[(FSO2)(n-C4F9SO2)N]-based polymer electrolyte for solid-state sodium batteries. *J Mater Chem A* **2017,** *5* (17), 7738-7743.
127. Alloin, F.; Sanchez, J. Y.; Armand, M., Electrochemical-Behavior of Lithium Electrolytes Based on New Polyether Networks. *J Electrochem Soc* **1994,** *141* (7), 1915-1920.
128. Evans, J.; Vincent, C. A.; Bruce, P. G., Electrochemical Measurement of Transference Numbers in Polymer Electrolytes. *Polymer* **1987,** *28* (13), 2324-2328.
129. Pandian, A. S.; Chen, X. C.; Chen, J. H.; Lokitz, B. S.; Ruther, R. E.; Yang, G.; Lou, K.; Nanda, J.; Delnick, F. M.; Dudney, N. J., Facile and scalable fabrication of polymer-ceramic composite electrolyte with high ceramic loadings. *J Power Sources* **2018,** *390*, 153-164.
130. Chintapalli, M.; Timachova, K.; Olson, K. R.; Mecham, S. J.; Devaux, D.; DeSimone, J. M.; Balsara, N. P., Relationship between Conductivity, Ion Diffusion, and Transference Number in Perfluoropolyether Electrolytes. *Macromolecules* **2016,** *49* (9), 3508-3515.
131. Ma, C. M.; Mao, Z. P.; Zhou, J.; Yan, J., A Drift Chamber with Uniform Electric-Field and Measurements of the Electron-Drift Velocity. *Chinese Phys* **1985,** *5* (3), 664-668.
132. Dong, H. T.; Hyun, J. K.; Rhodes, C. P.; Frech, R.; Wheeler, R. A., Molecular Dynamics Simulations and Vibrational Spectroscopic Studies of Local Structure in Tetraglyme : Sodium Triflate ($CH_3O(CH_2CH_2O)_4CH_3$: $NaCF_3SO_3$) solutions. *J. Phys. Chem. B* **2002,** *106* (18), 4878-4885.
133. Frech, R.; Rhodes, C. P.; York, S. S., A comparative study of ionic association in poly(ethylene oxide)-MCF3SO3 systems (M=lithium and sodium). In *Solid State Ionics V*, Nazri, G. A.; Julien, C.; Rougier, A., Eds. Materials Research Society: Warrendale, 1999; Vol. 548, pp 335-345.
134. Manning, J.; Frech, R., The Structure of Associated Ionic Species in Poly(Propylene Oxide) Alkali-Metal Trifluoromethanesulfonate Complexes. *Polymer* **1992,** *33* (16), 3487-3494.
135. Rhodes, C. P.; Frech, R., Cation-anion and cation-polymer interactions in (PEO)(n)NaCF3SO3 (n=1-80). *Solid State Ionics* **1999,** *121* (1-4), 91-99.
136. Rhodes, C. P.; Khan, M.; Frech, R., Crystalline phases of poly(ethylene oxide) oligomers and sodium triflate: Changes in coordination and conformation with chain length. *J Phys Chem B* **2002,** *106* (40), 10330-10337.
137. Torell, L. M.; Jacobsson, P.; Petersen, G., A Raman study of ion solvation and association in polymer electrolytes. *Polmers for advanced technologies* **1993,** *4* (2-3), 152-163.
138. Shim, J.; Kim, L.; Kim, H. J.; Jeong, D.; Lee, J. H.; Lee, J. C., All-solid-state lithium metal battery with solid polymer electrolytes based on polysiloxane crosslinked by modified natural gallic acid. *Polymer* **2017,** *122*, 222-231.
139. Kang, Y. K.; Cheong, K.; Noh, K. A.; Lee, C.; Seung, D. Y., A study of cross-linked PEO gel polymer electrolytes using bisphenol A ethoxylate diacrylate: ionic conductivity and mechanical properties. *J Power Sources* **2003,** *119*, 432-437.

140. Kim, G. T.; Appetecchi, G. B.; Carewska, M.; Joost, M.; Balducci, A.; Winter, M.; Passerini, S., UV cross-linked, lithium-conducting ternary polymer electrolytes containing ionic liquids. *J Power Sources* **2010,** *195* (18), 6130-6137.
141. Rupp, B.; Schmuck, M.; Balducci, A.; Winter, M.; Kern, W., Polymer electrolyte for lithium batteries based on photochemically crosslinked poly(ethylene oxide) and ionic liquid. *Eur Polym J* **2008,** *44* (9), 2986-2990.
142. Daigle, J. C.; Asakawa, Y.; Vijh, A.; Hovington, P.; Armand, M.; Zaghib, K., Exceptionally stable polymer electrolyte for a lithium battery based on cross-linking by a residue-free process. *J Power Sources* **2016,** *332*, 213-221.
143. Chiang, C. K.; Davis, G. T.; Harding, C. A.; Takahashi, T., Polymeric Electrolyte Based on Poly(Ethylene Imine) and Lithium-Salts. *Solid State Ionics* **1986,** *18-9*, 300-305.
144. Harris, C. S.; Shriver, D. F.; Ratner, M. A., Complex-Formation of Poly(Ethylenimine) with Sodium Triflate and Conductivity Behavior of the Complexes. *Macromolecules* **1986,** *19* (4), 987-989.
145. Paul, J. L.; Jegat, C.; Lassegues, J. C., Branched Poly(Ethyleneimine)-Cf3so3li Complexes. *Electrochim Acta* **1992,** *37* (9), 1623-1625.
146. Chen, Y.; Shi, Y.; Liang, Y.; Dong, H.; Hao, F.; Wang, A.; Zhu, Y.; Cui, X.; Yao, Y., Hyperbranched PEO-Based Hyperstar Solid Polymer Electrolytes with Simultaneous Improvement of Ion Transport and Mechanical Strength. *ACS Appl Energ Mater* **2019,** *2* (3), 1608-1615.
147. Lee, S.-I.; Schömer, M.; Peng, H.; Page, K. A.; Wilms, D.; Frey, H.; Soles, C. L.; Yoon, D. Y., Correlations between ion conductivity and polymer dynamics in hyperbranched poly (ethylene oxide) electrolytes for lithium-ion batteries. *Chemistry of Materials* **2011,** *23* (11), 2685-2688.
148. Xu, P. Y.; Guo, T. Y.; Zhao, C. H.; Broadwell, I.; Zhang, Q. G.; Liu, Q. L., Anion exchange membranes based on poly(vinyl alcohol) and quaternized polyethyleneimine for direct methanol fuel cells. *J Appl Polym Sci* **2013,** *128* (6), 3853-3860.
149. Zuo, D. Y.; Gong, Y. J.; Yan, Q. L.; Zhang, H. W., Preparation and characterization of hydroxyl ion-conducting interpenetrating polymer network based on PVA and PEI. *J Polym Res* **2016,** *23* (7), 126-132.
150. Min, S.; Kim, D., SAXS cluster structure and properties of sPEEK/PEI composite membranes for DMFC applications. *Solid State Ionics* **2010,** *180* (40), 1690-1693.
151. Tanaka, R.; Sakurai, M.; Sekiguchi, H.; Inoue, M., Improvement of room-temperature conductivity and thermal stability of PEO-LiClO4 systems by addition of a small proportion of polyethylenimine. *Electrochim Acta* **2003,** *48* (14-16), 2311-2316.
152. Tanaka, R.; Sakurai, M.; Sekiguchi, H.; Mori, H.; Murayama, T.; Ooyama, T., Lithium ion conductivity in polyoxyethylene/polyethylenimine blends. *Electrochim Acta* **2001,** *46* (10-11), 1709-1715.
153. Jung, Y. J.; Kim, S., New approaches to improve cycle life characteristics of lithium-sulfur cells. *Electrochem Commun* **2007,** *9* (2), 249-254.
154. Zhou, J.; Ji, H.; Liu, J.; Qian, T.; Yan, C., A new high ionic conductive gel polymer electrolyte enables highly stable quasi-solid-state lithium sulfur battery. *Energy Stor Mater* **2019,** *22*, 256-264.

155. Krauklis, A.; Echtermeyer, A., Mechanism of yellowing: Carbonyl formation during hygrothermal aging in a common amine epoxy. *Polymers* **2018,** *10* (9), 1017-1032.
156. Rosu, D.; Rosu, L.; Cascaval, C. N., IR-change and yellowing of polyurethane as a result of UV irradiation. *Polymer Degradation and Stability* **2009,** *94* (4), 591-596.
157. Khurana, R.; Schaefer, J. L.; Archer, L. A.; Coates, G. W., Suppression of lithium dendrite growth using cross-linked polyethylene/poly (ethylene oxide) electrolytes: a new approach for practical lithium-metal polymer batteries. *Journal of the American Chemical Society* **2014,** *136* (20), 7395-7402.
158. Pan, Q.; Smith, D. M.; Qi, H.; Wang, S.; Li, C. Y., Hybrid electrolytes with controlled network structures for lithium metal batteries. *Advanced Materials* **2015,** *27* (39), 5995-6001.
159. Wu, H.; Zhang, X. F.; Xu, D.; Li, B.; Jiang, Z. Y., Enhancing the interfacial stability and solvent-resistant property of PDMS/PES composite membrane by introducing a bifunctional aminosilane. *J Membrane Sci* **2009,** *337* (1-2), 61-69.
160. Lutkenhaus, J. L.; Olivetti, E. A.; Verploegen, E. A.; Cord, B. M.; Sadoway, D. R.; Hammond, P. T., Anisotropic structure and transport in self-assembled layered polymer-clay nanocomposites. *Langmuir* **2007,** *23* (16), 8515-8521.
161. Qian, M. B.; Sun, Y. Q.; Xu, X. D.; Liu, L. N.; Song, P. A.; Yu, Y. M.; Wang, H.; Qian, J., 2D-alumina platelets enhance mechanical and abrasion properties of PA612 via interfacial hydrogen-bond interactions. *Chem Eng J* **2017,** *308*, 760-771.
162. Phua, S. L.; Yang, L.; Toh, C. L.; Huang, S.; Tsakadze, Z.; Lau, S. K.; Mai, Y. W.; Lu, X. H., Reinforcement of Polyether Polyurethane with Dopamine-Modified Clay: The Role of Interfacial Hydrogen Bonding. *Acs Appl Mater Inter* **2012,** *4* (9), 4571-4578.
163. York, S.; Frech, R.; Snow, A.; Glatzhofer, D., A comparative vibrational spectroscopic study of lithium triflate and sodium triflate in linear poly (ethylenimine). *Electrochim Acta* **2001,** *46* (10-11), 1533-1537.
164. York, S. S.; Buckner, M.; Frech, R., Ion− Polymer and Ion− Ion Interactions in Linear Poly (ethylenimine) Complexed with LiCF3SO3 and LiSbF6. *Macromolecules* **2004,** *37* (3), 994-999.
165. Shi, Y.; Chen, Y.; Liang, Y.; Andrews, J.; Dong, H.; Yuan, M.; Ding, W.; Banerjee, S.; Ardebili, H.; Robertson, M. L., Chemically inert covalently networked triazole-based solid polymer electrolytes for stable all-solid-state lithium batteries. *J Mater Chem A* **2019,** *7* (34), 19691-19695.
166. He, R.; Echeverri, M.; Ward, D.; Zhu, Y.; Kyu, T., Highly conductive solvent-free polymer electrolyte membrane for lithium-ion batteries: Effect of prepolymer molecular weight. *J Membrane Sci* **2016,** *498*, 208-217.
167. Hong, T.; Cao, P.-F.; Zhao, S.; Li, B.; Smith, C.; Lehmann, M.; Erwin, A. J.; Mahurin, S. M.; Venna, S. R.; Sokolov, A. P.; Saito, T., Tailored CO2-philic Gas Separation Membranes via One-Pot Thiol–ene Chemistry. *Macromolecules* **2019,** *52*, 5819-5828.
168. Klongkan, S.; Pumchusak, J., Effects of nano alumina and plasticizers on morphology, ionic conductivity, thermal and mechanical properties of PEO-LiCF3SO3 solid polymer electrolyte. *Electrochim Acta* **2015,** *161*, 171-176.
169. Xu, X. R.; Xu, J. T.; Feng, L. X., Tensile behaviour of homogeneous ethylene copolymers. *Polymer international* **2002,** *51* (5), 458-463.

170. Boschin, A.; Johansson, P., Characterization of NaX (X: TFSI, FSI)–PEO based solid polymer electrolytes for sodium batteries. *Electrochim Acta* **2015,** *175*, 124-133.
171. Ruther, R. E.; Yang, G.; Delnick, F. M.; Tang, Z.; Lehmann, M. L.; Saito, T.; Meng, Y.; Zawodzinski Jr, T. A.; Nanda, J., Mechanically Robust, Sodium-Ion Conducting Membranes for Nonaqueous Redox Flow Batteries. *ACS Energy Letters* **2018,** *3* (7), 1640-1647.
172. Seo, D. M.; Boyle, P. D.; Sommer, R. D.; Daubert, J. S.; Borodin, O.; Henderson, W. A., Solvate structures and spectroscopic characterization of LiTFSI electrolytes. *The Journal of Physical Chemistry B* **2014,** *118* (47), 13601-13608.
173. Geise, G. M.; Freeman, B. D.; Paul, D. R., Sodium chloride diffusion in sulfonated polymers for membrane applications. *J Membrane Sci* **2013,** *427*, 186-196.
174. Bouchet, R.; Maria, S.; Meziane, R.; Aboulaich, A.; Lienafa, L.; Bonnet, J. P.; Phan, T. N. T.; Bertin, D.; Gigmes, D.; Devaux, D.; Denoyel, R.; Armand, M., Single-ion BAB triblock copolymers as highly efficient electrolytes for lithium-metal batteries. *Nat Mater* **2013,** *12* (5), 452-457.
175. Porcarelli, L.; Shaplov, A. S.; Bella, F.; Nair, J. R.; Mecerreyes, D.; Gerbaldi, C., Single-ion conducting polymer electrolytes for lithium metal polymer batteries that operate at ambient temperature. *ACS Energy Lett* **2016,** *1* (4), 678-682.
176. Tang, S.; Zhao, H., Glymes as versatile solvents for chemical reactions and processes: from the laboratory to industry. *RSC Adv* **2014,** *4* (22), 11251-11287.
177. Chernyak, Y., Dielectric constant, dipole moment, and solubility parameters of some cyclic acid esters. *J Chem Eng Data* **2006,** *51* (2), 416-418.
178. Kamcev, J.; Sujanani, R.; Jang, E.-S.; Yan, N.; Moe, N.; Paul, D. R.; Freeman, B. D., Salt concentration dependence of ionic conductivity in ion exchange membranes. *J Membrane Sci* **2018,** *547*, 123-133.
179. Saito, T.; Mather, B. D.; Costanzo, P. J.; Beyer, F. L.; Long, T. E., Influence of site-specific sulfonation on acrylic graft copolymer morphology. *Macromolecules* **2008,** *41* (10), 3503-3512.
180. Liu, J.; Pickett, P. D.; Park, B.; Upadhyay, S. P.; Orski, S. V.; Schaefer, J. L., Non-solvating, side-chain polymer electrolytes as lithium single-ion conductors: synthesis and ion transport characterization. *Polymer Chemistry* **2020,** *11* (2), 461-471.
181. Zheng, W.; Cornelius, C., Solvent tunable multi-block ionomer morphology and its relationship to modulus, water swelling, directionally dependent ion transport, and actuator performance. *Polymer* **2016,** *103*, 104-111.
182. Huang, F.; Largier, T. D.; Zheng, W.; Cornelius, C. J., Pentablock copolymer morphology dependent transport and its impact upon film swelling, proton conductivity, hydrogen fuel cell operation, vanadium flow battery function, and electroactive actuator performance. *J Membrane Sci* **2018,** *545*, 1-10.
183. Truong, P. V.; Black, R. L.; Coote, J. P.; Lee, B.; Ardebili, H.; Stein, G. E., Systematic Approaches To Tailor the Morphologies and Transport Properties of Solution-Cast Sulfonated Pentablock Copolymers. *ACS Applied Polymer Materials* **2018,** *1* (1), 8-17.
184. Chintapalli, M.; Chen, X. C.; Thelen, J. L.; Teran, A. A.; Wang, X.; Garetz, B. A.; Balsara, N. P., Effect of grain size on the ionic conductivity of a block copolymer electrolyte. *Macromolecules* **2014,** *47* (15), 5424-5431.

185. Puleo, A.; Muruganandam, N.; Paul, D., Gas sorption and transport in substituted polystyrenes. *Journal of Polymer Science Part B: Polymer Physics* **1989,** *27* (11), 2385-2406.
186. Jangu, C.; Savage, A. M.; Zhang, Z.; Schultz, A. R.; Madsen, L. A.; Beyer, F. L.; Long, T. E., Sulfonimide-containing triblock copolymers for improved conductivity and mechanical performance. *Macromolecules* **2015,** *48* (13), 4520-4528.
187. Saito, T.; Moore, H. D.; Hickner, M. A., Synthesis of midblock-sulfonated triblock copolymers. *Macromolecules* **2010,** *43* (2), 599-601.
188. Eisenberg, A.; Kim, J.-S., *Introduction to ionomers*. Wiley: 1998.
189. Willis, C. L.; Handlin Jr, D. L.; Trenor, S. R.; Mather, B. D., Sulfonated block copolymers, method for making same, and various uses for such block copolymers. Google Patents: 2010.
190. Kraton, Nexar Polymers. *https://www.kraton.com/products/pdf/NEXAR_brochure.pdf* **2014,** *last accessed Nov. 14 2021*.
191. Uhrig, D.; Schlegel, R.; Weidisch, R.; Mays, J., Multigraft copolymer superelastomers: Synthesis morphology, and properties. *Eur Polym J* **2011,** *47* (4), 560-568.
192. Galanos, E.; Grune, E.; Wahlen, C.; Müller, A. H.; Appold, M.; Gallei, M.; Frey, H.; Floudas, G., Tapered multiblock copolymers based on isoprene and 4-methylstyrene: influence of the tapered interface on the self-assembly and thermomechanical properties. *Macromolecules* **2019,** *52* (4), 1577-1588.
193. Yang, G.; Lehmann, M. L.; Zhao, S.; Li, B.; Ge, S.; Cao, P.-F.; Delnick, F. M.; Sokolov, A. P.; Saito, T.; Nanda, J., Anomalously High Elastic Modulus of a Poly (ethylene oxide)-Based Composite Electrolyte. *Energy Stor Mater* **2020,** *35*, 431-442.
194. Geise, G. M.; Falcon, L. P.; Freeman, B. D.; Paul, D. R., Sodium chloride sorption in sulfonated polymers for membrane applications. *J Membrane Sci* **2012,** *423*, 195-208.
195. Xin, N.; Sun, Y.; Radke, C. J.; Prausnitz, J. M., Osmotic and activity coefficients for five lithium salts in three non–aqueous solvents. *The Journal of Chemical Thermodynamics* **2019,** *132*, 83-92.
196. Hernandez-Luis, F.; Galleguillos, H. R.; Graber, T. A.; Taboada, M. E., Activity coefficients of LiCl in ethanol− water mixtures at 298.15 K. *Industrial & engineering chemistry research* **2008,** *47* (6), 2056-2062.
197. Hamer, W. J.; Wu, Y. C., Osmotic coefficients and mean activity coefficients of uni-univalent electrolytes in water at 25° C. *Journal of Physical and Chemical Reference Data* **1972,** *1* (4), 1047-1100.
198. Lehmann, M. L.; Yang, G.; Nanda, J.; Saito, T., Well-designed Crosslinked Polymer Electrolyte Enables High Ionic Conductivity and Enhanced Salt Solvation. *J Electrochem Soc* **2020,** *167* (7), 070539-070547.
199. Peng, J.; Carbone, L.; Gobet, M.; Hassoun, J.; Devany, M.; Greenbaum, S., Natural Abundance oxygen-17 NMR investigation of lithium ion solvation in glyme-based electrolytes. *Electrochim Acta* **2016,** *213*, 606-612.
200. Fish, D.; Smid, J., Solvation of lithium ions in mixtures of tetraethylene glycol dimethyl ether and propylene carbonate. *Electrochim Acta* **1992,** *37* (11), 2043-2049.
201. Pan, F.; Yang, J.; Jia, C.; Li, H.; Wang, Q., Biphenyl-lithium-TEGDME solution as anolyte for high energy density non-aqueous redox flow lithium battery. *J Energ Chem* **2018,** *27* (5), 1362-1368.

202. Shimizu, A.; Takenaka, K.; Handa, N.; Nokami, T.; Itoh, T.; Yoshida, J. I., Liquid Quinones for Solvent-Free Redox Flow Batteries. *Adv Mater* **2017,** *29* (41), 1606592-1606597.
203. Gu, S.; Cai, R.; Luo, T.; Chen, Z. W.; Sun, M. W.; Liu, Y.; He, G. H.; Yan, Y. S., A Soluble and Highly Conductive Ionomer for High-Performance Hydroxide Exchange Membrane Fuel Cells. *Angew Chem Int Edit* **2009,** *48* (35), 6499-6502.
204. Varcoe, J. R.; Atanassov, P.; Dekel, D. R.; Herring, A. M.; Hickner, M. A.; Kohl, P. A.; Kucernak, A. R.; Mustain, W. E.; Nijmeijer, K.; Scott, K.; Xu, T. W.; Zhuang, L., Anion-exchange membranes in electrochemical energy systems. *Energ Environ Sci* **2014,** *7* (10), 3135-3191.
205. Wang, Y. J.; Qiao, J. L.; Baker, R.; Zhang, J. J., Alkaline polymer electrolyte membranes for fuel cell applications. *Chem Soc Rev* **2013,** *42* (13), 5768-5787.
206. Noonan, K. J. T.; Hugar, K. M.; Kostalik, H. A.; Lobkovsky, E. B.; Abruna, H. D.; Coates, G. W., Phosphonium-Functionalized Polyethylene: A New Class of Base-Stable Alkaline Anion Exchange Membranes. *J Am Chem Soc* **2012,** *134* (44), 18161-18164.
207. Mohanty, A. D.; Tignor, S. E.; Krause, J. A.; Choe, Y. K.; Bae, C., Systematic Alkaline Stability Study of Polymer Backbones for Anion Exchange Membrane Applications. *Macromolecules* **2016,** *49* (9), 3361-3372.
208. Arges, C. G.; Ramani, V., Two-dimensional NMR spectroscopy reveals cation-triggered backbone degradation in polysulfone-based anion exchange membranes. *P Natl Acad Sci USA* **2013,** *110* (7), 2490-2495.
209. Nunez, S. A.; Hickner, M. A., Quantitative H-1 NMR Analysis of Chemical Stabilities in Anion-Exchange Membranes. *ACS Macro Lett* **2013,** *2* (1), 49-52.
210. Liu, D.; Xu, M. Z.; Fang, M. L.; Chen, J. L.; Wang, L., Branched comb-shaped poly(arylene ether sulfone) s containing flexible alkyl imidazolium side chains as anion exchange membranes. *J Mater Chem A* **2018,** *6* (23), 10879-10890.
211. Maurya, S.; Noh, S.; Matanovic, I.; Park, E. J.; Villarrubia, C. N.; Martinez, U.; Han, J.; Bae, C.; Kim, Y. S., Rational design of polyaromatic ionomers for alkaline membrane fuel cells with > 1 W cm(-2) power density. *Energ Environ Sci* **2018,** *11* (11), 3283-3291.
212. Olsson, J. S.; Pham, T. H.; Jannasch, P., Poly(arylene piperidinium) Hydroxide Ion Exchange Membranes: Synthesis, Alkaline Stability, and Conductivity. *Adv Funct Mater* **2018,** *28* (2), 1702758-1702768.
213. Hudak, N. S.; Small, L. J.; Pratt, H. D.; Anderson, T. M., Through-plane conductivities of membranes for nonaqueous redox flow batteries. *J Electrochem Soc* **2015,** *162* (10), A2188-A2194.
214. Chen, L.; Wang, X.; He, X.; Liu, S.; Chen, Y.; Zhou, W., Vinyl-addition type norbornene copolymer containing sulfonated biphenyl pendant groups for proton exchange membranes. *J Appl Polym Sci* **2013,** *127* (3), 2280-2289.
215. Pierre, F.; Commarieu, B.; Tavares, A. C.; Claverie, J., High Tg sulfonated insertion polynorbornene ionomers prepared by catalytic insertion polymerization. *Polymer* **2016,** *86*, 91-97.
216. Yao, H.; He, X.; Chen, L.; Chen, Y.; Chen, D., Vinyl-addition type norbornene copolymers containing flexible spacers and sulfonated pendant groups for proton exchange membranes. *J Appl Polym Sci* **2013,** *128* (6), 3540-3547.

217. Selhorst, R.; Gaitor, J.; Lee, M.; Markovich, D.; Yu, Y.; Treichel, M.; Olavarria Gallegos, C.; Kowalewski, T.; Kourkoutis, L. F.; Hayward, R. C.; Noonan, K. J. T., Multiblock Copolymer Anion-Exchange Membranes Derived from Vinyl Addition Polynorbornenes. *ACS Appl Energ Mater* **2021,** *4* (9), 10273-10279.
218. Mandal, M.; Huang, G.; Kohl, P. A., Anionic multiblock copolymer membrane based on vinyl addition polymerization of norbornenes: Applications in anion-exchange membrane fuel cells. *J Membrane Sci* **2019,** *570*, 394-402.
219. Gmernicki, K. R.; Hong, E.; Maroon, C. R.; Mahurin, S. M.; Sokolov, A. P.; Saito, T.; Long, B. K., Accessing Siloxane Functionalized Polynorbornenes via Vinyl-Addition Polymerization for CO2 Separation Membranes. *ACS Macro Lett* **2016,** *5* (7), 879-883.
220. Higgins, M. A.; Maroon, C. R.; Townsend, J.; Wang, X.; Vogiatzis, K. D.; Long, B. K., Evaluating the impact of functional groups on membrane-mediated CO2/N2 gas separations using a common polymer backbone. *J Pol Sci* **2020,** *58* (18), 2644-2653.
221. Akiyama, R.; Yokota, N.; Otsuji, K.; Miyatake, K., Structurally well-defined anion conductive aromatic copolymers: Effect of the side-chain length. *Macromolecules* **2018,** *51* (9), 3394-3404.
222. Dekel, D. R.; Rasin, I. G.; Brandon, S., Predicting performance stability of anion exchange membrane fuel cells. *J Power Sources* **2019,** *420*, 118-123.
223. Mahmoud, A. M. A.; Miyatake, K., Optimization of the pendant chain length in partially fluorinated aromatic anion exchange membranes for alkaline fuel cells. *J Mater Chem A* **2018,** *6* (29), 14400-14409.

VITA

Michelle Lehmann graduated from the University of Tennessee with a B.S. degree in chemical engineering and a chemistry minor in 2017. During that time, she was involved in undergraduate research under Dr. Robert Counce performing separations research. Upon graduation, Michelle joined the Soft Materials group at ORNL as a post-bachelor researcher. In August 2019, Michelle began her PhD studies under the guidance of Dr. Tomonori Saito. Her research focus has been the synthesis and characterization of polymer electrolytes and ion exchange membranes for a variety of electrochemical applications. Michelle has presented at MRS and ECS conferences and has published 14 peer reviewed publications.